ROBUST SMOOTH MODEL-FREE CONTROL METHODOLOGIES FOR INDUSTRIAL APPLICATIONS

by

Sohail Iqbal
Reg. No. PE 073003

A thesis submitted to the
Department of Electronic Engineering
in partial fulfillment of the requirements for the degree of
DOCTOR OF PHILOSOPHY IN ELECTRONIC ENGINEERING

Faculty of Engineering and Applied Sciences
Mohammad Ali Jinnah University
Islamabad
August, 2011

Dedicated to
all of my teachers
who taught me the unseen truths.

ABSTRACT

Model free control methodologies are popular in industry due to their easy implementation. Minor tuning of controller gains yields satisfactory performance from a dynamical system. The main drawback of the techniques is their lack of robustness. On the other hand, robust control techniques e.g. sliding mode control require mathematical model of the system and their aggressive control effort is the main barrier in their implementation for mechanical systems. The proposed robust smooth control techniques with robust state-disturbance observer in the closed loop are the solution to the problem. The proposed state-disturbance observer is model free and relies on input and output of the system only; consequently it estimates states as well as drift term of the system. The estimated drift term is used to cancel out internal and external disturbances of the system and this cancellation transforms the system into an nth order integrator system. The observed states are used to design any modern or classical state-space control technique e.g. pole placement, Linear Quadratic Regulator (LQR) or Linear Matrix Inequality (LMI) methods etc. The finite time stability analysis of robust state-disturbance observer is given in noisy and noise free environments. In this thesis, two novel control methodologies i.e. robust smooth real twisting second order sliding mode and robust feedback linearization are also proposed. The finite time stability analysis of the robust smooth real twisting control is proven using Lyapunov method along with homogeneity concepts. The stability analyses of overall closed loop systems are given using separation principle. Simulations as well as experimental results with academic bench mark DC motor validate the ideas. The proposed techniques are also compared with robust LMI based polytopic controller on an industrial stabilized platform to verify their usage for industry.

TABLE OF CONTENTS

LIST OF FIGURES

LIST OF TABLES

Chapter 1

INTRODUCTION

It is a long standing aspiration of the control engineer to achieve a specified level of closed-loop performance and robustness from a system in finite span of time. The problem becomes more crucial when only outputs are available, the system do not have specific mathematical model and it also contains substantial internal uncertainties and significant external disturbances.

PID (Proportional-Integral-Derivative) control (Ogata, 2009; Franklin *et al*, 2010) is popular due to its simplicity and facility to tune its parameters without any detailed knowledge of the plant. However it is not a robust scheme. In nonlinear systems, feedback linearization (Isidori, 1995; Slotine and Li, 1991) can provide desired performance, but it requires all parameters of the system to be well known; and again it is not robust. Sliding Mode Control (SMC) (Utkin, 1992; Edwards and Spurgeon, 1998) can provide desired performance and robustness in presence of internal uncertainties and external disturbances, but the associated chattering effects resulting from the use of discontinuous terms in the control law are an obstacle to its implementation - especially for mechanical systems.

In the last decade, a number of methods have been proposed to avoid the chattering effects. Saturation approaches (Slotine and Li, 1991) and Sigmoid approximations (Burton and Zinober, 1986) have been used to smooth the transition near switching surface by changing the dynamics in small vicinity of the surface. Such approaches risk possible reductions in accuracy. Another well known approach for the purpose is equivalent control (Utkin, 1992), that involves convex combination of control effort on both sides of the sliding surface. This method maintains system trajectories on the constraint manifold, if the system dynamics are exactly known that is not always possible.

Other approaches that do not compromise performance have recently been proposed. The terminal sliding mode method (Man *et al*, 1994) is built on a nonlinear switching manifold and can significantly improve the transient performance of the closed loop

system. The technique does not satisfy Lipschitz conditions (Yu and Man, 2002) and has an unbounded right-hand side (Levant, 2003). In dynamical sliding modes (Sira-Ramirez, 1993) the surface is not only dependent upon the states but also on the inputs of the system. This method adds additional dynamics to the compensated system and hence increases the overall complexity. Higher Order Sliding Modes (HOSM) (Emel'yanov *et al*, 1996; Levant, 1993; Fridman and Levant, 1996; Bartolini, Ferrara and Usai, 1998) is the most prominent and effective technique to remove chattering effects whilst preserving the important properties of traditional first order SMC. The main shortcoming of this method is its sensitivity to unmodeled fast dynamics (Shtessel, Shkolnikov and Levant, 2007).

1.1 Motivation

The motivation of this thesis is to develop novel control methodologies for industrial systems. The techniques should be model-free, robust and smooth, moreover desired performance from the system can be achieved within finite time in the presence of uncertainties and disturbances.

The industrial systems are very complex and no ready to use mathematical model of the system is available. If the model is available then its parameters are unknown or highly time varying. Unmodeled and ignored dynamics are also big issues. Model free control environment, e.g. PID (Ogata, 2009; Franklin *et al*, 2010), Fuzzy Control (Lee, 90) and Neural Network (Hunt *et al*, 92) may be good options, but these approaches are not robust in nature or time consuming.

The environmental disturbances and uncertainties are also big issues. Robust control e.g. sliding mode control (Utkin, 1992; Edwards and Spurgeon, 1998) is a solution of the problem for rejection of the disturbances and copes with the uncertainties. The states of the plant are required to implement the robust control techniques. States observers (Kalman, 1960; Luenberger, 1964; Utkin, 1999; Khalil, 2002; Davila Fridman and Levant, 2005) can be used to estimate the states, but it require mathematical model of the system.

Generally robust control produces aggressive control actions to cope with the disturbance effects. The controller gain should be greater than upper bounds of the internal and external (matched) uncertainties. This aggressive control causes chattering effects

in the system input channel. Some industrial systems are too sensitive and cannot allow the chattering effects in their control law. The robust smooth control (Shtessel, Shkolnikov and Levant, 2007) may be an option for handling of such kind of problems.

The smooth controllers alone are not robust and give degraded performance in perturbed and uncertain circumstances. The robustness can be incorporated if the disturbances are cancelled out after its estimations. It requires disturbance observer (Radke and Gao, 2006) in closed loop of the system to estimate drift terms effects in the system.

For design of robust smooth control methodology, system states and disturbance observations are required. A robust state-disturbance observer can estimate simultaneously both the things. Such observer can ensure model-free, robust and smooth characteristics in closed loop systems.

To establish the results of methodology based on robust state-disturbance observer, the feedback linearization control techniques can yield a linear closed loop dynamics. The control gain matrix can be designed using any modern or classical state-space technique e.g. pole placement, LQR or LMI methods etc, such that the coefficients of the system are Hurwitz and meet the desired performance and robustness objectives in the closed loop system.

To achieve above goals, first of all an observer is required that can estimate states as well as drift terms of the system in the absence of detailed mathematical model of the system. The observer can help control techniques to reject the disturbance effects in the closed loop. In this way robust smooth control and robust feedback linearization techniques are feasible to implement in industrial environment.

1.2 Contributions

This thesis comprises four novel contributions as follows:

First of all a robust exact observer is proposed that is derived from robust exact differentiator (Levant, 1998; Levant, 2003; Shtessel, Shkolnikov and Levant, 2007). The observer can estimate the states as well as drift terms i.e. combined effect of internal and external disturbances of the system, without detailed knowledge of the mathemat-

ics of the system. Finite time convergence of the proposed observer for relative degree less than or equal to the system order is also proven in noisy and noise free environments.

Secondly, a novel robust smooth real twisting second order sliding mode control is proposed in combination with disturbance observer to provide robustness as well as accuracy. A Lyapunov method combined with homogeneity concept is used to prove exponential stability of the nominal system. The overall stability of the closed loop system is established with the help of separation principle.

Thirdly, a robust feedback linearization with stable zero dynamics is introduced for nonlinear systems. The robust state-disturbance observer is incorporated in closed loop system to estimate states as well as drift terms. The drift term estimates are used to compensate the nonlinear dynamics of the system and observed states are used to design a linear control law. The complete closed loop stability of the system is proven using separation principle.

Fourthly, a novel technique is proposed to formulate the polytopic system for highly uncertain system. System identification is used to extract distinct model of the system at different operating conditions. The different identified models are vertices of a convex hull and used to build the polytopic systems.

1.3 Disseminations

Following are the outcome of the PhD research published in journals and proceeding of international conferences.

1.3.1 Journal Publications

i. **S. Iqbal,** C. Edwards, A. I. Bhatti, (2011)**,** *Output-Feedback Smooth Second-Order Sliding Mode Controller for Relative Degree Two Systems*, Submitted to **Asian Journal of Control** on invitation of the chief Editor (ISI Thomson IF: 0.84)

ii. **S. Iqbal**, A. I. Bhatti, (2011), *Load Varying Polytopic Based Robust Controller Design in LMI Framework for a 2DOF Stabilized Platform*, **Arabian Journal for Science and Engineering**, Vol. 36 (2), pp. 311 – 327. (ISI Thomson IF: 0.224).

iii. M. Iqbal, A. I. Bhatti, **S. Iqbal**, Q. Khan, (2011), *Robust Parameter Estimation of Nonlinear Systems using Sliding Mode Differentiator Observer*, **IEEE Transactions on Industrial Electronics**, Vol. 58(2), pp. 680 – 689. (ISI Thomson IF: 5.468).

iv. Q. Khan, A. I. Bhatti, **S. Iqbal**, M. Iqbal, (2011), *Dynamic Integral Sliding Mode for MIMO Uncertain Nonlinear Systems*, **International Journal of Control, Automation and Systems**. Vol. 9(1), pp.151 – 160. (ISI Thomson IF: 0.770).

1.3.2 International Conferences Publications

v. **S. Iqbal**, C. Edwards, A. I. Bhatti, (2011), *Robust Feedback Linearization using Higher Order Sliding Mode Observer*, in proceeding of **50th IEEE Conference on Decision and Control and European Control Conference (CDC-ECC'11)**, December 12– 15, Orlando, Florida, USA.

vi. **S. Iqbal**, C. Edwards, A. I. Bhatti, (2011), *Robust Output Feedback Linearization for Minimum Phase Systems*, in proceeding of **18th IFAC World Congress (IFAC WC'11)**, August 28 – September 2, Milano, Italy.

vii. **S. Iqbal**, C. Edwards, A. I. Bhatti, (2010), *A Smooth Second-Order Sliding Mode Controller for Relative Degree Two Systems*, Proceeding of **36th Annual Conference of the IEEE Industrial Electronics Society (IECON'10)**, Glendale, AZ, USA, Nov 07-10, 2010.

viii. Q. Ahmed, A. I. Bhatti, **S. Iqbal**, I. H. Kazmi, (2010), *2-Sliding Mode Based Robust Control for 2-DOF Helicopter*, Proceeding of 11th **International Workshop on Variable Structure Systems (VSS'10)**, Mexico City, June 26-28, 2010.

ix. M. Iqbal, A. I. Bhatti, **S. Iqbal**, Q. Khan, I. H. Kazmi, (2009), *Fault Diagnosis of Nonlinear Systems Using Higher Order Sliding Mode Technique*, Proceedings of the **7th Asian Control Conference (ASCC'09),** Hong Kong, China, August 27-29, 2009, pp 875 - 880.

x. M. Iqbal, A.I. Bhatti, **S. Iqbal**, Q. Khan, H.I. Kazmi, (2009), *Parameter estimation of uncertain nonlinear MIMO three tank systems using higher order sliding modes*, Proceeding of **IEEE International Conference Control and Automation, (ICCA'09)** on 9-11 Dec. 2009, pp. 1931 – 1936.

xi. Q. Ahmed, A. I. Bhatti, **S. Iqbal**, (2009), *Nonlinear Robust Decoupling Control Design for Twin Rotor System*, Proceedings of the **7th Asian Control Conference (ASCC'09)**, Hong Kong, China, August 27-29, 2009, pp 937 - 942.

xii. Q. Ahmed, A. I. Bhatti, **S. Iqbal**, (2009), *Robust Decoupling Control Design for Twin Rotor System using Hadamard Weights*, Proceeding of **18th IEEE International Conference on Control Applications 2009 IEEE Multi-conference on Systems and Control (MSC'09)**, Saint Petersburg, Russia, July 8-10, 2009, pp. 1009 – 1014

xiii. M. Iqbal, A. I. Bhatti, **S. Iqbal** and Q. Khan, (2009), *Parameter Estimation based Fault Diagnosis of Uncertain Nonlinear Three Tank System using HOSM Differentiator Observer*, Proceedings of the **13th IEEE International Multi-conference, (INMIC'09)**, Islamabad, Pakistan, 14-15 December 2009.

xiv. H. Kazmi, A. I. Bhatti and **S. Iqbal**, (2009), *A Nonlinear Observer for PEM Fuel Cell System*, Proceedings of **13th IEEE International Multi-conference, (INMIC'09)**, Islamabad, Pakistan, 14-15 December 2009, pp

xv. Iqbal, M., A. I. Bhatti, **S. Iqbal**, Q. R. Butt, (2009), *LMI Based Controller Synthesis of an Uncertain Three Tank System*, **6th International Bhurban Conference on Applied Sciences and Technology (IBCAST'09)**, pp. 192 - 196

xvi. **S. Iqbal**, A. I. Bhatti, Q. Ahmed, (2008), *Determination of Realistic Uncertainty Bounds for the Stewart Platform with Payload Dynamics*, Proceeding of **17th IEEE International Conference on Control Applications, IEEE Multi-conference on Systems and Control, (MSC'09)**, San Antonio, Texas (USA), September 3-5, 2008

xvii. **S. Iqbal**, A. I. Bhatti, Q. Ahmed, (2008), *Dynamic Analysis and Robust Control Design for Stewart Platform with Moving Payloads*, **Proceedings of 17th IFAC World Congress (IFAC WC '08)**, 5 – 11 July 2008, Seoul, Korea.

xviii. **S. Iqbal**, A. I. Bhatti, M. Akhtar, S. Ullah, (2007) *Design and Robustness Evaluation of an H_∞ Loop Shaping Controller for a 2DOF Stabilized Platform*, Proceedings of **European Control Conference (ECC'07),** Kos, Greece 2 – 5 July 2007, ISBN: 978-960-89028-5-5, pp 2098-2104.

xix. **S. Iqbal**, A. I. Bhatti, (2007), *Robust Sliding-Mode Control for Stewart Platform*, Proceeding of **5th International Bhurban Conference on Applied**

Sciences and Technology (IBCAST'07), 8 – 11 Jan 2007, Islamabad, Pakistan.

xx. **S. Iqbal**, A. I. Bhatti, (2006), *Direct Sliding-Mode Control for Stewart Manipulator*, Proceeding of **10th IEEE International Multitopic Conference (INMIC'06)**, 23 – 24 Dec 2006, Islamabad, Pakistan, ISBN 1-4244-0794-x, pp 421-426.

xxi. **S. Iqbal**, M. Akhtar, N. Mehdi, (2005), *System Identification and H_∞ Loop-Shaping Design for a 3DOF Stabilized Platform*, proceeding of the **4th International Bhurban Conference on Applied Sciences and Technology (IBCAST'05)**, 13 – 18 Jun 2005, Bhurban`, Pakistan.

1.4 Thesis Structure

The thesis consists of six chapters. First chapter explains introduction of thesis containing motivation, dissemination and structure.

In the second chapter, necessary theoretical background is given for better understanding of rest of the thesis. Firstly an introduction of feedback linearization is summarized and its pros and cons are given. After that, standard sliding mode and higher order sliding mode are discussed in detail. Afterwards general idea of smooth sliding mode control is presented. In the last, robust exact differentiator is discussed.

In the third chapter, a robust smooth second order sliding mode controller for relative degree two systems is proposed. Due to the smooth nature of the controller, a robust disturbance observer is also introduced as part of the closed loop system. The observer estimates the drift terms of the system to compensate its effects. A Lyapunov function is used along with homogeneity-based approach to prove finite time stability of the proposed smooth controller. The stability of the complete closed loop system is given by using separation principle. The proposed scheme is verified through simulations as well as experimentations on a benchmark DC motor.

In the fourth chapter, synthesis of robust feedback linearization procedure for nonlinear systems with stable zero dynamics is explored employing state-disturbance observer for estimation of the states as well as drift terms simultaneously on the basis of just available output of the system. The detailed knowledge of the mathematical model of the system is no more crucial. Finite time convergence of the complete closed

loop system is proved and thus a form of separation principle is satisfied i.e., the controller and observer can be designed separately. The simulation and experimental results verify robustness as well as performance of the proposed technique.

Fifth chapter deals with robustness and performance evaluation of the proposed techniques on an industrial application. Generally PID control is used as benchmark for such comparison, but due to lack of robustness its evaluation with the robust techniques would not be reasonable. In this scenario robust H_∞ control based on LMI optimization is chosen for the evaluation. A parallel robot stabilized platform is used as an experimental rig. In the chapter a novel idea to construct polytopic model of the system is proposed. Different models of the system are extracted using system identification method at distinct load conditions. These models are then used to construct vertices of a polytopic system for the parallel manipulator. Experimental results show that controller based on LMI optimization is inferior to the proposed techniques results.

In the last chapter, drawn conclusions are listed and future work is proposed for researchers working in this area.

1.5 Summary

This chapter provides the overview of the thesis. In the next chapter basic foundations of the contributions are discussed.

Chapter 2

MATHEMATICAL BACKGROUND

Mostly physical engineering systems in industry have approximate mathematical models and only inputs and outputs of the system could be available. Sensors and their installations for measurement of the internal states come with expensive and very difficult scenarios. The industrial systems are affected by significant internal and external disturbances due to heavy uncertainties in the environment. In these circumstances, it is a great challenge for a control engineer to achieve desired closed-loop performance and robustness from the systems.

This thesis presents two novel robust smooth control techniques for solution of the industrial systems. First technique proposes a smooth second order real twisting controller using the robust state-disturbance observer. In the second technique, robust feedback linearization control is suggested using robust exact state and disturbance observer.

In this chapter, important and necessary definitions are given in detail for ready reference to understand the research work, which also provide a theoretical foundation for the thesis.

2.1 Input-Output Linearization

Input-output linearization fully or partially transforms a nonlinear system into equivalent linear form by cancelling out the nonlinearities through feedback (Slotine and Li, 1991). In this technique, the derivatives of output $y^{(i)}$ are not proportional to control input for all $i = 1, \dots, k-1$ and $y^{(k)}$ is directly proportional to the input with non-zero coefficient of proportionality in reasonable domain. The procedure comprises of following steps (Slotine and Li, 1991):

- Output y of the system is differentiated until input u appears in dynamical equation of the system.
- Choose input u such that it cancels out the nonlinear dynamics and ensure tracking error convergence.

- Analyze unobservable dynamics of the system.

Consider a single input single output dynamical system (Sastry, 1999)

$$\dot{x} = f(x) + g(x)u \tag{2.1.1a}$$

$$y = h(x) \tag{2.1.1b}$$

with well defined relative degree *r* i.e. control appears at *rth* derivative of the system. In the equation $x \epsilon \mathcal{R}^n$ is state vector, $u \epsilon \mathcal{R}$ is control effort, $y \epsilon \mathcal{R}$ is output, the vector functions $f(.)$ and $g(.)$ are smooth vector fields, locally defined over the tangent space of $\mathcal{R}^n$, and $h(x)$ is the smooth scalar function of $\mathcal{R}^n$. Note that $f(.)$ and $g(.)$ are referred as drift term and control input fields respectively.

Let the Lie derivative (directional derivative) of $h(x)$ in the direction of $f(x)$ is a scalar function defined by $L_f h(x) = \frac{\partial h}{\partial x^T} f(x)$, similarly the scalar function $L_g L_f h(x)$ is the Lie derivative of $L_f h(x)$ in the direction of $g(x)$ (Sastry, 1999). In the following calculation, it is assumed that states x of system (2.1.1) are defined in open set U of $\mathcal{R}^n$ and the relative degree of the system about specific equilibrium point $x_0 \epsilon U$ is equal to the system's order. In other words, the system does not have any internal dynamics. Differentiating output y *n*-times in (2.1.1b) (Sastry, 1999), we get

$$y^{(k)} = \begin{cases} L_f^k h(x) & \forall\, k = 1, \dots, n-1 \\ L_f^k h(x) + L_g L_f^{k-1} h(x) u(t) & k = n \end{cases} \tag{2.1.2}$$

If $L_g L_f^{n-1} h(x)$ is bounded away from zeros for all $x \epsilon U$, the control law can be chosen as

$$u = \frac{1}{L_g L_f^{n-1} h(x)} \left(-L_f^n h(x) + v \right) \tag{2.1.3}$$

where v is the new input. The control (2.1.3) cancels out the nonlinearities of the system (2.1.1) and yields it into a simple nth order integrator relationship between new input variable v to output *y,* i.e.

$$y^{(n)} = v \tag{2.1.4}$$

The convergence of this nth order integrator is simple due to linear control techniques such as pole placement or others. Let the tracking error of the system is $\xi = y - y_d$ and choosing the new control input such that

$$v = y_d^{(n)} - \lambda_1 \xi - \lambda_2 \dot{\xi} - \cdots - \lambda_n \xi^{(n-1)}$$

here all λ_i are positive constants. The new control yields the error dynamics of the system (Slotine and Li, 1991)

$$\xi^{(n)} + \lambda_n \xi^{(n-1)} + \cdots + \lambda_2 \dot{\xi} + \lambda_1 \xi = 0 \tag{2.1.5}$$

exponentially stable and its convergence is dependent upon the λ_i, coefficients of the Hurwitz polynomial.

Now suppose that the system has relative degree $r \leq n$, then internal dynamics are not directly related to the output of the system. A diffeomorphic transformation $(\xi, \eta) = T(x)$ can transform the system (2.1.1) into so called normal form (Sastry, 1999) as follows:

$$\begin{aligned}
\dot{\xi}_1 &= \xi_2 \\
&\vdots \\
\dot{\xi}_{r-1} &= \xi_r \\
\dot{\xi}_r &= b(\xi, \eta) + a(\xi, \eta) u(t) \\
\dot{\eta} &= q(\xi, \eta) \\
y &= x
\end{aligned} \tag{2.1.6}$$

here $b(\xi, \eta) = L_f^r h(x),\ a(\xi, \eta) = L_g L_f^{r-1} h(x),\ q(\xi, \eta) = L_f \eta(\xi, \eta)$ in (ξ, η) coordinates, $\eta \in \mathcal{R}^{n-r}$ are the internal dynamics and it is not directly decoupled with input *u* or in other words have not a direct dependence on the input *u*, i.e. $L_g \eta = 0$ (Sastry, 1999). Note that in (2.1.6), first *r* equations are in controllable canonical form and last *n-r* equations are unobservable. The input-output linearization procedure can be represented with structure as shown in Figure 2.1.

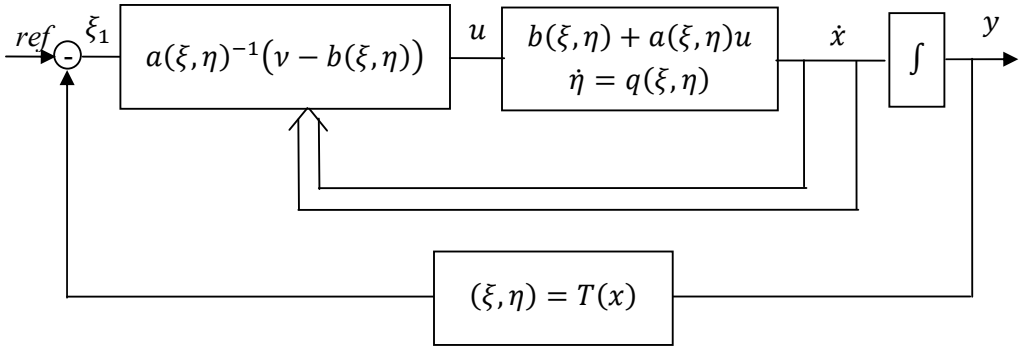

Figure 2.1: *Input-Output Linearization Structure*

Problems in Feedback Linearization

Input-output linearization is very powerful tool for analyzing and controlling nonlinear dynamical systems. But at the same time this method has some limitations (Slotine and Li, 1991):

i. Exact mathematical model of the system, correct measurement of states and accurate knowledge of system parameters are required to formulate the control law so it can cancel out the nonlinearities in the system and introduce linear dynamics.
ii. If the observer is embedded in the closed loop for measurement of states, its stability analysis is also required.
iii. It is not applicable to all nonlinear systems, e.g., relative degree should be certain, zero dynamics should be stable, etc.
iv. It is not robust against disturbances and parametric variations of the system.

To overcome the robustness issues, sliding mode control is suggested. sliding mode control and its variants are discussed in the following lines in detail.

2.2 Sliding Mode Control

Sliding mode control (Utkin, 1977; Utkin, 1992; Edwards and Spurgeon, 1998) is a variant of Variable Structure System (VSS). Traditionally, VSS is comprised of a variety of structures in different portions of state-space of closed loop system. The detached structures may be unstable alone. The certain rules are defined to switch control efforts online between the structures to achieve desire performance. The closed loop system contains new features that were not at hand in any base structure.

In sliding mode control, a "custom-designed" linear or nonlinear function $s(x)$, named as sliding variable is defined. When a constraint $s(x) = 0$ is imposed on sliding variable, it becomes sliding manifold (or sliding surface in the linear case). The approach contains two phases namely reaching and sliding phases. In the reaching phase, system trajectories are directed towards the sliding manifold with the help of appropriate control law. In the sliding phase, the trajectories motion is kept on the sliding manifold with the help of the control law and the trajectories are steered towards the equilibrium points automatically due to inherent design of the sliding manifold. In this technique, a reduced order dynamics are achieved for the compensated system and the system dynamics is independent from unknown system parameters.

The features of sliding mode control are ultimate accuracy, robustness against external disturbances, model reduction and finite-time stability. The main drawback is dangerous chattering effect that can be unacceptable for mechanical systems, e.g. aircraft, missile and robotic manipulators. Other shortcomings are: it can only be applicable if the system has relative degree one with respect to sliding variable and all states used in the construction of the sliding variable must be known.

In the sliding phase, the control that helps the trajectories to stay on the surface is called equivalent control that will be dealt with in the following lines.

2.2.1 Equivalent Control

The equivalent control (Utkin, 1992) is an average of the high frequency switching that applies after reaching the system trajectories on sliding manifold so that it stays the trajectories on the manifold afterwards. A low pass filter is used for averaging the high frequency control law. Let a dynamical system be

$$f(x) = Ax + Bu, \tag{2.3.1}$$

where $x \in \mathcal{R}^n$ is state vector, $u \in \mathcal{R}$ is control effort and *A, B* are matrices of appropriate dimensions. Let a constraint manifold $s(x) = 0$ be followed by the system (Slotine and Li, 1991). Then

$$\begin{aligned} f_+(x) &= Ax + Bu_+ \qquad if\ s < 0, \\ f_-(x) &= Ax + Bu_- \qquad if\ s > 0, \end{aligned} \tag{2.3.2}$$

and trajectory f_{eq} on the surface can be possible by applying the average control effort u_{eq}, (Slotine and Li, 1991), i.e.

$$f_{eq}(x) = Ax + Bu_{eq} \tag{2.3.3}$$

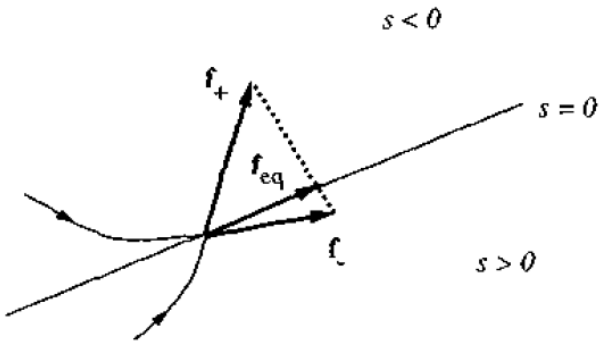

Figure 2.2: *The Equivalent Control (Slotine and Li, 1991)*

Geometrically, equivalent control can be written as the convex combination of control efforts on both sides of the sliding surface (see Fig. 2.2), i.e.

$$u_{eq} = \alpha u_+ + (1-\alpha)u_-, \qquad 0 < \alpha < 1, \tag{2.3.4}$$

where α can be found by equating $\dot{s} = 0$ i.e. the resultant trajectories are tangential to the sliding manifold (Slotine and Li, 1991). The equivalent control cannot be implemented practically because system model is always approximate and disturbances are unknown.

A design example of a simple pendulum is considered to illustrate the details of sliding mode control.

2.2.2 Design Example

Consider nonlinear model of a simple pendulum (Edwards and Spurgeon, 1998)

$$ml^2\ddot{\theta} + mglsin\theta = u \tag{2.3.5}$$

where m is the mass, l is the length, g is the force of gravity, θ is the pendulum position and u is the control input. Let $x_1 = \theta$ and $x_2 = \dot{\theta}$, the state-space model of the system can be written as

$$\dot{x}_1 = x_2$$

$$\dot{x}_2 = -\frac{g}{l}sinx_1 + \frac{1}{ml^2}u \tag{2.3.6}$$

In sliding mode control first step is to design sliding variable i.e.

$$s = \lambda\, x_1 + \, x_2$$

By taking the first derivative of the sliding variable, we get

$$\dot{s} = \lambda\, \dot{x}_1 + \, \dot{x}_2$$

by putting the value of $\dot{x}_1\ and\ \dot{x}_2$ from (2.3.6), we get,

$$\dot{s} = \lambda\, x_2 - \frac{g}{l}sinx_1 + \frac{1}{ml^2}u \tag{2.3.7}$$

For equivalent control put $\dot{s} = 0$ in equation (2.3.7) we get,

$$u_{eq} = ml^2\left(-\lambda\, x_2 + \frac{g}{l}sinx_1\right)$$

and the sliding mode control can be given as

$$u = u_{eq} - Ksign(\sigma) \tag{2.3.8}$$

The control law in (2.3.8) is robust and accurate along with harmful chattering effects for mechanical systems. In the last decade, a numbers of methods have been proposed to avoid these chattering effects e.g. saturation approximation (Slotine and Li, 1991), equivalent control (Utkin, 1992), terminal sliding mode (Man *et al*, 1994), dynamical sliding mode (Sira-Ramirez, 1993), sliding-sector method (Furuta and Pan, 2000) and high-order sliding mode (Levant, 1993; Levant, 2003; Levant, 2005). To overcome the shortcoming of conventional sliding mode control, higher order sliding modes are introduced in 1980s by Russian scientists Emel'yanov and Levant. In the next Section, we will discuss the approach and its popular algorithms.

2.3 Higher Order Sliding Mode

The Higher Order Sliding Mode (HOSM) (Emel'yanov *et al*, 1996; Levant, 1993; Fridman and Levant, 1996; Bartolini, Ferrara and Usai, 1998) is an extension of traditional sliding mode control theory. Let sliding order of the dynamical system is denoted by variable *r*. The *rth* order sliding mode is said to be taking place, if a control law with nonlinear sliding variable steers not only the sliding variable but also its $r-1$ successive derivatives towards zero manifold in finite time and stay there afterwards in the presence of bounded disturbance (Levant, 1993) i.e.

$$\sigma = \dot{\sigma} = \cdots = \sigma^{(r-1)} = 0$$

As the sliding order increases, the chattering effect reduces in vicinity of the sliding manifold and the control effort becomes more and more continuous. The fact can be understood by the following arguments. In sliding mode, a system starts chattering when its trajectories are in the vicinity of sliding manifold. When the sliding order of a system is increased, its sliding manifold dimension is reduced e.g. in third order sliding mode, the sliding manifold is only a point as shown in Figure 2.3. In this way the harmful chattering effects vanished in the higher derivatives of the sliding variable.

In other words, the sliding accuracy provided by HOSM is proportional to the *rth* power of the time interval, i.e.

$$sup|\sigma| \leq \mathcal{O}(\tau^r),$$

where $\mathcal{O}$ = constant > 0. This means, that we can achieve better accuracy and attenuation in chattering effects as the sliding order is increased, graphically it can be illustrated through Figure 2.4.

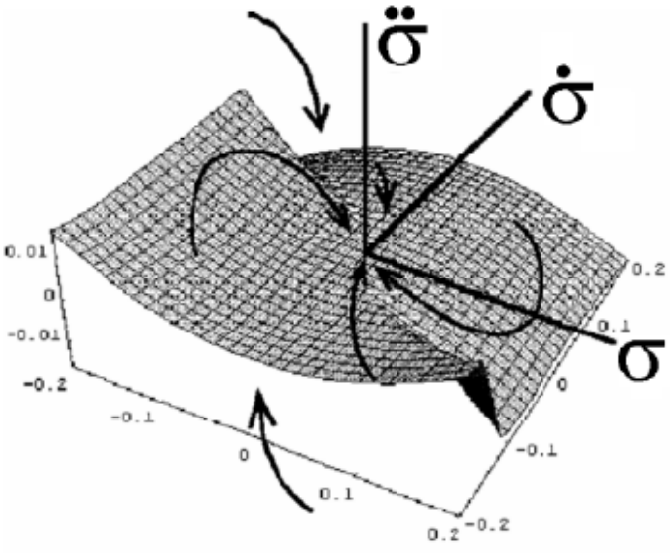

***Figure 2.3**: Third Order Sliding Mode Trajectory (Levant, 2003)*

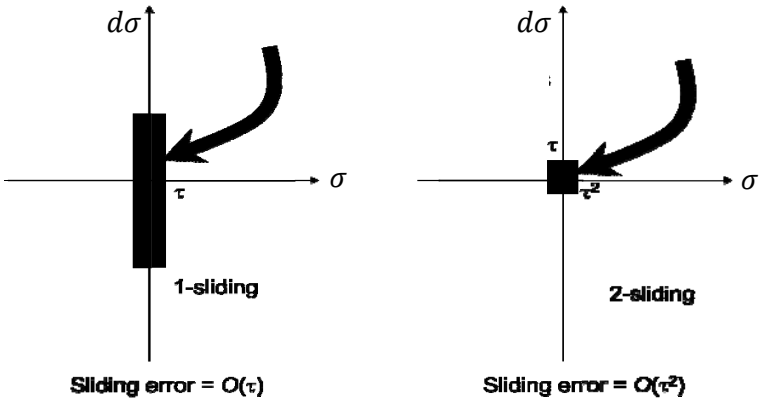

***Figure 2.4**: The Sliding accuracy in sliding mode*

Standard sliding mode is also a special case of higher order sliding mode herein the order of the mode is equal to one. In the first order sliding mode control, the system trajectories hit the sliding manifold more or less vertically (see Figure 2.5a) whereas in higher order sliding the trajectories hit the manifold tangentially (Emel'yanov, Korovin and Levantovsky, 1996). This fact reduces the chances for the trajectories to leave the HOSM manifold thereafter. The Figure 2.5b demonstrates the tangential ap-

proaching of the system trajectory towards sliding manifold in second order sliding mode.

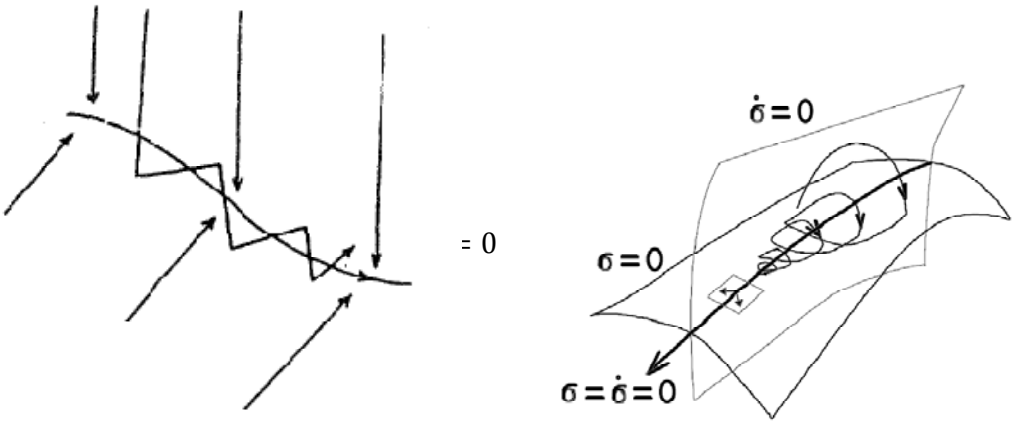

(a) First Order Sliding Mode (Emel'yanov et al, 1996)

(b) Second Order Sliding Mode (Levant, 2003)

***Figure 2.5**: Trajectory Motion in First and Second Order Sliding Modes*

Unlike standard sliding mode, higher order can handle any relative degree with respect to sliding variable. HOSM also reduces the total dynamic order of a system in finite time, in other words, the system dynamics turn to algebraic equations. Moreover it also deals well with matched uncertainty and the disturbance of a system.

In HOSM, sliding order of the system can artificially be increased up to *rth* degree, but Second Order Sliding Mode (SOSM) is most popular due to ease of its implementation. In the next Section, SOSM and its algorithms are discussed.

2.4 Second Order Sliding Mode

The algorithm that steers the system trajectories in the vicinity of sliding manifold such that $\sigma \to 0$ and $\dot{\sigma} \to 0$ in finite time and keeping them there afterwards in the presence of bounded disturbance is called second order sliding mode, mathematically it can be written as

$\sigma = \dot{\sigma} = 0$

The SOSM has been successfully implemented on many practical problems, e, g. (Bartolini, Ferrara, Punta, 2000), (Levant *et al.*, 2000), (Khan, Spurgeon and Puleston, 2001), (Spurgeon *et al.*, 2002), (Bartolini *et al*., 2003), (Khan, Goh and Spurgeon,

2003), (Massey and Shtessel, 2005), (Khan and Spurgeon 2006), (Ferrara and Lombardi, 2007), (Baev, Shtessel and Shkolnikov, 2008), (Butt and Bhatti, 2008), (Qaiser *et al*., 2009a; Qaiser *et al*., 2009b), (Iqbal, Edwards and Bhatti, 2010), (Iqbal, Edwards and Bhatti, 2011), (Iqbal *et al*, 2011), (Khan *et al*, 2011a), (Khan *et al*, 2011b), (Khan *et al*, 2011c), (Qadeer *et al*., 2011a) and (Qadeer *et al*., 2011b);

There are a number of SOSM algorithms; practically real twisting and super twisting algorithms are most popular. In the forth coming subsections, both algorithms are discussed in detail.

2.4.1 Real Twisting Algorithm

Real twisting is historically a first second-order sliding mode controller. It is used to avoid chattering and provides good robustness properties. This algorithm requires the measurement of $\dot{\sigma}$ for the implementations. It is also sensitive to sampling interval τ. The controller twists the state trajectories about the origin and converge them to the origin in finite time. This algorithm can be applied for relative degree one as well as for relative degree two systems. For relative degree 1, control law can be applied as (Levant, 1993)

$$\dot{u} = \begin{cases} -u, & if\ |u| > 1 \\ -\alpha_m sign\sigma, & if\ \sigma\dot{\sigma} \leq 0;\ |u| \leq 1 \\ -\alpha_M sign\sigma, & if\ \sigma\dot{\sigma} > 0;\ |u| \leq 1 \end{cases} \tag{2.4.1}$$

where $\alpha_M > \alpha_m > C/K_m,$ and $0 < \rho \leq 0.5,$

The $\dot{u}$ value commutes at each axis crossing which requires availability of $\dot{\sigma}$. The above equation (2.5.1) can also be written as

$$\dot{u} = \begin{cases} -u, & if\ |u| > 1 \\ -r_1 sign\ \sigma - r_2 sign\ \dot{\sigma} \leq 0, & if\ |u| \leq 1 \end{cases}$$

where $r_1 > r_2 > 0$, $\alpha_M = r_1 + r_2$ and $\alpha_m = r_1 - r_2$. The problem with this method is that $\dot{\sigma}$ is not available all the times. To solve the problem, $sign(\dot{\sigma})$ can be replaced with $sign(\Delta\sigma)$, where $\Delta\sigma = \sigma(t) - \sigma(t_i - t_{i-1})$ and $t\ \epsilon\ [t_i, t_{i-1})$ (Levant, 1993).
For relative degree 2, the control law can be applied as (Levant, 1993)

$$\dot{u} = \begin{cases} -K_m sign\ \sigma, & if\ |u| > 1 \\ -K_M sign\ \sigma, & if\ |u| \leq 1 \end{cases}$$

Graphically, the convergence of real twisting control can be seen in Figure 2.6.

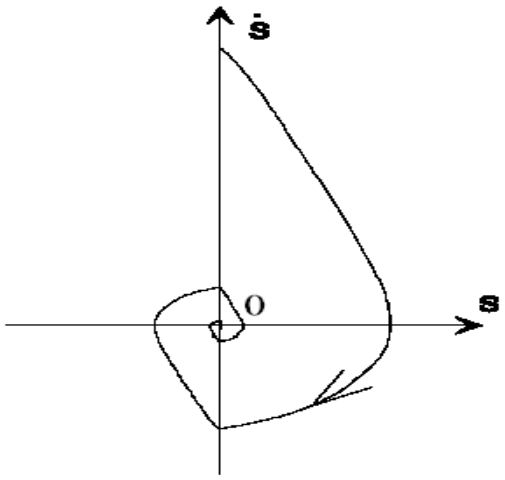

Figure 2.6: *Real Twisting Algorithm convergence (Levant, 1993)*

The stability analysis of real twisting algorithm is given in Appendix A.

2.4.2 Super Twisting Algorithm

The super twisting is the only algorithm that derives both sliding variable and its derivative to zero manifolds in finite time without measurement of $\dot{\sigma}$. The algorithm can be used instead of standard sliding mode to avoid chattering. Another advantage of the algorithm is that it is not sensitive to sampling time interval τ. The control can be written as (Levant, 1993)

$u = -\lambda|\sigma|^{\rho} sign\sigma + u_1$

$\dot{u}_1 = -\alpha\, sign\sigma$

If the controller gains satisfy the conditions $\lambda, \alpha, \sigma_0 > 0$ and $0 < \rho \leq 0.5$ then sliding variable converges to zero manifolds in finite time. The algorithm can also be written as

$$\boldsymbol{u = -\lambda|\sigma|^{\rho} sign\sigma - \alpha \int sign(\sigma)\, dt} \quad (2.4.2)$$

Here control is continuous, because the chattering effects are smoothed out due to the power of sliding variable and integral in the second terms of (2.4.2) respectively. The drift term of the compensated system can be cancelled out with the help of $\alpha \int sign(\sigma)dt$ after finite time. Graphically, the convergence of the algorithm can be shown in Figure 2.7.

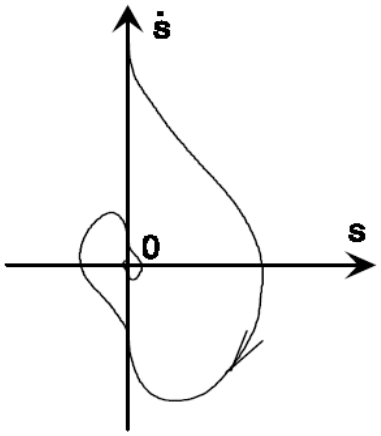

***Figure 2.7**: Super Twisting Algorithm convergence (Levant, 1993)*

The stability analysis of super twisting algorithm is discussed in Appendix B.

2.5 Smooth Sliding Mode Control

Higher order sliding mode provides reduction in chattering effects, but it is sensitive to unmodeled fast dynamics (Shtessel, Shkolnikov and Brown, 2003). The chattering can appear sooner or later in the systems using HOSM control. Some sensitive systems require completely chatter free control. In cascaded systems, a control in outer loop needs to be smooth where the profile generated by it must be followed by inner loop e.g. in missile and autopilot systems; guidance loop generated accelerations command must be followed by the inner loop to track line-of-sight. Following are the examples of some smooth sliding mode control.

The modified sliding mode control proposed by (Utkin, 95) is

$$u = -k|\sigma|^{1/2} sign(\sigma) \tag{2.5.1}$$

where $k > 0$ and σ is sliding surface, is smooth due to its time varying gain.

The Smooth Second Order Sliding Mode (SSOSM) control is recently proposed by (Shtessel, Shkolnikov and Levant, 2007),

$$u = -\lambda|\sigma|^{2/3} sign\sigma + u_1$$

$$\dot{u}_1 = -\alpha\,|\sigma|^{1/3} sign\sigma \tag{2.5.2}$$

where $\lambda, \alpha > 0$ and σ is sliding surface. The control is smooth due to variable gain in (2.5.2).

The gain in smooth control decreases as the trajectories approaches to sliding manifold and control effort remains smooth. The smooth control can achieve accuracy as well as performance only in the absence of uncertainties and disturbances.

The smooth controllers can provide desire objectives if the disturbance can be estimated with the help of disturbance observers (Radke and Gao, 2006) and canceled out within close-loop systems. The robust exact differentiator (Levant, 1998; Levant, 2003) can act as a disturbance observer as used by (Shtessel, Shkolnikov and Levant, 2007).

Robust exact differentiator proposed by Levant is discussed in the next Section. The concepts of the differentiator can help to understand robust state-disturbance observer, a contribution of the thesis.

2.6 Robust Exact Differentiator

A differentiation for a signal may be achieved through a simple first order closed loop integrator system. The achieved differentiation is not robust and the disturbances can degrade its performance. If we use sliding mode control in the feedback that is robust in nature, it gives chattering effects in the differentiation and requires a low pass filter to smoothen out the results at the cost of robustness. A robust and continuous controller in the feedback loop can solve the problem of robust exact differentiation. The super twisting algorithm is continuous as well as robust so that it is the best candidate for the differentiator loopback. The closed loop differentiator with super twisting algorithm can be illustrated with the help of Figure 2.8. Consider a signal $f(t)$, defined on $[0,\infty)$ is assumed to be unknown but differentiable with bounds $\left|\dot{f}(t)\right| < L$, where $L > 0$ is a 'Lipschitz constant'.

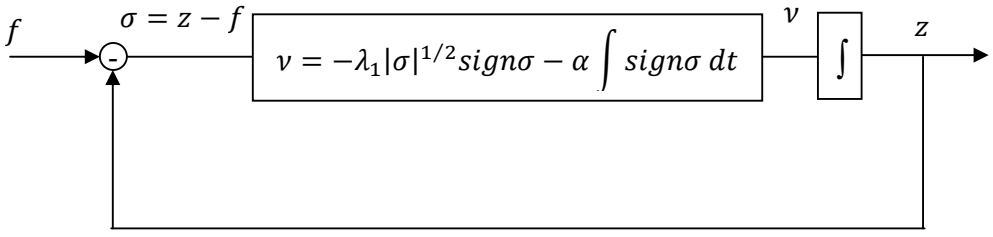

Figure 2.8: Basic Idea of Robust Exact Differentiator

Now the super twisting algorithm will drive the sliding surface and its first derivative towards zero manifolds in finite time i.e.

$$\sigma = \dot{\sigma} = 0$$

This fact ensures the availability of the first derivative of function f in finite time i.e.

$$z - f = \dot{z} - \dot{f} = 0$$

$$z = f \qquad \text{and} \qquad \dot{z} = v = \dot{f}$$

In the same way, exact higher derivatives of the function f can be estimated using higher order sliding mode in presence of bounded noise.

The structure of robust exact differentiator (Levant, 1998, 2003) can be given as:

$$\begin{aligned}
&\dot{z}_0 = v_0 \\
&v_0 = -\lambda_0 |z_0 - f(t)|^{n/(n+1)}\, sign\big(z_0 - f(t)\big) + z_1 \\
&\dot{z}_1 = v_1 \\
&v_1 = -\lambda_1 |z_1 - v_0|^{(n-1)/n}\, sign(z_1 - v_0) + z_2 \\
&\quad \vdots \\
&\dot{z}_{n-1} = v_{n-1} \\
&v_{n-1} = -\lambda_{n-1} |z_{n-1} - v_{n-2}|^{1/2} sign(z_{n-1} - v_{n-2}) + z_n \\
&\dot{z}_n = -\lambda_n sign(z_n - v_{n-1})
\end{aligned} \tag{2.6.1}$$

where $\lambda_i > 0$.

2.7 Summary

This chapter provides the basic foundation of the thesis. The main concepts of feedback linearization, sliding mode control, higher order sliding mode control are given. Moreover the idea of smooth second order sliding mode control and its prerequisite robust exact differentiator is given.

In the next chapter, robust smooth real twisting second order sliding mode along with robust disturbance observer is discussed and its simulations and experimental results are given.

Chapter 3

ROBUST SMOOTH REAL TWISTING SECOND ORDER SLIDING MODE

Many physical systems require robustness as well as performance in finite interval of time against unknown internal and external disturbances. These systems may also be sensitive to any chattering effect and require smooth control efforts, hence conventional sliding mode control cannot be a good option. Examples are multi-loop cascaded systems, in which the command generated by outer-loop is followed by inner-loop. A simple PID control cannot afford discontinuity in the outer-loop commands and may become unstable. The problem becomes severe when only outputs are available and mathematical model of the system is not exactly known.

Higher Order Sliding Modes (HOSM) (Emel'yanov, Korovin, and Levantovsky, 1996; Levant, 1993; Fridman and Levant, 1996; Bartolini, Ferrara and Usai, 1998) is an effective technique to remove chattering effects whilst preserving the important properties of traditional first order SMC. It also eliminates relative degree restrictions of the conventional SMC. But the main shortcoming of this method is its sensitivity to unmodeled fast dynamics (Shtessel, Shkolnikov and Brown, 2003).

Recently proposed Smooth Second Order Sliding Mode (SSOSM) controller (Shtessel, Shkolnikov and Levant, 2007) based on super twisting algorithm for relative degree one systems is a good choice to cope with the problem. In work (Shtessel, Shkolnikov and Levant, 2007) a modified robust exact differentiator (Levant, 1998 and 2003) is introduced in the closed loop to compensate internal dynamics and external disturbances or more generically “drift terms” of the system. In this way chattering free control is achieved *with robustness*. The problem with this approach is that the system should have relative degree one with respect to sliding manifold, whereas many mechanical systems have relative degree two for example robotic manipulators.

In this chapter, a smooth second order sliding mode controller is suggested for relative degree two systems. The robust disturbance observer is proposed to compensate for

the drift term. Stability analysis of the observer is given in detail. The finite time convergence of overall closed loop system is also proven. Furthermore simulation studies of the proposed technique on a DC motor are presented. In the last, experiments validate the theoretical contribution of the chapter.

3.1 Problem Statement

The chapter builds on the SSOMC framework for relative degree two systems with respect to the sliding manifold by using the "twisting" algorithm (Levant, 1993; Orlov, 2005). Whilst this control law is smooth, it may be sensitive to external and internal disturbances. To overcome this problem, a robust disturbance observer is employed in the closed loop system to compensate for the drift term precisely.

The proposed controller can provide robust performance even mathematical model of the system is not exactly known. Another advantage of the proposed technique is that it does not require aggressive control and employs the nominal control effort required to compensate the disturbances. Finite time convergence of the controller is established using Lyapunov method combined with homogeneity-based approach (Levant, 2008; Orlov, 2005). The stability of the closed loop system is proven using separation principle. The resulting overall system is finite time stable and robust against (sufficiently) smooth uncertain disturbances.

3.2 Smooth Real Twisting Control

Consider a SISO system, whose sliding variable dynamics with respect to the input are of relative degree two:

$$\ddot{\sigma} = f(\sigma, \dot{\sigma}, t) + u \tag{3.2.1}$$

In (3.2.1) the switching surface $\sigma \in \mathcal{R}$, and $f(\sigma, \dot{\sigma}, t)$ is a bounded and sufficiently smooth uncertain function. The control signal $u \in \mathcal{R}$ is required to provide smooth control action.

In this case only states of the system are available. The system dynamics are not completely known. A disturbance observer is required to estimate the drift term $f(\sigma, \dot{\sigma}, t)$. The control action u is then developed on the basis of the estimated information and under the assumption that $f(\sigma, \dot{\sigma}, t)$ is exactly canceled out by its estimate. The nominal system is then represented by a double integrator system:

$$\ddot{\sigma} = u$$

In the system above, let the variables $\sigma_0 = \sigma$ and $\sigma_1 = \dot{\sigma}$. The proposed smooth control law is given as

$$u = -k_1|\sigma_0|^{(p-2)/p} sign(\sigma_0) - k_2|\sigma_1|^{(p-2)/(p-1)} sign(\sigma_1) \tag{3.2.2}$$

where $k_1,\ k_2 > 0$ and $p \geq 2$ is employed. Then the closed loop system can be written in state space form as follows,

$$\dot{\sigma_0} = \sigma_1$$

$$\dot{\sigma_1} = -k_1|\sigma_0|^{(p-2)/p} sign(\sigma_0) - k_2|\sigma_1|^{(p-2)/(p-1)} sign(\sigma_1) \tag{3.2.3}$$

Theorem 3.1: *The system in (3.2.3) is globally uniformly finite time stable. Moreover the system generates a smooth second order sliding motion only at the origin.*

Proof: The only possible equilibrium point for system (3.2.3) is the origin, i.e. $\sigma_0 = \sigma_1 = 0$. Consider a candidate Lyapunov function

$$V(\sigma_0, \sigma_1) = \frac{p}{2(p-1)} k_1|\sigma_0|^{2(p-1)/p} + \frac{1}{2}\sigma_1^2$$

that is differentiable, radially unbounded and positive definite. Its derivative with respect to time is

$$\dot{V} = k_1|\sigma_0|^{(p-2)/p}\ \dot{\sigma_0} sign(\sigma_0) + \sigma_1\dot{\sigma_1}$$

It can be written as

$$\begin{aligned}\dot{V}\ = {} & k_1|\sigma_0|^{(p-2)/p}\sigma_1 sign(\sigma_0) - k_1|\sigma_0|^{(p-2)/p}\sigma_1 sign(\sigma_0) \\ & - k_2|\sigma_1|^{(p-2)/(p-1)}\sigma_1 sign(\sigma_1)\end{aligned}$$

and therefore

$$\dot{V}(t, \sigma) = -k_2|\sigma_1|^{(2p-3)/(p-1)} \tag{3.2.4}$$

Since $(0, 0)$ is the only possible equilibrium point for the system in (3.2.3), applying LaSalle's invariance principle (Slotine and Li, 1991) for smooth systems, the only possible trajectory of (3.2.3) on the invariant manifold $\dot{V} = 0$ is $\Sigma \equiv 0$, where $\Sigma = [\sigma_0 \quad \sigma_1]^T$. This shows that the system is globally uniformly asymptotically stable with respect to the origin.

Moreover, it can be easily verified that system (3.2.3) is homogeneous, and its homogeneity degree is equal to –1 by using the transformation

$(t, \Sigma) \mapsto (\kappa t, d_\kappa \Sigma) \qquad \forall \kappa > 0$

The dilation d_κ is defined as

$d_\kappa : (\sigma_0, \sigma_1) \mapsto (\kappa^p \sigma_0, \kappa^{p-1} \sigma_1)$

Then according to (Bhatt and Bernstein, 2000; Bacciotti and Rosier, 2001) the system (3.2.3) is globally uniformly finite time stable at the origin. This means that the trajectories of the system with *smooth control* belong to the surface $\sigma = \dot{\sigma} = 0$ after a finite time interval. This proves the theorem. ■

Remark 3.1: *The motion in the system (3.2.3) can be reasonably called a Second-Order Sliding Mode.*

Theorem 3.1 relates to the control of a double integrator system $\ddot{\sigma} = u$, whereas the real problem to be tackled is the control of system (3.2.1). This will be addressed in the next Section by the use of a robust disturbance observer to estimate drift terms of the system.

3.3 Robust Disturbance Observer

Since the proposed control law in (3.2.2) is smooth; the closed loop dynamics (3.2.1) can be sensitive to $f(\sigma_0, \sigma_1, t)$. The overall closed system therefore requires a good estimate of the drift term to compensate robustness. Assume that the outputs σ_0, σ_1 and input u are available and the control u is Lebesgue-measurable. The tion $f(\sigma_0, \sigma_1, t)$ is assumed to be unknown but $(n-1)$ times differentiable with bounds $\left| f^{(n-1)}(\sigma_0, \sigma_1, t) \right| < L$, where $L > 0$ is a 'Lipschitz constant'. Then the modified robust exact differentiator (Levant, 1998, 2003) can be introduced into the closed loop to estimate the drift term, and the drift term is used to design equivalent control for the system.

For notational convenience, define $\hat{f} \equiv \hat{f}_1$. The proposed observer structure can be written as follows

$\dot{\hat{\sigma}}_0 = \hat{\sigma}_1$

$\dot{\hat{\sigma}}_1 = \hat{f}_1 + u$

$$\hat{\dot{f}}_1 = -\lambda_n L^{1/n} |\hat{\sigma}_1 - \sigma_1|^{(n-1)/n} \, sign(\hat{\sigma}_1 - \sigma_1) + \hat{\sigma}_2$$
$$\dot{\hat{\sigma}}_2 = \hat{\dot{f}}_2$$

$$\hat{\dot{f}}_2 = -\lambda_n L^{1/(n-1)} \left|\hat{\sigma}_2 - \hat{\dot{f}}_1\right|^{n/(n-1)} sign\left(\hat{\sigma}_2 - \hat{\dot{f}}_1\right) + \hat{\sigma}_3$$

$$\vdots$$

$$\dot{\hat{\sigma}}_{n-1} = \hat{\dot{f}}_{n-1}$$

$$\hat{\dot{f}}_{n-1} = -\lambda_2 L^{1/2} \left|\sigma_{n-1} - \hat{\dot{f}}_{n-2}\right|^{1/2} sign\left(\sigma_{n-1} - \hat{\dot{f}}_{n-2}\right) + \hat{\sigma}_n$$

$$\dot{\hat{\sigma}}_n = -\lambda_1 L \, sign\left(\hat{\sigma}_n - \hat{\dot{f}}_{n-1}\right) \tag{3.3.1}$$

The parameters λ_i can be chosen recursively as suggested in (Levant, 2003). The observer (3.3.1) has a different structure to the one in (Shtessel, Shkolnikov and Levant, 2007) because a relative degree *2* system is considered in (3.2.1).

Theorem 3.2: *Suppose the parameters of the observer $\lambda_1, \dots, \lambda_{n+1}$ are properly chosen and the output of the system σ_0, σ_1 and the input signal u are bounded and Lebesgue-measurable. Then in the absence of noise the following equalities are established in finite time:* $\hat{\sigma}_0 = \sigma_0, \dots, \hat{\sigma}_{n-1} = \sigma_{n-1}$ and $\sigma_n = f^{(n-2)}(\sigma, \dot{\sigma}, t)$.

Proof: Define

$$\varphi_0 = \hat{\sigma}_0 - \sigma_0$$

$$\varphi_1 = \hat{\sigma}_1 - \sigma_1$$

$$\varphi_2 = \hat{\sigma}_2 - f(\sigma_0, \sigma_1, t)$$

$$\vdots$$

$$\varphi_n = \hat{\sigma}_n - f^{(n-2)}(\sigma, \dot{\sigma}, t) \tag{3.3.2}$$

From system (3.2.1) and the observer described in (3.3.1),

$$\hat{\sigma}_2 - \hat{\dot{f}}_1 = \hat{\sigma}_2 - \dot{\hat{\sigma}}_1 + u = \hat{\sigma}_2 - \dot{\varphi}_1 - \dot{\sigma}_1 + u$$
$$= \varphi_2 + f(\sigma, \dot{\sigma}, t) \; - \dot{\varphi}_1 - f(\sigma, \dot{\sigma}, t) - u + u = \varphi_2 - \dot{\varphi}_1$$

$$\vdots$$

$$\hat{\sigma}_n - \hat{\dot{f}}_{n-1} = \hat{\sigma}_n - \dot{\hat{\sigma}}_{n-1} = \hat{\sigma}_n - \dot{\varphi}_{n-1} - f^{(n-2)}(\sigma, \dot{\sigma}, t)$$
$$= \varphi_n - \dot{\varphi}_{n-1}$$

By using these definitions, the observer in (3.3.1) can be written as

$$\dot{\varphi}_1 = v_1$$

$$v_1 = -\lambda_{n+1} L^{1/(n+1)} |\varphi_1|^{n/(n+1)}\, sign(\varphi_1) + \varphi_2$$

$$\vdots$$

$$\dot{\varphi}_{n-1} = v_{n-1}$$

$$v_{n-1} = -\lambda_2 L^{1/2} |\varphi_{n-1} - v_{n-2}|^{1/2}\, sign(\varphi_{n-1} - v_{n-2}) + \varphi_n$$

$$\dot{\varphi}_n \in -\lambda_1 L\, sign(\varphi_n - v_{n-1}) + [-L, +L] \qquad (3.3.3)$$

The structure in (3.3.3) above is similar to the robust exact differentiator (Levant 1998; Levant 2003). The resulting differential inclusion can be understood in the Flippov sense (Flippov, 1988). It is easy to see that the differential inclusion in (3.3.3) is invariant with respect to the dilation

$$t \mapsto \kappa t \text{ and } \varphi_i \mapsto \kappa^{n-i+1} \varphi_i \qquad \forall \kappa > 0,\ i = 1, \dots, n$$

and therefore the system is homogenous: furthermore its homogeneity degree is equal to –1. Therefore $\varphi_i \to 0$ in finite time and the following exact equalities are obtained (in finite time):

$$\varphi_0 = \hat{\sigma}_0 - \sigma_0 = 0 \implies \hat{\sigma}_0 = \sigma_0$$

$$\varphi_1 = \hat{\sigma}_1 - \sigma_1 = 0 \Longrightarrow \hat{\sigma}_1 = \sigma_1$$

$$\varphi_2 - \dot{\varphi}_1 = 0 \Longrightarrow \hat{\sigma}_2 - f(\sigma_0, \sigma_1, t) - \dot{\hat{\sigma}}_1 + \dot{\sigma}_1 = 0$$

$$\Longrightarrow \hat{\sigma}_2 - f(\sigma_0, \sigma_1, t) = 0 \Longrightarrow \hat{\sigma}_2 = f(\sigma_0, \sigma_1, t)$$

$$\varphi_2 - \hat{f} = 0 \implies \hat{f} = f(\sigma_0, \sigma_1, t)$$

$$\vdots$$

$$\varphi_n - \dot{\varphi}_{n-1} = 0 \Longrightarrow \hat{\sigma}_n = f^{(n-2)}(\sigma_0, \sigma_1, t)$$

This proves the theorem. ■

Theorem 3.2 assumes the inputs and outputs of the system in (3.2.1) are noise free. The next theorem explores the impact of noise on input and output.

Theorem 3.3**:** *Suppose the input signal u is bounded and Lebesgue-measurable and the output noise are bounded then, the following inequalities can be established in finite time for some positive constants* μ_i.

$$|\hat{\sigma}_0 - \sigma_0| \leq \mu_0 \varepsilon$$

$$|\hat{\sigma}_1 - \sigma_1| \leq \mu_1 \varepsilon^{(n-1)/n}$$

$$\vdots$$

$$\left|\hat{\sigma}_n - f^{(n-2)}(\sigma_0, \sigma_1, t)\right| \leq \mu_n \varepsilon^{1/n} \qquad (3.3.4)$$

where the noise on input is $u \in \left[-k\varepsilon^{(n-1)/n}, k\varepsilon^{(n-1)/n}\right]$ and output is $\sigma \in [-\varepsilon, \varepsilon]$.

Proof: By using definitions (3.3.2), the observer (3.3.1) can be rewritten as (3.3.3). The structure in (3.3.3) is similar to the robust exact differentiator (Levant 1998; Levant 2003). If noise is present i.e. $\varepsilon \neq 0$, the output $\varphi \in [-\varepsilon, \varepsilon]$ and the input $u \in \left[-k\varepsilon^{(n-1)/n},\ k\varepsilon^{(n-1)/n}\right]$, then the bounds in (3.3.4) can be obtained using arguments similar to (Levant, 2003). The system (3.3.3) is homogenous and its homogeneity degree is equal to –1 with respect to transformation:

$$G_\kappa: (t, \varphi_i, \varepsilon) \mapsto \left(\kappa t,\ \kappa^{n-i+1}\varphi_i,\ \kappa^n \varepsilon\right) \qquad \forall \kappa > 0, i = 1, .., n$$

Again by using the definitions (3.3.2) and suppose that the noise $\varphi_0 = \mu_0 \varepsilon \sin\left((\mu_0/\varepsilon)^{1/n}\right)$. It is easy to prove the inequalities given in (3.3.4). This proves the theorem. ■

3.3.1 Control Law

For the system in (3.2.1) consider the control law

$$u = -\hat{f} - k_1 |\sigma_0|^{(p-2)/p} sign(\sigma_0) - k_2 |\hat{\sigma}_1|^{(p-2)/(p-1)} sign(\hat{\sigma}_1) \qquad (3.3.5)$$

with $p = n + 1, n \geq 2$ and where $\hat{f}$ will be obtained by using the robust disturbance observer (3.3.1). The closed loop system is given by

$$\dot{\sigma_0} = \sigma_1$$

$$\dot{\sigma_1} = f(\sigma_0, \sigma_1, t) - \hat{f} - k_1 |\sigma_0|^{(p-2)/p} sign(\sigma_0) - k_2 |\hat{\sigma}_1|^{(p-2)/(p-1)} sign(\hat{\sigma}_1)$$

The idea is that in finite time, the term $\hat{f}$ can cancel the drift signal $f(\sigma_0, \sigma_1, t)$, and the dynamics above will become (3.2.3).

The result of this Section will now be formally stated:

Theorem 3.4: *Suppose the drift term* $f(\sigma_0, \sigma_1, t)$ *in (3.2.1) is differentiable and* $\left| f^{(n-1)}(\sigma_0, \sigma_1, t) \right| < L$*, where L is the 'Lipschitz constant'. Then the closed loop system arising from (3.2.1), (3.3.1) and control law (3.3.5), is finite time stable.*

Proof: The proof of this theorem is a consequence of Theorems 3.1 – 3.3, by introducing the following definitions (3.3.2). As shown in Theorem 3.2, the system (3.3.1) can easily be transformed into (3.3.3) by using above definitions. The resulting system is homogenous and its homogeneity degree is equal to –1 by using the dilation:

$t \mapsto \kappa t$ and $\varphi_i \mapsto \kappa^{n-i+1}\varphi_i \qquad \forall \kappa > 0, i = 1, .., n$

Consider the σ-dynamics in (3.2.1) with control law (3.3.5) and the observer in (3.3.1). When exact measurements of $\hat{f}$ is available, the term $\hat{f}$ can be cancelled by $f(\sigma_0, \sigma_1, t)$ in finite time. Subsequently the dynamics (3.2.3) can be established. Following Theorem 3.1 and the separation principle, the overall closed loop system is finite time stable. This proves the theorem. ■

In the next Section, simulations of the proposed control law on a mathematical model of a DC motor are given.

3.4 Simulation Example

In this Section, the control technique is demonstrated on a benchmark DC motor (Utkin *et al*, 1999) with the following dynamics

$$L_0 \frac{di}{dt} = u - Ri - k_e\omega$$

$$J\frac{d\omega}{dt} = k_t i - \tau_l \qquad (3.4.1)$$

In system (3.4.1), u is the input terminal voltage, ω and i are the states of the system and represent shaft speed and armature current respectively. The motor load torque is defined as $\tau_l = B\omega$. All the parameters of the DC motor and their nominal values are listed in Table 3.1.

Let ω_r be the reference shaft speed, and $e = \omega_r - \omega$ be the tracking error. Define $x_1 = e$ and $x_2 = \dot{e}$, then the error dynamical system using equation (3.4.1) can be represented as:

$\dot{x}_1 = x_2$`

$\dot{x}_2 = f(x_1, x_2, t) + bu$ (3.4.2)

where the function $f(x_1, x_2, t)$ is

$f(x_1, x_2, t) = -a_1 x_1 - a_2 x_2 + \ddot{\omega}_r + a_2 \dot{\omega}_r + a_1 \omega_r + \frac{R}{JL_0}\tau_l + \frac{1}{J}\dot{\tau}_l$ (3.4.3)

Name	***Symbol***	***Values/Units***
Inertia of the Motor Rotor and Load	*J*	*0.001 Kg. m^2*
Armature Resistance	*R*	*0.5 Ω*
Armature Inductance	L_0	*1.0 mH*
Back-EMF Constant	K_e	*0.001 V/rad*
Torque Constant	K_t	*0.008 Nm/A*
Coefficient of Viscous Friction	*B*	*0.01 Nm s /rad*

Table 3.1*: The DC Motor Parameters*

Now the drift term depends upon the reference speed and load torque. The constants are defined as $a_1 = K_t K_e/(JL_0)$, $a_2 = R/L_0$, $b = -K_t/(JL_0)$. To ensure the existence of an inequality of the form $|\dot{f}(x_1, x_2, t)| < L$, where L is the 'Lipschitz constant', a second order low-pass pre-filter for reference signal is introduced.

A second order sliding surface $x_1 = x_2 = 0$ is chosen for the DC motor. Only the states of the system are available. Assume that $f(x_1, x_2, t)$ is unknown and also has to estimate. The robust disturbance observer in (3.3.1) is used to estimate the drift nal $\hat{f}$,

$\dot{\hat{x}}_1 = \hat{x}_2$

$\dot{\hat{x}}_2 = \hat{f} + bu$

$\hat{f} = -\lambda_2 L^{1/2} |\hat{x}_2 - x_2|^{1/2} \, sign(\hat{x}_2 - x_2) + \hat{x}_3$

$\dot{\hat{x}}_3 = -\lambda_1 L \, sign(\hat{x}_3 - \hat{f})$ (3.4.4)

The smooth second order sliding mode control law described earlier is used with parameters $p = 3, m = 2, k_1 = 5$ and $k_2 = 6$ is given as

$u = \frac{1}{b}\left(-\hat{f} - k_1 |x_1|^{1/3} \, sign(x_1) - k_2 |\hat{x}_2|^{1/2} \, sign(\hat{x}_2)\right)$ (3.4.5)

where $\hat{f}$ is the estimate of the drift term (3.4.3). The observer parameters used in the simulations are $\lambda_1 = 3.3$, $\lambda_2 = 2.2$ and $\lambda_1 = 1.1$.

Figure 3.1 shows the simulation results of the proposed smooth "twisting" controller for speed control of the DC motor. As illustrated, the speed signal efficiently follows the reference signal.

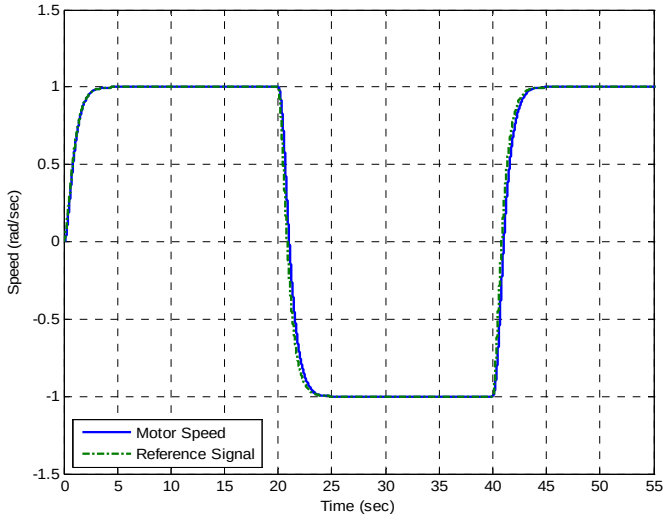

Figure 3.1: *The Speed Response of DC Motor*

Figure 3.2 shows the resultant acceleration of the motor.

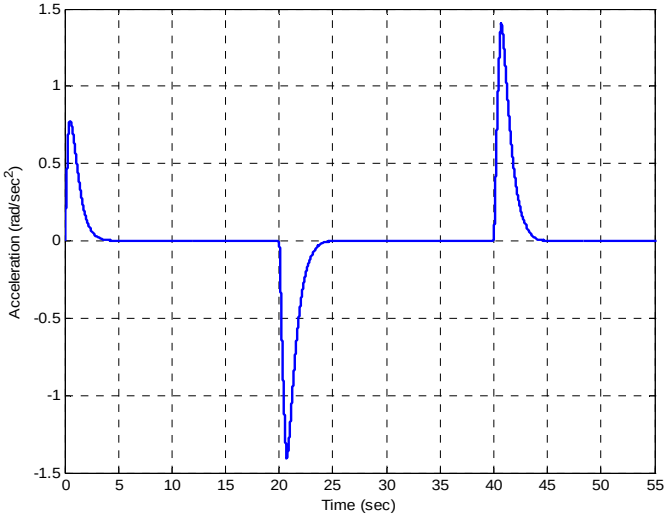

Figure 3.2*: The Acceleration Response of DC Motor*

Figure 3.3 demonstrates the tracking of the drift term by the proposed observer. As shown in the figure, the observer precisely tracks the drift signal exactly after a certain (finite) time.

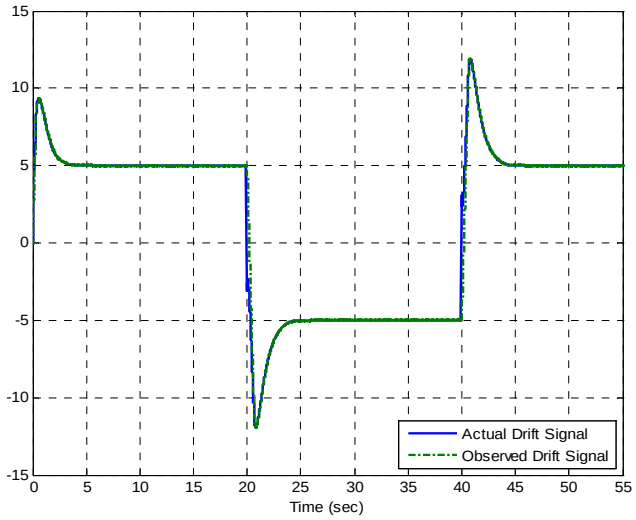

Figure 3.3: *The Actual and Observed Drift Terms*

Figure 3.4 shows the motor current. Note that the current is not explicitly controlled; its behavior is a result of acceleration control. The current is determined through the second term of (3.4.1) whilst assuming that the load torque is available, i.e.

$$i = \frac{J}{k_t}\dot{\omega} + \frac{1}{k_t}\tau_l$$

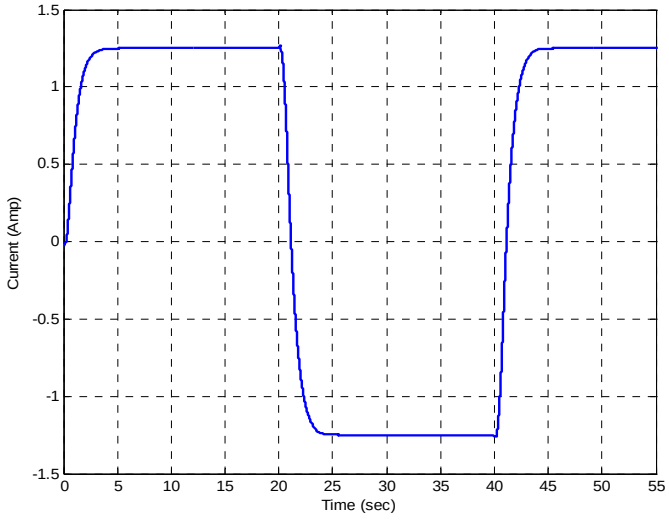

Figure 3.4*: The Current Response of the Speed Controller for DC Motor*

As depicted in Figure 3.4 the results are very good compared to a more conventional SMC design (see for example Utkin, 1999; Figure 10.5 pp 177).

Figure 3.5 shows the control effort generated by the smooth real twisting controller.

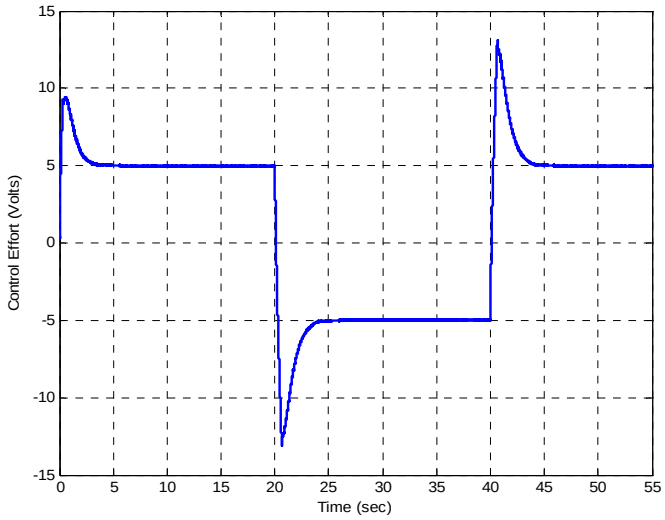

***Figure 3.5**: The Controller Effort of DC Motor for Step Reference*

The validity of the proposed controller is discussed below when the motor output is required to track a continuous sinusoidal waveform as the reference speed.

Figure 3.6 shows sinusoidal speed control of the DC motor with the smooth controller. The plots show that the signal is tracked precisely.

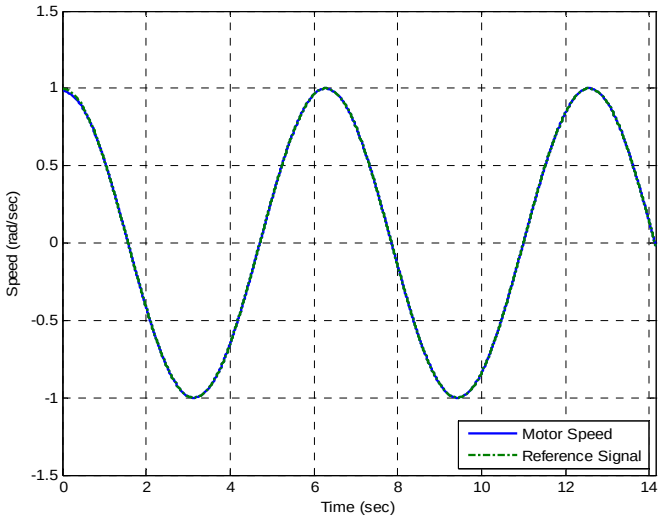

***Figure 3.6:** The Sinusoidal Speed Reference Response*

Figure 3.7 depicts the results from the proposed observer. The drift signal is followed in less than one second and well tracked thereafter.

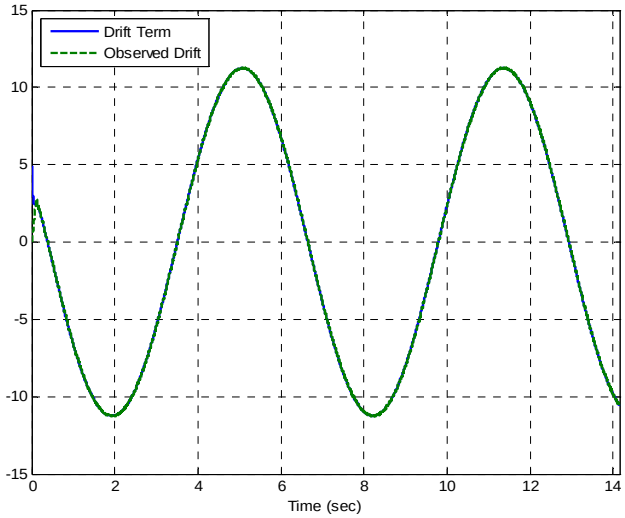

***Figure 3.7**: The Actual and Observed Drift Term*

Figure 3.8 shows the current waveform generated by the DC motor for sinusoidal reference signal.

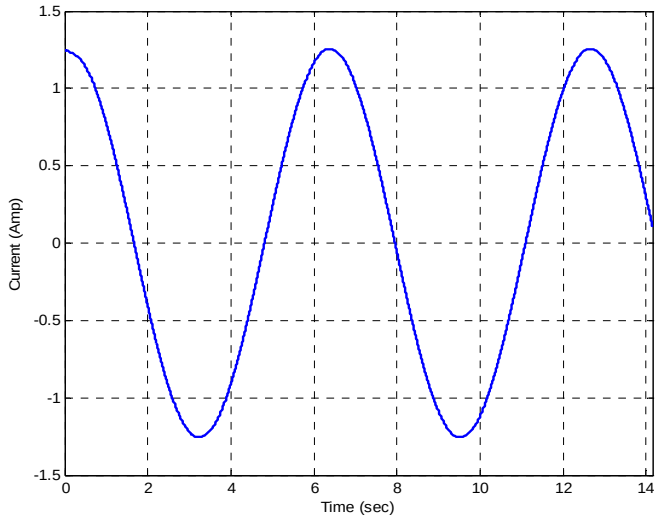

***Figure 3.8:** The Current Response for the Sinusoidal Speed Reference*

Figure 3.9 shows the control effort generated by the controller to track the reference sinusoidal speed.

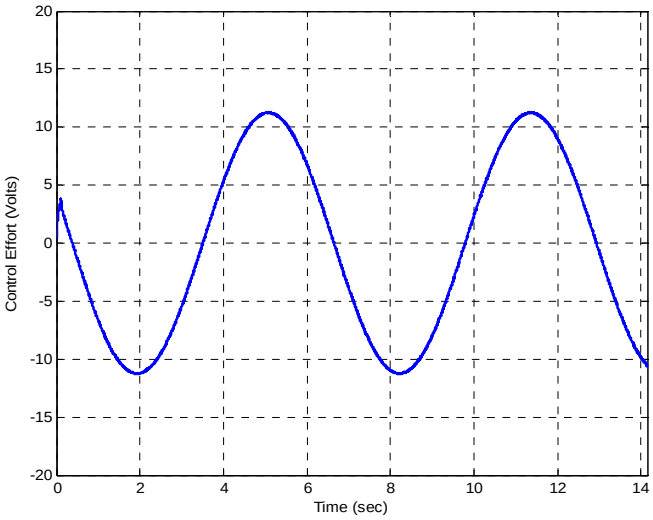

***Figure 3.9**: The Controller Effort of DC Motor for Sinusoidal Speed Reference*

To verify the robustness of the proposed controller, certain parameters of the DC motor have been varied with time – specifically the viscous friction coefficient and the armature resistance are increased by 100% (unknown to the controller) during the simulation. These changes do not affect the performance of the controller significantly. Figure 3.10 demonstrates the speed response of the DC motor with purturbations in the parmeters. The two subplots at the bottom of the figure show the variation in the friction and resistance respectively.

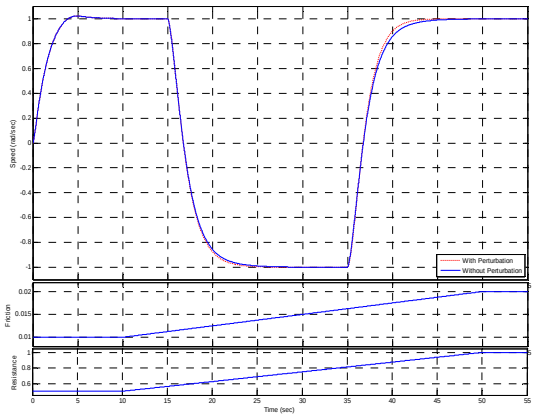

***Figure 3.10**: The Speed Response of DC Motor with Parameters Perturbation*

3.5 Experimental Results

For stringent performance and robustness analysis of the proposed controller an academic benchmark DC-motor (MS150) manufactured by Feedback Instrumentation has been used at Control Teaching Lab, Department of Engineering, University of Leicester. Figure 3.11 shows the experimental setup.

***Figure 3.11**: The DC Motor and dSPACE Setup*

The input of the motor is voltage (in Volts) and the angular speed output (in radians per second) can be measured through a taco-generator. An aluminum disk is mounted on the motor shaft to increase the inertia of the motor. The disk rotates between the two poles of a magnet, to reproduce the effect of frictional load. The key parameters of the DC-servomotor are given in Table 3.2 as listed by the manufacturer.

Name	***Symbol***	***Values/Units***
Inertia of the Motor Rotor and Load	J	$4.42x\ 10^{-4} Kg.\ m^2$
Armature Resistance	R	$3.2\ \Omega$
Armature Inductance	L_0	$8.6\ x\ 10^{-3}\ H$
Back-EMF Constant	K_e	$60\ x\ 10^{-3}\ V/rad$
Torque Constant	K_t	$17\ x\ 10^{-3}\ Nm/A$

***Table 3.2**: The MS-150 DC Motor Parameters*

A dSPACE® card (DS1102) was chosen as the interface for real time implementation of the controller from the Matlab/Simulink® environment. The card provides four channels of 16-bit A/D conversion and two channels of 16-bit D/A data conversion. The setup uses a TMS320C31 floating-point DSP processor with 128 K x 32-bit RAM.

For the experiment, the observer structure from (3.4.4) and the control law from (3.4.5) have been used. The values of b_0, λ_1, λ_2 and λ_3 need to be tuned. The initial guesses for the observer and controller gains were obtained through simulations.

Figure 3.12 shows the experimental results of the proposed control scheme for a square reference signal. The two plots in the figure show the speed response of the DC motor and its corresponding control effort. As illustrated below, the measured speed tracks the reference precisely.

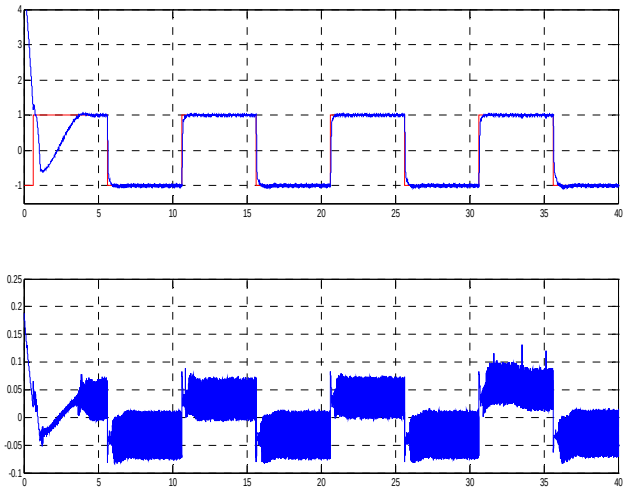

***Figure 3.12**: The Experimental Result of Square Wave Signal for DC Motor.*

The Figure 3.12 shows that chattering effects in the control effort, but its amplitude is very small i.e. 0.05 Volts.

The performance of the proposed controller has also been examined with respect to a continuous sinusoidal waveform as a reference speed. The speed response of the DC motor with the sine wave reference signal is shown in Figure 3.13. The plots demonstrate that the trajectory is followed accurately with low control effort.

To verify the robustness of the proposed controller, the friction load, with the help of a magnetic brake, has been increased by 300% during the experiment. Figure 3.14 demonstrates the speed response of the DC motor subject to this perturbation. In the experiment the brake has been applied at 13 seconds and released after 33 seconds. The graph shows that these changes do not affect the performance of the controller significantly.

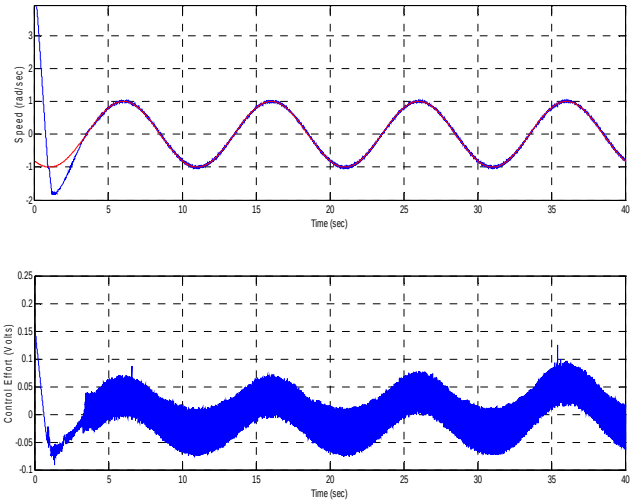

***Figure 3.13**: The Experimental Result of Sine Wave Signal for DC Motor.*

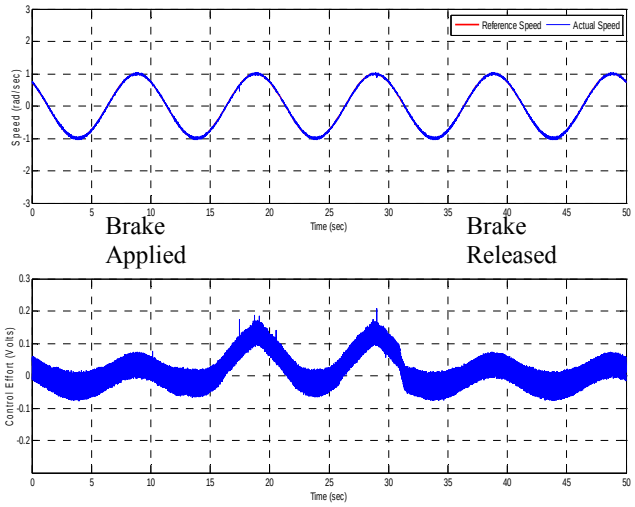

***Figure 3.14**: The Speed Response with Perturbation in Friction Load*

The experimental results associated with the proposed scheme offers an opportunity for achieving desired and robust performance without detailed knowledge of the plant system model.

3.6 Summary

In this chapter, a new smooth second order sliding mode control law for relative degree two systems using a modified real twisting algorithm is presented. A robust dis-

turbance observer is used to compensate for the drift term in the closed-loop dynamics. Finite time stability of the overall system is proven using a homogeneity-based approach.

In the next chapter, a new version of the disturbance observer is presented i.e. states as well as drift term is observed using modified robust state-disturbance differentiator. Moreover with the help of the observer, a control using feedback linearization technique is proposed.

Chapter 4

ROBUST FEEDBACK LINEARIZATION

It is a great challenge to achieve desired output performance from a nonlinear system in the presence of significant uncertainties. The problem becomes more difficult when only output information is available and the system model is not exactly known. Usually observers e.g. Kalman filters (Kalman, 1960), Luenberger observers (Luenberger, 1964), sliding mode observers (Edwards and Spurgeon, 1998), high gain observers (Khalil, 2002) and second order sliding mode observers (Davila *et al*, 2005) are used to reconstruct the state information on the basis of a nominal model of the system. The estimated state information is then used in robust or adaptive control schemes to achieve the desired results.

A different approach to address the same problem is to estimate the disturbance or drift terms which constitute the combined effects of model uncertainties, unknown parameters, the influence of internal dynamics, etc; and cancel them via feedback action (Radke and Gao, 2006). For this approach the model is transformed into the Generalized Controllable Canonical Form (GCCF) (Isidori, 1995; Slotine and Li, 1991) and the state vector and drift terms are estimated via a High Gain Observer (HGO) (Khalil, 2002) or a "modified" robust exact differentiator (Levant, 1998 and Levant, 2003). On the basis of this information, a feedback linearization control (Isidori, 1995; Slotine and Li, 1991) is used to convert the system into an equivalent linear system. Examples based on HGO schemes can be seen in (Esfandiari and Khalil, 1992; Khalil, 1999; Freidovich and Khalil, 2006) and case studies with robust exact differentiator can be reviewed in (Massey and Shtessel, 2005; Hall and Shtessel, 2006; Besnard, Shtessel, and Landrum, 2007; Shtessel, Shkolnikov and Levant, 2007; Iqbal, Edwards and Bhatti, 2010; Iqbal, Edwards and Bhatti, 2011).

In this decade, robust feedback linearization has been successfully demonstrated by various authors. In (Esfandiari and Khalil, 1992; Khalil, 1999), an output feedback controller for nonlinear systems using a HGO is proposed which robustly estimates an appropriate number of derivatives of the output together with the drift terms. An out-

put feedback controller for nonlinear systems has been proposed in (Bartolini *et al*, 2002) that estimates the derivatives of the outputs with the help of the robust exact differentiator (Levant, 1998). These derivatives are then used to create a sliding surface for a second order sliding mode controller. Feedback linearization based on a nominal model recently presented by (Freidovich and Khalil, 2006). In the design of (Freidovich and Khalil, 2006) the extended HGO is used to estimate the unmeasured derivatives of the output "plus" one. This extra derivative facilitates estimation of the uncertainties in the system. In (Benallegue, Mokhtari and Fridman, 2008), robust feedback linearization was also undertaken by using a higher order sliding mode observer (Davila, Fridman and Levant, 2005). However in the work of (Benallegue, Mokhtari and Fridman, 2008) the states and external disturbance effects were estimated based on nominal model of the plant.

In this chapter first of all, the problem is formulated for the proposed robust feedback linearization. Secondly the structure of the robust state-disturbance observer and its finite time stability is proven. After that, a case study involving DC motor to validate the proposed technique through simulation is considered. In the last, implementation of the idea on a DC motor rig is discussed.

4.1 Problem Statement

In this chapter the authors proposed a technique for feedback linearization of nonlinear systems with internal ("unobserved") dynamics on the basis of modified robust exact differentiator (Levant 1998; Levant 2003). This observer can estimates the states as well as the drift terms based only on the available input and output of the system, and without detail knowledge of the mathematics of the system. The methodology is similar to the work of (Freidovich and Khalil, 2006) however in our case, a HOSM observer rather than a HGO is employed to estimate the required derivatives and uncertainties.

The idea here is first transform the error dynamics of the system into GCCF, and then use modified robust exact differentiator to estimate the states as well as the combined effect of the drift terms. The controller then nullifies the effects of the drift terms, and imposes specific linear closed loop dynamics. The states and the drift term estimates are all obtained in finite time using the observer. Consequently, a type of separation

principle holds and the controller and observer can be designed independently. One key benefit of this scheme over robust control (sliding mode or higher order sliding mode) approaches is that it does not require conservative upper bounds on the nonlinear terms and does not result in aggressive control action. The overall closed loop structure arising from using the proposed technique can be depicted as shown in Figure 4.1.

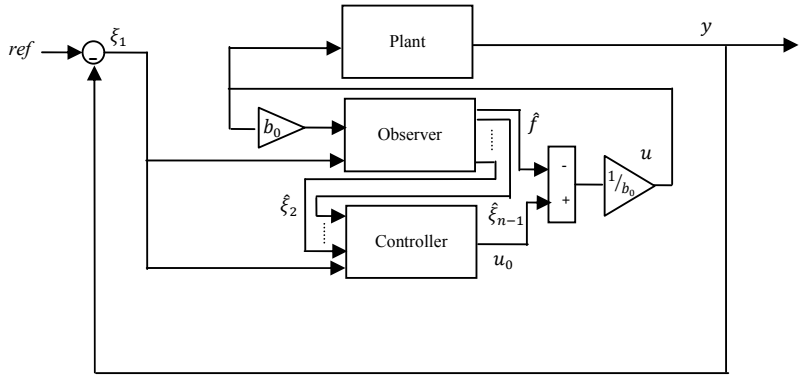

Figure 4.1: *The Proposed Controller-Observer Structure*

4.2 Robust Feedback Linearization

Consider a Single Input Single Output (SISO) dynamical system with well defined relative degree $r \leq n$ which can be written in Generalized Controllable Canonical Form (GCCF) (Isidori, 1995; Slotine and Li, 1991) as follow

$$\begin{aligned}
\dot{\xi}_1 &= \xi_2 \\
\dot{\xi}_2 &= \xi_3 \\
&\vdots \\
\dot{\xi}_r &= f(t,\xi,z) + g(t,\xi)u \\
\dot{z} &= \psi(t,\xi,z) \\
y &= \xi_1
\end{aligned} \tag{4.2.1}$$

where $\xi \in \mathcal{R}^r$ is observable state vector, $z \in \mathcal{R}^{n-r}$ is the zero dynamics, $u \in \mathcal{R}$ is the control input and $f(.)$ and $g(.)$ are smooth vector fields.

Assumption 4.1*:* The zero-dynamics $\dot{z} = \psi(t,\xi,z)$ is input-to-state stable, so the system (4.2.1) is minimum phase (Isidori, 1995; Khalil, 2002).

The system in (4.2.1) can be written in the form

$$\dot{\xi} = A\xi + B[f(t,\xi,z) + g(t,\xi)u]$$
$$\dot{z} = \psi(t,\xi,z)$$
$$y = C\xi \tag{4.2.2}$$

where $A = \begin{bmatrix} 0 & 1 & 0 & \cdots & 0 \\ 0 & 0 & 1 & \cdots & 0 \\ 0 & 0 & 0 & \cdots & \vdots \\ \vdots & \vdots & \vdots & \ddots & 1 \\ 0 & 0 & 0 & 0 & 0 \end{bmatrix}$, $B = \begin{bmatrix} 0 \\ 0 \\ \vdots \\ 0 \\ 1 \end{bmatrix}$, $C = \begin{bmatrix} 1 \\ 0 \\ \vdots \\ 0 \\ 0 \end{bmatrix}^T$.

Suppose $\hat{\xi}$ is the estimate of the state vector $\xi(t)$ and $g\left(t,\hat{\xi}\right)$ is the input gain of the system, reconstructed using the observed states. Then system (4.2.2) can be written in the form

$$\dot{\xi} = A\xi + B\left[f(t,\xi,z,\Delta_u) + g\left(t,\hat{\xi}\right)u\right]$$
$$\dot{z} = \psi(t,\xi,z)$$
$$y = C\xi \tag{4.2.3}$$

where $\Delta_u = g(t,\xi) - g\left(t,\hat{\xi}\right)$ is uncertainty in the input channel.

If all the states (including zero dynamics) are available and the function $f(.)$ is precisely known in (4.2.3) and $g\left(t,\hat{\xi}\right) \neq 0$, then a feedback linearization control law for the system is given by

$$u = \frac{1}{g\left(t,\hat{\xi}\right)}\left(-f(t,\xi,z,\Delta_u) - K\xi\right) \tag{4.2.4}$$

where $K^T \in \mathcal{R}^n$ is a design gain vector. Using this control law in (4.2.3) yields linear closed loop dynamics

$$\dot{\xi} = (A - BK)\xi \tag{4.2.5}$$

The gain matrix K can be designed using any modern or classical state-space technique e.g. pole placement, LQR or LMI methods etc, such that $A - BK$ is Hurwitz and the states ξ meet the desired performance objectives of the closed loop system.

However, in reality, in most engineering systems only the output of the system is available and the function $f(.)$ is unknown (or not known perfectly). As a result the ideal control law in (4.2.4) is not realizable. Instead the control law

$$u = \frac{1}{g(t,\hat{\xi})}\left(-\hat{f} - K\hat{\xi}\right) \tag{4.2.6}$$

is employed where $\hat{f}$ and $\hat{\xi}$ are estimates of $f(.)$ and $\xi(t)$ respectively. If the states and the drift term are correctly estimated so that $\hat{f} \to f(.)$ and $\hat{\xi} \to \xi(t)$ in finite time, the effect of control (4.2.4) can be achieved, and the desired performance indicated in (4.2.5) can be obtained in finite time.

Assumption 4.2*: it is assumed that $g(t,\xi)$ is bounded away from zero for all $\xi \in \mathcal{R}^r$.*

The following Section proposes an observer structure to generate the estimates $\hat{\xi}$ and $\hat{f}$ in (4.2.6) which converge to the true values in finite time.

4.3 Robust State-Disturbance Observer

Since only the output of the system (4.2.3) is available and the closed loop dynamics (4.2.5) is also sensitive to unknown drift term $f(.)$, so the control law (4.2.4) is not realistic. The overall closed system therefore requires a good estimate of the states and the drift signals to cancel out its effects.

Assume the control $u(t)$ is Lebesgue-measurable and the unknown drift tion $f(.)$ is $n-r$ times differentiable and satisfies $\left|f^{(n-r)}(.)\right| < L$, where $L > 0$ is the Lipshitz constant. Then the 'robust state-disturbance observer' can be introduced as a part of the closed loop to compensate undesired disturbances and estimate precisely the unmeasured but observable states in finite time. The approach of (Freidovich and Khalil, 2006) is similar in terms of methodology, but instead HGO is used to obtain the estimates.

For notational convenience define $\hat{f} \equiv \hat{f}_1$. The proposed observer structure can be written as follows

$$\dot{\hat{\xi}}_1 = v_1$$

$$v_1 = -\lambda_{n+1} L^{1/(n+1)} \left|\hat{\xi}_1 - \xi_1\right|^{n/(n+1)} sign\left(\hat{\xi}_1 - \xi_1\right) + \hat{\xi}_2$$

$$\dot{\hat{\xi}}_2 = v_2$$

$$v_2 = -\lambda_n L^{1/n} \left|\hat{\xi}_2 - v_1\right|^{(n-1)/n} sign\left(\hat{\xi}_2 - v_1\right) + \hat{\xi}_3$$

$$\vdots$$

$$\dot{\hat{\xi}}_r = \hat{f}_1 + g\left(t,\hat{\xi}\right)u,$$

$$\hat{f}_1 = -\lambda_{n-r+2} L^{1/(n-r+2)} \left|\hat{\xi}_r - v_{r-1}\right|^{(n-r+1)/(n-r+2)} sign\left(\hat{\xi}_r - v_{r-1}\right) + \hat{\xi}_{r+1}$$

$$\vdots$$

$$\dot{\hat{\xi}}_n = \hat{f}_{n-r+1}$$

$$\hat{f}_{n-r+1} = -\lambda_2 L^{1/2} \left|\hat{\xi}_n - \hat{f}_{n-r}\right|^{1/2} sign\left(\hat{\xi}_n - \hat{f}_{n-r}\right) + \hat{\xi}_{n+1}$$

$$\dot{\hat{\xi}}_{n+1} = -\lambda_1 L \, sign\left(\hat{\xi}_{n+1} - \hat{f}_{n-r+1}\right) \tag{4.3.1}$$

The parameters λ_i can be chosen recursively as suggested in (Levant, 2003). The observer (4.3.1) has a different structure to the one in (Shtessel, Shkolnikov and Levant, 2007; Iqbal, Edwards and Bhatti, 2010) because a relative degree $r \leq n$ system is considered in (4.2.3). Note that the estimates of the higher derivatives of the drift term have no direct relevance to the internal dynamics of the system.

Theorem 4.1: *Suppose the parameters of the observer* $\lambda_1,\ \lambda_2, \dots, \lambda_{n+1}$ *are properly chosen and the output of the system* $\xi_1(t)$ *and the input signal* $u(t)$ *are bounded and Lebesgue-measurable. Then in the absence of noise the following equalities are established in finite time :* $\hat{\xi}_i = \xi_i,\ \forall\, i = 1, \dots, r;\ \hat{\xi}_{r+1} = f(t, \xi, z, \Delta_u);\ \hat{\xi}_{j+1} = f^{j-r}(t, \xi, z, \Delta_u),\ \forall\, j = r+1, \dots, n.$

Proof: Define

$$\varphi_1 = \hat{\xi}_1 - \xi_1$$

$$\varphi_2 = \hat{\xi}_2 - \dot{\xi}_1$$

$$\vdots$$

$$\varphi_r = \hat{\xi}_r - \xi_1^{(r-1)}$$

$$\varphi_{r+1} = \hat{\xi}_{r+1} - f(t, \xi, z, \Delta_u)$$

$$\vdots$$

$$\varphi_n = \hat{\xi}_n - f^{(n-r-1)}(t, \xi, z, \Delta_u)$$

$$\varphi_{n+1} = \hat{\xi}_{n+1} - f^{(n-r)}(t, \xi, z, \Delta_u) \tag{4.3.2}$$

From system (4.2.1) and the observer described in (4.3.1),

$$\hat{\xi}_2 - v_1 = \hat{\xi}_2 - \dot{\hat{\xi}}_1 = \hat{\xi}_2 - \dot{\xi}_1 - \dot{\varphi}_1$$

$$= \varphi_2 - \dot{\varphi}_1$$

$$\vdots$$

$$\hat{\xi}_{r+1} - \hat{f}_1 = \hat{\xi}_{r+1} - \dot{\hat{\xi}}_r + g(.)u$$
$$= \hat{\xi}_{r+1} - \dot{\varphi}_r - \xi_1^{(r)} + g(.)u$$
$$= \hat{\xi}_{r+1} - \dot{\varphi}_r - f(.) - g(.)u + g(.)u$$
$$= \hat{\xi}_{r+1} - f(.) - \dot{\varphi}_r$$
$$= \varphi_{r+1} - \dot{\varphi}_r$$
$$\vdots$$
$$\hat{\xi}_{n+1} - \hat{f}_{n-r+1} = \hat{\xi}_{n+1} - \dot{\hat{\xi}}_n$$
$$= \hat{\xi}_{n+1} - \dot{\varphi}_n - f^{(n-r)}(.)$$
$$= \varphi_{n+1} - \dot{\varphi}_n$$

By using these definitions, the observer in (4.3.1) can be written as

$$\dot{\varphi}_1 = v_1$$
$$v_1 = -\lambda_{n+1} L^{1/(n+1)} |\varphi_1|^{n/(n+1)}\, sign(\varphi_1) + \varphi_2$$
$$\dot{\varphi}_2 = v_2$$
$$v_2 = -\lambda_2 L^{1/n} |\varphi_2 - v_1|^{(n-1)/n}\, sign(\varphi_2 - v_1) + \varphi_3$$
$$\vdots$$
$$\dot{\varphi}_n = v_n$$
$$v_n = -\lambda_2 L^{1/2} |\varphi_n - v_{n-1}|^{1/2}\, sign(\varphi_n - v_{n-1}) + \varphi_{n+1}$$
$$\dot{\varphi}_{n+1}\, \epsilon - \lambda_1 L\, sign(\varphi_{n+1} - v_n) + [-L, +L] \qquad (4.3.3)$$

The structure in (4.3.3) is similar to the exact differentiator from (Levant 1998; Levant 2003). The resulting differential inclusion can be understood in the Flippov sense (Flippov, 1988). It is easy to see that the differential inclusion in (4.3.3) is invariant with respect to the dilation

$t \mapsto \kappa t$ and $\varphi \mapsto \kappa^{n-i+1}\varphi_i \qquad \forall \kappa > 0,\ i = 0, \dots, n$

and therefore the system is homogenous: furthermore its homogeneity degree is equal to –1. Therefore in the absence of noise, the quantities $\varphi_i \to 0$ in finite time and the following exact equalities are obtained (in finite time):

$$\varphi_1 = \hat{\xi}_1 - \xi_1 = 0 \implies \hat{\xi}_1 = \xi_1$$
$$\varphi_2 - v_1 = \varphi_2 - \dot{\varphi}_1 = 0 \implies \hat{\xi}_2 - \dot{\xi}_1 - \dot{\hat{\xi}}_1 + \dot{\xi}_1 = 0$$

$$\Longrightarrow \hat{\dot{\xi}}_2 - \dot{\xi}_1 = 0$$
$$\Longrightarrow \hat{\dot{\xi}}_2 = \dot{\xi}_1 = \xi_2$$
$$\vdots$$
$$\varphi_r - v_{r-1} = \varphi_r - \dot{\varphi}_{r-1} = 0 \Longrightarrow \hat{\xi}_r = \xi_1^{(r-1)} = \xi_r$$
$$\varphi_{r+1} - v_r = \varphi_{r+1} - \dot{\varphi}_r = 0$$
$$\Longrightarrow \hat{\xi}_{r+1} - f(.) - \hat{\dot{\xi}}_r + \xi_1^{(r)}$$
$$\Longrightarrow \hat{\xi}_{r+1} - f(.)$$
$$\Longrightarrow \hat{\xi}_{r+1} = f(.)$$
$$\varphi_{r+2} - v_{r+1} = \varphi_{r+2} - \dot{\varphi}_{r+1} = 0$$
$$\Longrightarrow \hat{\xi}_{r+2} - \dot{f}(.) - \hat{\dot{\xi}}_{r+1} + \dot{f}(.) = 0$$
$$\Longrightarrow \hat{\xi}_{r+2} - \dot{f}(.) = 0$$
$$\Longrightarrow \hat{\xi}_{r+2} = \dot{f}(.)$$
$$\vdots$$
$$\varphi_n - v_{n-1} = \varphi_n - \dot{\varphi}_{n-1} = 0 \Longrightarrow \hat{\xi}_n = f^{(n-r-1)}(.)$$
$$\varphi_{n+1} - v_n = \varphi_{n+1} - \dot{\varphi}_n = 0 \Longrightarrow \hat{\xi}_{n+1} = f^{(n-r)}(.)$$

This proves the theorem. ■

Theorem 4.1 assumes the inputs and outputs of the system in (4.2.3) are noise free. The next theorem explores the impact of noise on the estimates ξ.

Theorem 4.2**:** *Suppose in presence of noise, the output noise is bounded, i.e.* $\xi_1 \in [-\varepsilon, \varepsilon]$ *and the input signal is also bounded and Lebesgue-measurable, i.e.* $u \in \left[-k\varepsilon^{(n-1)/n}, k\varepsilon^{(n-1)/n}\right]$. *Then the following inequalities can be established in finite time for some positive constants* μ_i *and* η_i.

$$\left|\hat{\xi}_1 - \xi_1\right| \leq \mu_1 \varepsilon$$
$$\left|\hat{\xi}_2 - \dot{\xi}_1\right| \leq \mu_2 \varepsilon^{(n-1)/n}$$
$$\vdots$$
$$\left|\hat{\xi}_r - \xi_1^{(r-1)}\right| \leq \mu_r \varepsilon^{(n-r-1)/n}$$
$$\left|\hat{\xi}_{r+1} - f(.)\right| \leq \mu_{r+1} \varepsilon^{(n-r-2)/n}$$
$$\vdots$$
$$\left|\hat{\xi}_i - f^{i-r-1}(.)\right| \leq \mu_i \varepsilon^{(n-i-1)/n}, \quad \forall\, i = r+1, \ldots, n \qquad (4.3.4)$$

Proof: By using definitions (4.3.2), the observer in (4.3.1) can be rewritten as (4.3.3). The structure in (4.3.3) is similar to the robust exact differentiator (Levant 1998; Levant 2003). The system in (4.3.3) is homogenous and its homogeneity degree is equal to –1 with respect to the transformation:

$$G_\kappa: (t, \varphi, \varepsilon) \mapsto \left(\kappa t,\ \kappa^{n-i+1}\varphi_i,\ \kappa^{n+1}\varepsilon\right) \qquad \forall \kappa > 0, i = 0, .., n$$

Furthermore, assuming that the noise can be represent by $\varphi_1 = \mu_1 \varepsilon \sin\left((\mu_1/\varepsilon)^{1/n}\right)$, it is easy to prove the inequalities given in (4.3.4). This proves the theorem. ■

Theorem 4.1 and 4.2 demonstrate the finite time convergence of the observer given in (4.3.1). In the next theorem, the stability analysis for the complete closed-loop system is given.

Theorem 4.3: *Assume that the zero dynamics of the system are stable, the drift term* $f(t, \xi, z, \Delta_u)$ *in (4.2.3) is a smooth vector field on* $\mathcal{R}^n$*, and moreover,* $\hat{\xi}_n$ *and* $\hat{f}$ *are exactly estimated. Then the closed loop system (4.2.3) with control law in (4.2.6) and the observer in (4.3.1) is stable.*

Proof: When exact measurements of $\hat{\xi}_n$ and $\hat{f}$ are available from the observer (4.3.1), the term $\hat{f}$ can cancel the drift term $f(t, \xi, z, \Delta_u)$ and the dynamics in (4.2.5) could be established in finite time. Designing *K* by using any modern or classical state-space methods ensures that $A - BK$ is Hurwitz and the closed loop system associated with (4.2.3) is stable.

As shown in Theorem 4.1, the observer in (4.3.1) can easily be transformed into structure (4.3.3) by using the definitions (4.3.2). The resulting system is homogenous and its homogeneity degree is equal to –1 by using following dilation:

$$t \mapsto \kappa t \text{ and } \varphi_i \mapsto \kappa^{n-i+1}\varphi_i \qquad \forall \kappa > 0, i = 1, .., n+1$$

Here the zero dynamics of the system are assumed to be stable, the observer in (4.3.1) is finite time stable and the control law (4.2.6) is bounded and convergent. Utilizing the separation principle, the overall closed loop system is stable. This proves the theorem.

■

4.4 Simulation Studies

The results are verified through simulations using the proposed control law on mathematical models of DC motor. Two cases are considered here, one is for relative degree *'r'* being equal to system order *'n'* and in the second case, relative degree is taken to be less than order of system.

4.4.1 Relative degree $r = n$

For relative degree equal to system order, the proposed control scheme is demonstrated on the same DC motor that used in previous chapter. Details of dynamical model and DC motor parameters are given in Section 3.4 of chapter 3.

A pole placement technique is chosen for the choice of the feedback gain *K*. For these simulations, two poles are placed at -3 and -3. The controller parameters to achieve this are $k_1 = 9$ and $k_2 = 6$. Thus the proposed controller is given by

$$u = \frac{1}{b_0}\left(-\hat{f} - k_1 x_1 - k_2 \hat{x}_2\right) \tag{4.4.4}$$

where $\hat{f}$ is the estimate of the drift term (4.4.3) and $\hat{x}_2$ is the estimate of the state x_2.

The proposed observer structure for the system is as follows:

$$\dot{\hat{x}}_1 = v_1$$

$$v_1 = -\lambda_3 L^{1/3} |\hat{x}_1 - x_1|^{2/3}\, sign(\hat{x}_1 - x_1) + \hat{x}_2$$

$$\dot{\hat{x}}_2 = \hat{f} + b_0 u$$

$$\hat{f} = -\lambda_2\, L^{1/2} |\hat{x}_2 - v_1|^{1/2}\, sign(\hat{x}_2 - v_1) + \hat{x}_3$$

$$\dot{\hat{x}}_3 = -\lambda_1 L\, sign\left(\hat{x}_3 - \hat{f}\right) \tag{4.4.5}$$

where $\lambda_1 = 2.1,\ \lambda_2 = 4.2$ and $\lambda_3 = 8.4$.

Figure 4.2 shows the simulation results of the proposed speed controller for the DC motor. The first subplot demonstrates the speed response and the second subplot displays the control effort. As illustrated, the speed tracks the reference signal very effectively. Moreover, the control input does not exhibit any chattering effects.

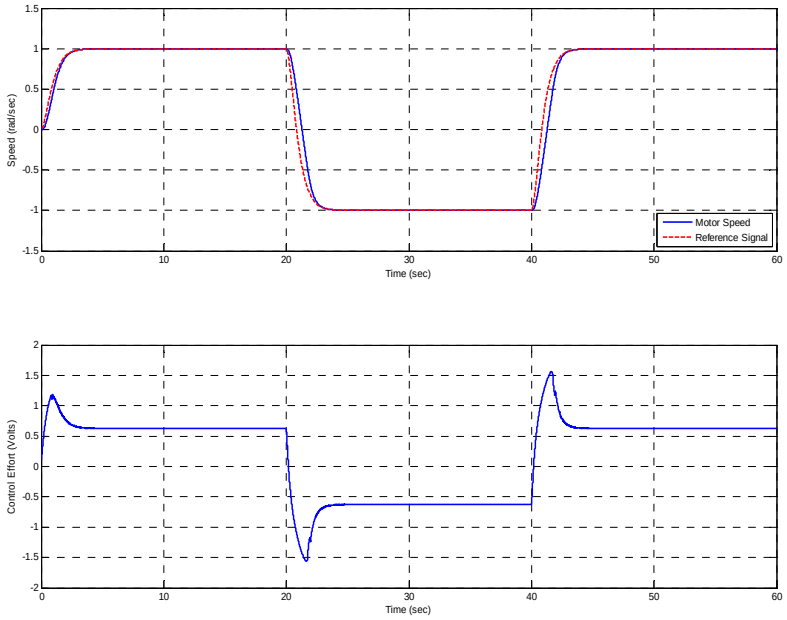

***Figure 4.2**: The Speed Response of DC Motor*

Figure 4.3 shows the tracking of the drift term by the proposed observer. As shown in the figure, the observer precisely tracks the drift signal after a certain (finite) time.

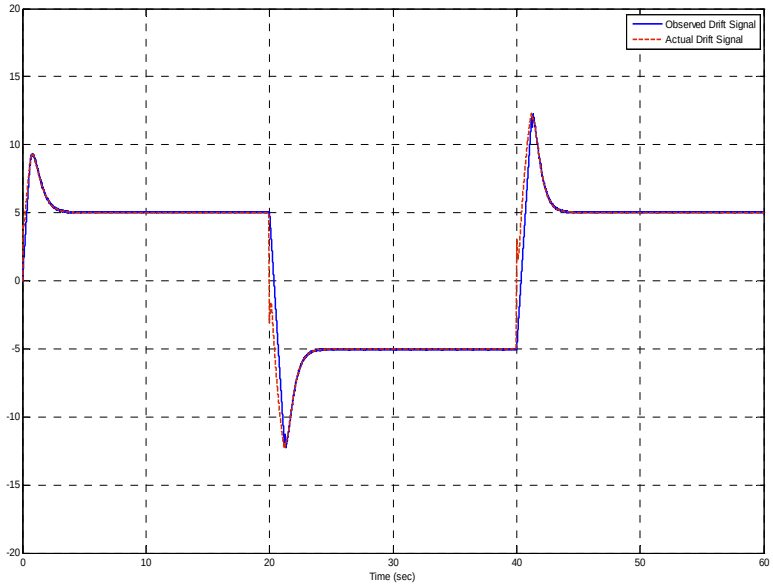

***Figure 4.3**: The Actual and Observed Drift Term*

Figure 4.4 shows a comparison between the actual and observed state. It is clear from the figure that the observed state follows the actual state component x_2 accurately.

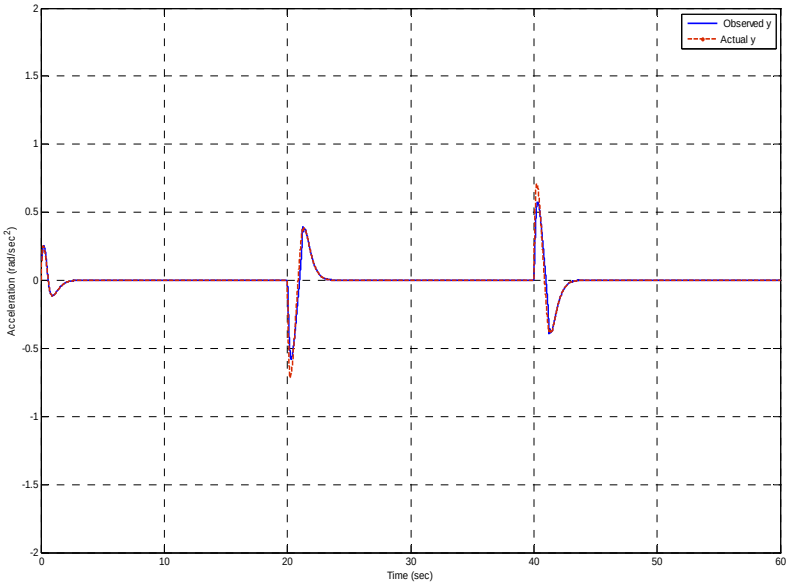

***Figure 4.4**: The Actual and Observed State* $\boldsymbol{x_2}$

4.4.2 Relative degree $r < n$

In this section, the proposed control scheme is demonstrated for a DC motor with a rigid arm (Freidovich and Khalil, 2006). The dynamics are given by

$$J\ddot{\theta} = k_c u - F \tag{4.4.6}$$

where in system (4.4.6), J represents the total moment of inertia of the rotor and the arm, k_c is the motor input constant, u is the applied terminal voltage and θ represents shaft position. The term F is the unknown frictional torque and can be represent by the dynamical LuGre model as given in (Canudas de Wit *et al*, 1995)

$$F = z + \sigma_1(\varepsilon_0 \dot{z}) + \sigma_2 \dot{\theta}$$

$$\varepsilon_0 \dot{z} = \dot{\theta} - \frac{|\dot{\theta}|}{s(\dot{\theta})} z \tag{4.4.7}$$

where ε_0 is the reciprocal of the average stiffness of the bristles, σ_1 is the damping coefficient of the bristles, $\sigma_2$is the viscous friction, and the Stribeck curve can be defined as,

$$s(\dot{\theta}) = \begin{cases} F_{c+} + (F_{s+} - F_{c+})e^{-(\dot{\theta}/v_s)^2} & \dot{\theta} > 0 \\ F_{c-} + (F_{s-} - F_{c-})e^{-(\dot{\theta}/v_s)^2} & \dot{\theta} < 0 \\ \left(s(0_+) + s(0_-)\right)/2 & \dot{\theta} = 0 \end{cases} \quad (4.4.8)$$

where v_s is the Stribeck velocity of the motor and $F_{c\pm}$ and $F_{s\pm}$ are the coulomb and static frictions respectively.

Let θ_r be the reference shaft position, and $\xi_1 = \theta_r - \theta$ be the tracking error, then $\dot{\xi}_1 = \xi_2 = \dot{\theta}_r - \dot{\theta}$ and $\dot{\xi}_2 = \ddot{\theta}_r - \ddot{\theta}$. It is easy to verify, as discussed in (Canudas de Wit *et al*, 1995), that the zero dynamics are input-to-state stable.

The system (4.4.6) can be represented as

$$\begin{aligned} \dot{\xi}_1 &= \xi_2 \\ \dot{\xi}_2 &= f(t, \xi, z, \Delta_u) + g\left(t, \hat{\xi}\right)u \\ \dot{z} &= \psi(t, \xi, z) \end{aligned} \quad (4.4.9)$$

where $f(.) = \ddot{\theta}_r - F + \Delta_u$, $g(.) = \frac{k_c}{J}, \psi(.) = \frac{1}{\varepsilon_0}\left(\dot{\theta} - \frac{|\dot{\theta}|}{s(\dot{\theta})}z\right)$ and Δ_u is the difference between the actual and nominal value of the input constant.

All the parameters of the DC motor and their nominal values are listed in Table 4.1.

Name	***Value***	***Name***	***Value***
J	*0.095 Kg. m²*	F_{c+}	*0.023.* k_c *N*
k_c	*2.5*	F_{c-}	*0.021.* k_c *N*
σ_1	*1.5 Ns/m*	F_{s+}	*0.058.* k_c *N*
σ_2	*0.004 Ns/m*	F_{s-}	*0.052.* k_c *N*
ε_0	*0.01*	v_s	*0.01 m/s*

Table 4.1*: The DC Motor (with Rigid Arm) Parameters*

A pole placement technique has been chosen for synthesizing the choice of the feed-back gain *K*. For this simulation, two poles are placed at -1 and -1. The controller parameters to achieve this are $k_1 = 1$ and $k_2 = 2$. Thus the proposed controller is given as

$$u = \frac{1}{b_0}\left(-\hat{f}_1 - k_1\xi_1 - k_2\hat{\xi}_2\right) \quad (4.4.10)$$

where $\hat{f}_1$ is the estimate of the drift term $f(.)$ and $\hat{\xi}_2$ is the estimate of the state ξ_2. The proposed observer structure for the system is as follows:

$$\dot{\hat{\xi}}_1 = v_1$$
$$v_1 = -\lambda_3 L^{1/3} \left|\hat{\xi}_1 - \xi_1\right|^{2/3} sign\left(\hat{\xi}_1 - \xi_1\right) + \hat{\xi}_2$$
$$\dot{\hat{\xi}}_2 = \hat{f}_1 + b_0 u$$
$$\hat{f}_1 = -\lambda_2 L^{1/2} \left|\hat{\xi}_2 - v_1\right|^{1/2} sign\left(\hat{\xi}_2 - v_1\right) + \hat{\xi}_3$$
$$\dot{\hat{\xi}}_3 = -\lambda_1 L\, sign\left(\hat{\xi}_3 - \hat{f}_1\right) \qquad (4.4.11)$$

where $\lambda_1 = 5,\ \lambda_2 = 10$ and $\lambda_3 = 5$.

Figure 4.5 shows the simulation results of the proposed controller with a sinusoidal reference signal. The first subplot demonstrates the speed response and the second subplot displays the control effort. As illustrated, the speed tracks the reference signal very effectively. Moreover the control force does not exhibit any chattering effects.

Figure 4.6 demonstrates the tracking of the drift term by the proposed observer. As shown in the figure, the observer accurately tracks the drift signal after a certain (finite) time.

Figure 4.7 shows a comparison between actual and observed state. It is obvious from the figure that the observed state follows the actual state component ξ_2 accurately.

The validity of the proposed controller for a square waveform as the reference speed for the DC motor is discussed in the following lines.

Figure 4.8 shows the simulation results of the proposed controller for speed control of the DC motor with a square wave reference signal. The first subplot shows the tracking of reference signal and second subplot demonstrates the controller effort. As illustrated, the speed follows the reference signal precisely.

Figure 4.9 exhibits the tracking of the drift term by the proposed observer. As shown in the figure, the observer precisely tracks the drift signal after a certain (finite) time.

Figure 4.10 shows the actual and observed state ξ_2 of the system. The graph reveals that the state is estimated exactly.

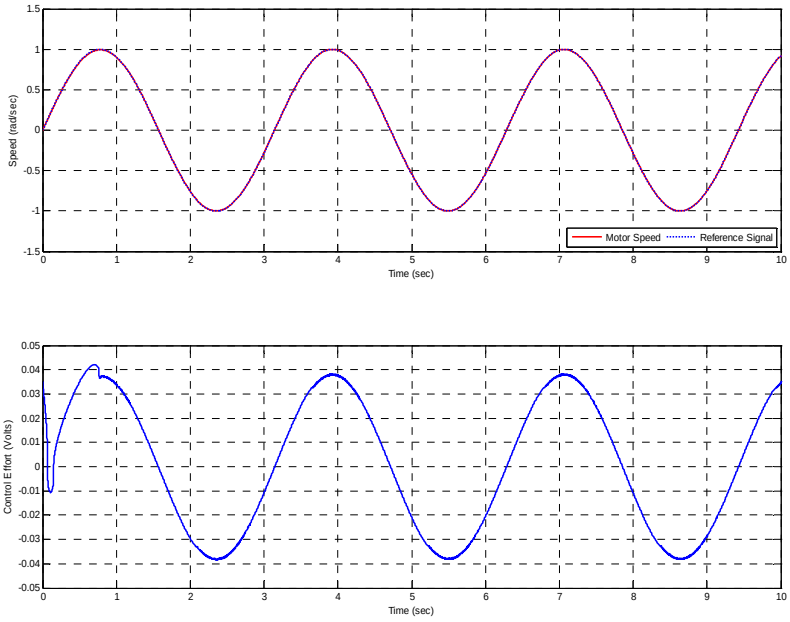

Figure 4.5: *The Speed Response and Control Effort of Sinusoidal Reference*

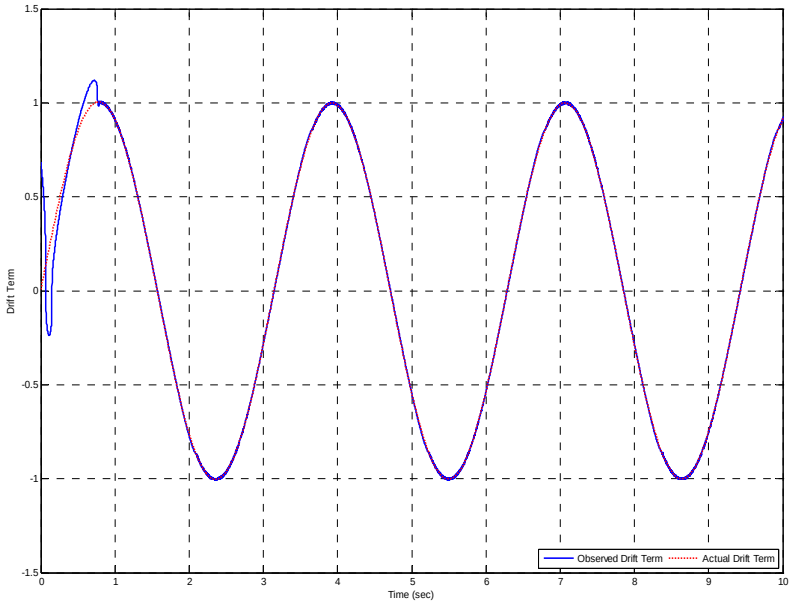

Figure 4.6: *The Actual and Observed Drift Term*

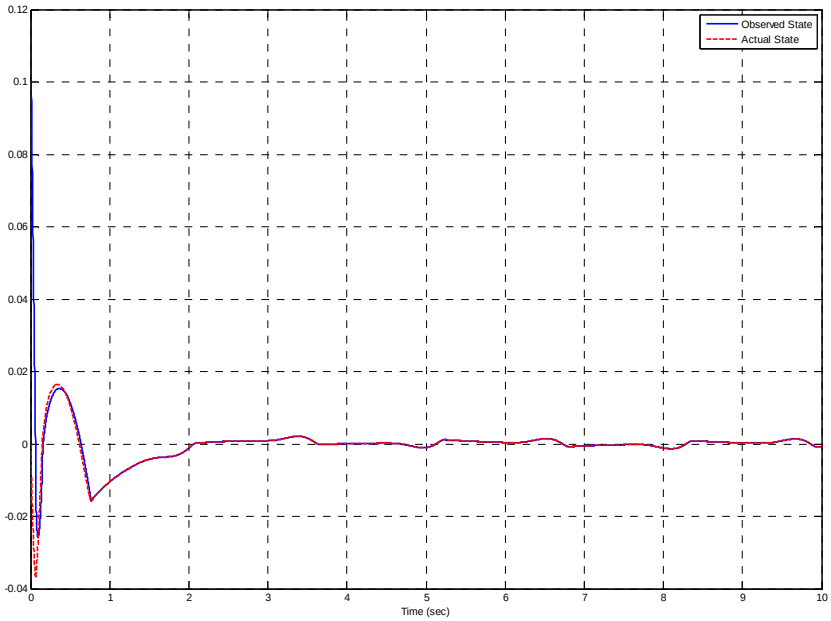

Figure 4.7: *The Actual and Observed State* $\boldsymbol{\xi_2}$

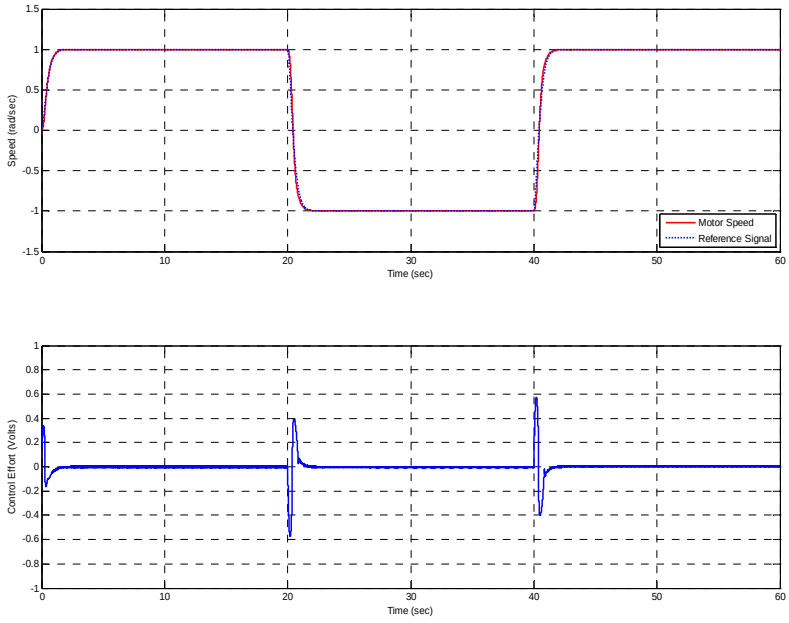

Figure 4.8: *The Speed Response and Control Effort*

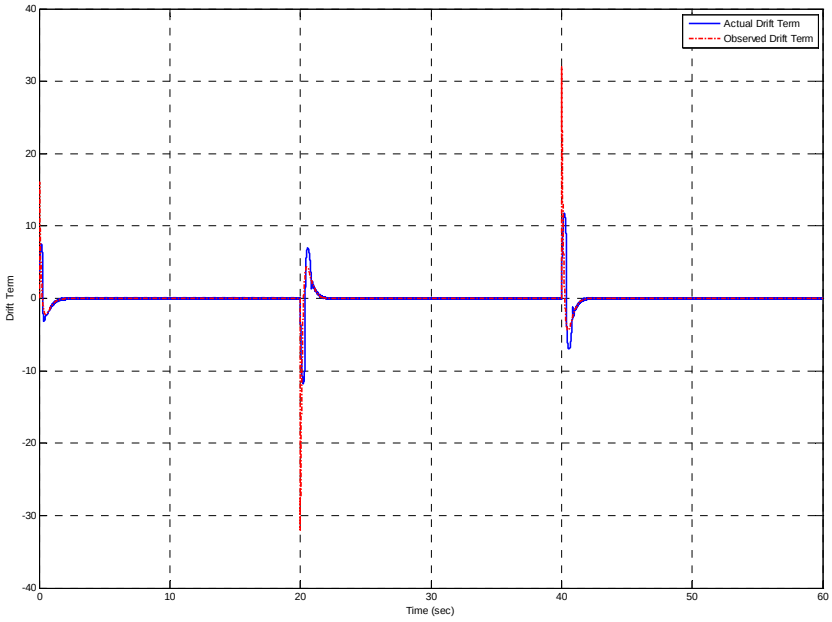

Figure 4.9: *The Actual and Observed Drift Terms*

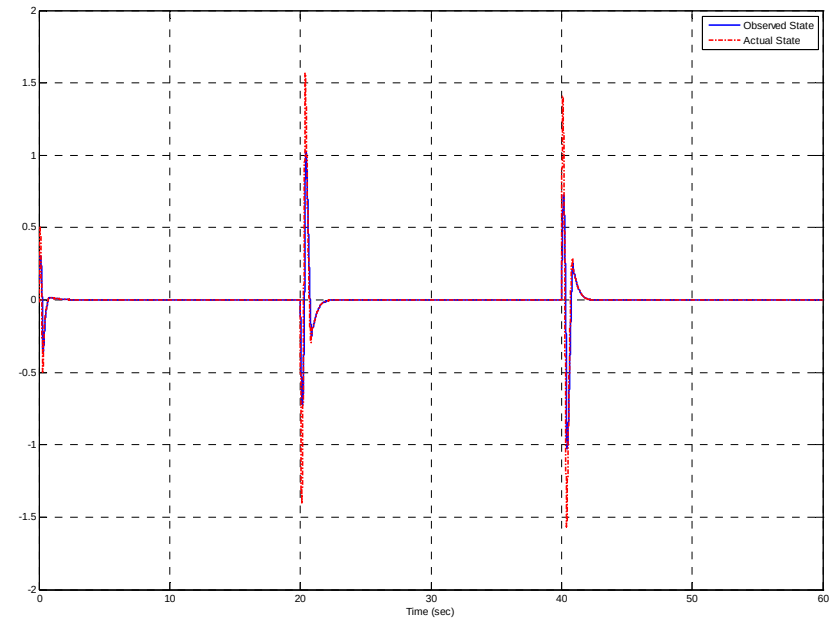

Figure 4.10: *The Actual and Observed State* $\boldsymbol{\xi_2}$

The results compare favourably with those of (Freidovich and Khalil, 2006).

4.5 Experimentation Results

To perform performance and robustness analysis of the proposed controller, an academic benchmark DC-motor (MS150) manufactured by Feedback Instrumentation has been used. The detail of experimental setup is given in the chapter 3.

For the experiment, the observer structure from (4.4.5) and the control law from (4.4.4) have been used. The values of b_0, λ_1, λ_2 and λ_3 need to be tuned. Initial guesses for these parameters were the values used in the simulations. The controller gains k_1 and k_2, are the ones described earlier to place the linear closed-loop poles at -3 and -3.

Figure 4.11 shows the experimental results of the proposed control scheme for a square reference signal. The two plots in the figure show the speed response of the DC motor and its corresponding control effort. As illustrated below, the measured speed tracks the reference precisely.

The performance of the proposed controller has also been examined with respect to a continuous sinusoidal waveform as a reference speed. The sinusoidal speed response of the DC motor with the sine reference signal is shown in Figure 4.12. The plots demonstrate that the trajectory is followed accurately with low control effort.

To verify the robustness of the proposed controller, the friction load, with the help of a magnetic brake, has been increased by 300% during the experiment. Figure 4.13 demonstrates the speed response of the DC motor subject to this perturbation. In the experiment the brake has been applied at 16.5 seconds and released after 31 seconds. The graph shows that these changes do not affect the performance of the controller significantly.

The experimental results from the proposed scheme for feedback linearization based on the robust state-disturbance observer validate the theory given in the earlier sections. The suggested strategy also offers an opportunity for achieving desired and robust performance, without the detailed knowledge of the plant system model.

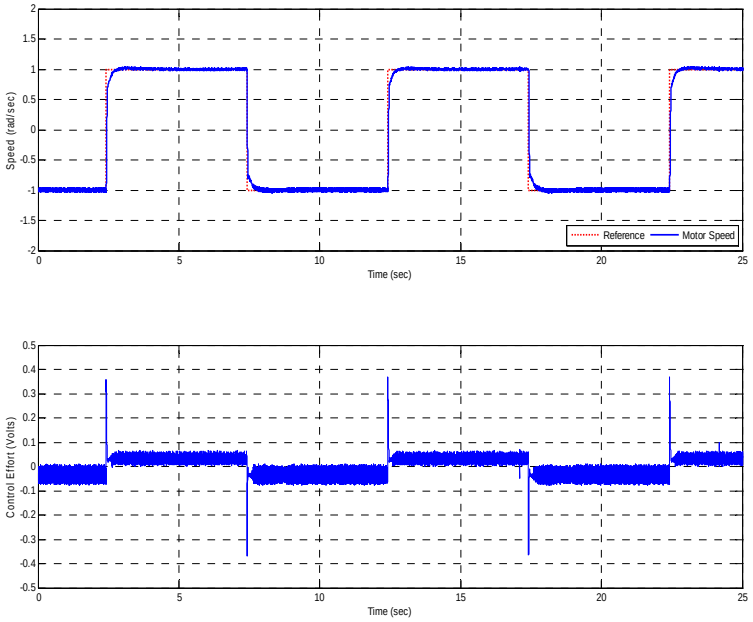

Figure 4.11: *The Experimental Result of Square Wave Reference*

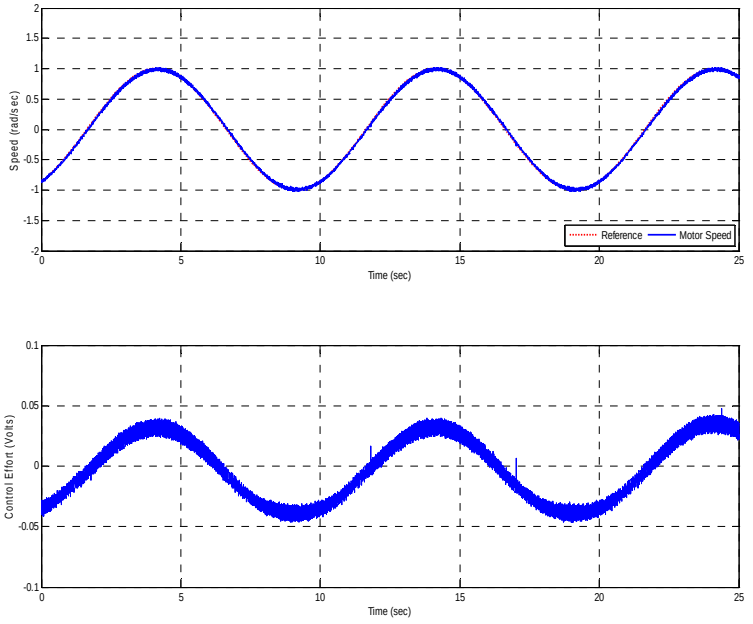

Figure 4.12: *The Experimental Result of Sinusoidal Wave Reference*

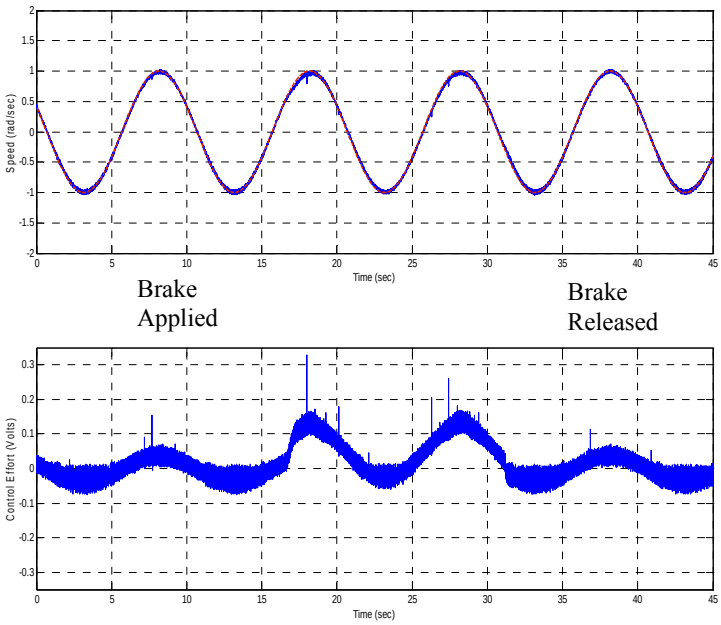

Figure 4.13: *The Speed Response with Perturbation in Friction Load*

4.6 Summary

In the chapter, a new technique for robust feedback linearization based only on output information is proposed. A robust state-disturbance observer is used to estimate the states and drift terms of the system. Finite time stability of the observer is proved, so that the separation principle can be applied. Simulation and experimental results verify the robustness and performance levels of the proposed technique.

In the next chapter, a comparative study for both controllers proposed in this chapter and previous chapter is given with a Robust LMI control design on a stabilized platform.

Chapter 5

EVALUATION OF THE PROPOSED TECHNIQUES ON INDUSTRIAL APPLICATION

Previously proposed robust control techniques, smooth second order sliding mode and robust feedback linearization control using robust state-disturbance observer, were tested only on academic bench mark DC motor. For industrial usage these methodologies need to be evaluated on industrial applications. The purpose of this chapter is robustness and performance analysis of the proposed techniques with industrial applications.

Mostly PID control is used as a point of reference for the evaluations of novel control techniques. The problem with PID control is that it is not robust, so its comparison with the robust techniques will be unjustified. H_∞ control with LMI optimization is a well established robust technique and can be used as a bench mark. Moreover the proposed techniques provide model-free control, therefore the comparison should be performed on an industrial application whose mathematical model is not well established.

5.1 Evaluation Strategy

The previously proposed techniques are compared with H_∞ control method with LMI optimization on an industrial parallel robot named stabilized platform. The stabilized platform is locally assembled and has no predefined mathematical model. A state space model of the system is required to implement any modern or robust control technique. System identification is used to extract the model of the system. Polytopic system based Linear Matrix Inequalities (LMI) is used to synthesize the H_∞ robust controller. In this work, a novel approach is used to construct the polytopic model of the system.

The polytopic system is formulated by different uncertain LTI systems as its vertices. Such system in LMI framework covers a long range of uncertainties through convex

hull. The convex hull contains LTI models which are developed traditionally via two techniques. Firstly, linearization of nonlinear model about different operating points gives distinct LTI models. Secondly nonlinear model gives LTI systems by considering a range value of uncertain affine parameters. The two methods depend evidently upon static operating points and numeric values of uncertain parameters respectively.

These two techniques do not cover dynamic uncertain scenario such as moving payload on the platform. In this work to account for such situation, a novel approach is proposed to formulate a polytopic system. In the proposed technique, system identification is employed to develop LTI models under dynamic operating conditions to construct vertices of differential inclusion. Subsequently this polytopic system is used to design controller with mixed H_2 / H_∞ synthesis with pole placement constraints in LMI framework (Khargonekar and Rotea, 1991).

The stabilized platform is used as a case study to validate proposed technique. Mainly these platforms serve as a basis for different payloads at different times. These payloads could be satellite antenna, camera, billiard tables, etc with symmetric or asymmetric structures in nature, so the mass and Moment of Inertia (MOI's) of payloads would always be uncertain. The uncertainties in payload affect the dynamical behavior of the overall system.

In the rest of the chapter, an introduction of industrial application i.e. stabilized platform and its characteristics are given to familiarize the reader with the experimental rig. After that, the detail of novel approach is given to formulate the polytopic model with the help of system identification at distinct payloads conditions. Afterward system analysis of distinct identified model is preceded. Next, control design is given in LMI framework with mixed H_2/H_∞ synthesis and pole placement constraints. In the last, performance and robustness evaluation of the proposed techniques on an industrial application is done with the LMI control.

5.2 Industrial Application: Stabilized Platform

The management of ocean-going luxury cruises goes to great lengths to isolate its critical systems from the slow persistent vibrations caused by sea waves. Systems like satellite tracking antennas or critical items such as surgery tables or even billiard tables need to be isolated from the sea waves related pitching and rolling of the ocean-

liners. Stabilized platforms are used as mounts for systems which are meant to be decoupled from sea waves.

A two Degree Of Freedom (2DOF) parallel manipulator stabilized platform is constructed to reject such torque disturbances and kept its top plate leveled with respect to horizontal axis. The schematic diagram of the stabilized platform is shown in Figure 5.1. The stabilized platform has a top-plate and a base-plate linked by two variable-length electro-mechanical actuators with the help of spherical joints. Angular motion of the top plate with respect to the base plate is produced by reducing or extending the actuators' length. The proper coordination of the actuators enables the top plate to reject the disturbances produced at the base plate with high accuracy.

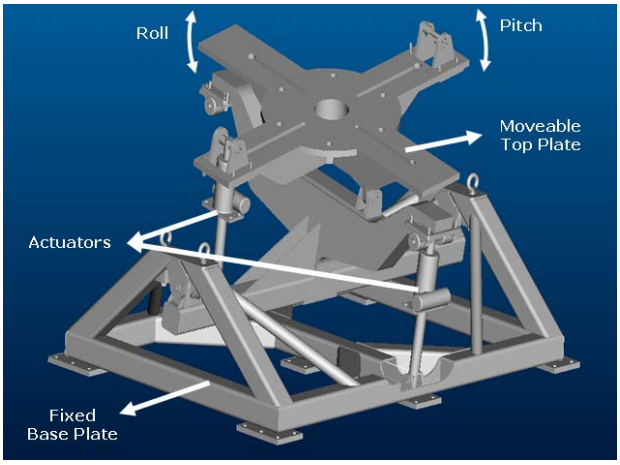

Figure 5.1: *The Schematic Diagram of Stabilized Platform*

The input range of power amplifier through Data Acquisition Card (DAC) is ± 10 Volts which corresponds with the whole range of the actuator position to correct errors in roll and pitch. The maximum voltage commands produced by the controller should lie in these limits. The outputs of the stabilized platform are the top-plate angular positions sensed by highly precise sensors. These outputs are again fedback to the controller for errors adjustment. A control system stabilizes the platform based on this information. The controller produces two separate voltages commands for each actuator. The reduction or extension of the actuators enables the top plate (payload) to reject the disturbances effectively. This sensor-controller-actuator package allows the stabilized platform to be self-correcting. The detailed block-diagram of the plant is given in Figure 5.2.

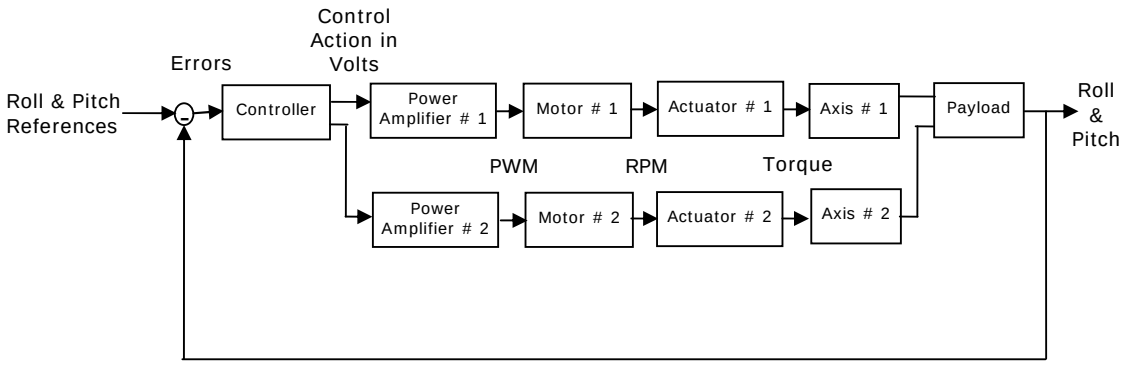

***Figure 5.2**: Block Diagram of the Stabilized Platform*

The mechanical limits of stabilized platform both in roll and pitch are ±10 degrees. The stabilized platform cannot compensate disturbances beyond these limits and become saturated. The key characteristics of the stabilized platform are provided in Table 5.1.

Parameter	***Value***
Platform Weight	*550 Kg*
Platform Max Roll Range	*±10°*
Platform Max Pitch Range	*±10°*
Platform Dimensions (length x width x height)	*1.7 m x 1.4 m x 1 m*
Top plate Radius	*0.7 m*
Payload Weight Capacity	*650 Kg*

***Table 5.1**: The Stabilized Platform and Payload Characteristics*

In practical situations, the stabilized platform may be used with different load conditions. The structure of these payloads can either be symmetric or asymmetric. The mass and Moment Of Inertia (MOIs) of these payloads will always be indeterminate. The controller design problem for these platforms is really a great challenge. One may model the platform using nonlinear differential equations and considering variation in mass and MOIs of payloads as uncertainties. However as the authors have shown in (Iqbal and Bhatti, 2008), these uncertainties are adequately large and can degrade the performance of the system. The various linear models of stabilized platform are obtained by using system identification with distinct symmetric and asymmetric payloads. System identification detailed procedures for the stabilized platform can be seen

in Appendix C. In the next Section, analyses of the identified models of the stabilized platform are given.

5.3 System Analysis

The system identification method is used to extract the state space models for the stabilized platform under three different payload conditions. First model is identified without any load. Second model is identified with symmetric load of volume 1.7x1.4 x1 m^3 and 550 Kg weight. Third model is identified with 500 Kg asymmetric satellite antenna.

The continuous-time counterparts for the three models are obtained by TUSTIN approximation. A pole-zero plots for these systems are shown in Figure 5.3. These plots illustrate that the identified models have very slow dynamics and also have non-minimum phase behavior. The damping ratios of these systems are 0.961, 0.686 and 0.0714 respectively. Moreover for asymmetric payload; poles are shifted towards origin. This shows a slow response and more oscillatory behavior is expected with these types of loads.

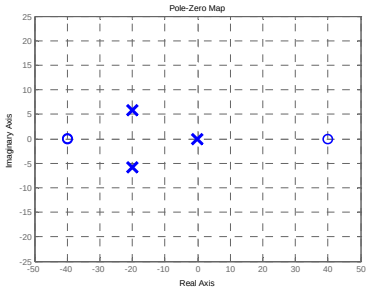

(a) Without Payload

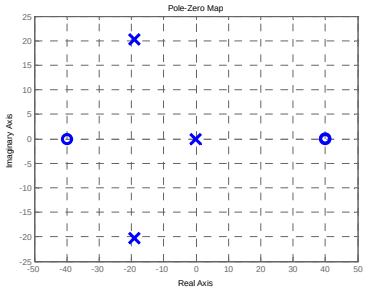

(b) Symmetric Payload

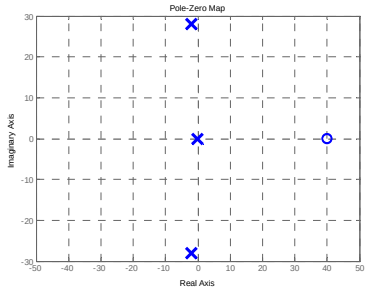

(c) Asymmetric Payload

Figure 5.3: *Pole-Zero Plots of Three Identified Models*

It is obvious from the identification process that the system model is sensitive to size and shape of the payload being used. These models i.e. without payload, symmetric payload and asymmetric payload have signification parameter variations due to the different load conditions. The characteristics of three identified models of stabilized platform are given in Table 5.2.

Stabilized Platform Models	***Bandwidth (Hz)***	***Damping Ratio***
Without payload	*0.105*	*0.961*
Symmetric payload	*0.09*	*0.686*
Asymmetric payload	*0.0445*	*0.0714*

***Table 5.2**: Characteristics of the System with Different Payload*

The Bode plots for three models are shown in Figure 5.4. The output signal is at 90° lead with respect to input signal thus the actual phase difference is 270° degrees. The Bode diagram shows that the gain decreases and phase lag increases with increase in load. Moreover it is interesting to note that the phase margin drastically increases when asymmetric payload was used. The Bode plots reveal that tracking turns out to be poorer for loaded system while noise sensitivity is decreased, whereas the bandwidth of the system with symmetric and asymmetric loads also decreases.

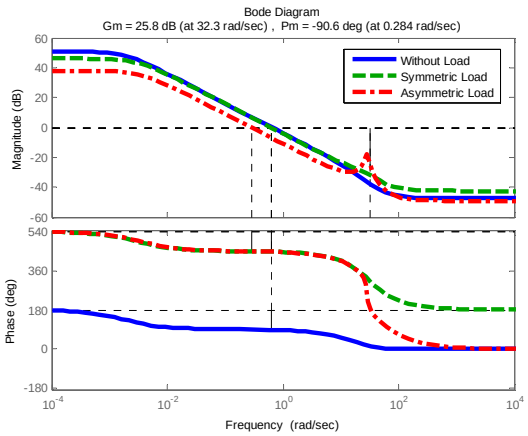

***Figure 5.4:** Bode Plot of Three Identified Models*

The Root locus plots of three identified models are shown in Figure 5.5. It can easily be seen from these plots that asymmetric load model has lowest natural frequency and it is closer to instability.

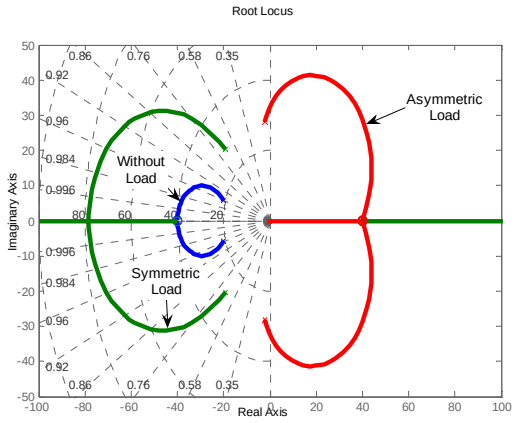

Figure 5.5: *Root Locus of Three Identified Models*

The rank of the controllability and observability matrices are full, so the systems are fully controllable and observable. The state-space matrices of three identified model are given in Appendix C. These identified models are used to formulate a polytopic model. The polytope is employed to design robust controller using Mixed H_2/H_∞ synthesis with pole-placement constraints (Chilali and Gahinet, 1996; Khargonekar and Rotea, 1991). In the next section polytopic formulation is given.

5.4 Polytopic System Formulation

The resulting identified state-space models of stabilized platform i.e. without payload, symmetric payload and asymmetric payload can be written as

$$\left.\begin{aligned}\dot{x} &= A^i x + B^i u\\ y &= C^i x + D^i u\end{aligned}\right\} \qquad \forall\, i = 1,2,3 \tag{5.4.1}$$

The system matrices of the above dynamical system can be written as a combination of system matrices as follows;

$$\Pi_i(t) = \begin{bmatrix} A^i(t) & B^i(t) \\ C^i(t) & D^i(t) \end{bmatrix} \qquad \forall\, i = 1,2,3 \tag{5.4.2}$$

The combination (5.4.2) can be constructed into convex set of polytopic system model as given below;

$$\Pi(t)\, \epsilon\, Co(\Pi_1, \Pi_2, \Pi_3) \coloneqq \left\{ \sum_{i=1}^{k} \alpha_i \Pi_i : \alpha_i \geq 0,\ \sum_{i=1}^{k} \alpha_i = 1 \right\} \tag{5.4.3}$$

where $Co(.)$ is the convex hull and nonnegative numbers α_i are called the polytopic system coordinate of Π.

5.5 LMI Control Design

The LMI theory offers a multi-objective mixed H_2/H_∞ synthesis with pole-placement constraints to solve practical problems (Chilali and Gahinet, 1996; Khargonekar and Rotea, 1991). The H_2 achieves greater noise rejection against random disturbance. H_∞ mostly deals with robust stability and does not allow to place the poles in desired regions of interest. In contrast pole-placement helps to achieve satisfactory time response and closed-loop damping.

In $\boldsymbol{H_2/H_\infty}$with pole-placement constraints synthesis, the output $\boldsymbol{z_\infty}$ is associated with $\boldsymbol{H_\infty}$ performance. The $\boldsymbol{z_2}$ is related with $\boldsymbol{H_2}$ performance. The $\boldsymbol{T_{wz_\infty}}$and $\boldsymbol{T_{wz_2}}$are related with the closed loop transfer function from $\boldsymbol{w}$ to $\boldsymbol{z_\infty}$ and from $\boldsymbol{w}$ to $\boldsymbol{z_2}$ respectively. Let *d* denotes disturbance in the system and white noise *n* are the elements of uncertainty vector $\boldsymbol{w}$, the $\boldsymbol{z_\infty}$ is the regulation error of the system and the $\boldsymbol{z_2}$ is the combination of states and control effort. Both $\boldsymbol{z_2}$ and $\boldsymbol{z_\infty}$ should be minimized in order to achieve LMI optimization. Therefore the LMI constraints can be written as

$$\left.\begin{aligned} w &= [d \quad n]^T \\ z_\infty &= e \\ z_2 &= [x \quad u]^T \end{aligned}\right\} \tag{5.5.1}$$

The new $\widehat{\boldsymbol{A}}$, $\widehat{\boldsymbol{B}}$, $\widehat{\boldsymbol{C}}$ and $\widehat{\boldsymbol{D}}$ of the augmented system can be composed as follows:

$$\widehat{\boldsymbol{A}} = \boldsymbol{A}$$

$$\widehat{\boldsymbol{B}} = [\boldsymbol{B_1} \quad \boldsymbol{B_2}]$$

$$\hat{C} = \left[\begin{array}{ccc} C_1 & C_2 & C_3 \\ \hline 1 & 0 & 0 \\ 0 & 1 & 0 \\ 0 & 0 & 1 \\ \hline 0 & 0 & 0 \end{array}\right] \qquad \hat{D} = \left[\begin{array}{c:c} D_{11} & D_{12} \\ \hline 0 & 0 \\ 0 & 0 \\ 0 & 0 \\ 0 & 1 \end{array}\right] \qquad \text{where} \quad D_{22} = \begin{bmatrix} 0 & 0 & 0 & 1 \end{bmatrix}^T \tag{5.5.2}$$

The equation (5.4.1) can be extended to polytopic system formulation with definitions given in (5.5.1) and (5.5.2):

$$\left.\begin{aligned} \dot{x} &= Ax + B_1 w + B_2 u \\ z_\infty &= C_1 x + D_{11} w + D_{12} u \\ z_2 &= C_2 x + D_{22} u \end{aligned}\right\} \tag{5.5.3}$$

The state-feedback control law $u = Kx$ guarantees (Chilali and Gahinet, 1996)

- to place the closed loop pole in some prescribed LMI stability regions.
- H_∞ performance such that $\left\|T_{\omega z_\infty}\right\| < \gamma$ where $\gamma > 0$.
- H_2 performance such that $\left\|T_{\omega z_2}\right\| < \nu$ where $\nu > 0$.

The equation (5.5.3) can be further simplified as

$$\left.\begin{aligned} \dot{x} &= (A + B_2K)x + B_1w \\ z_\infty &= (C_1 + D_{12}K)x + D_{11}w \\ z_2 &= (C_2 + D_{22}K)x \end{aligned}\right\} \tag{5.5.4}$$

The final closed-loop polytopic design principle for the system can be represented as shown in Fig 5.6.

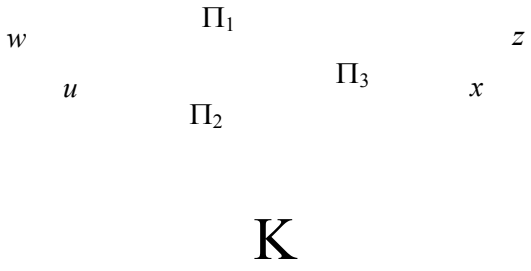

Figure 5.6: *The Polytopic State Feedback Control*

5.6 Pole Placement Region

The required pole-placement region can be designed using half-plane, disk and conic sector regions characterized by $\boldsymbol{S = (\alpha, r, \theta)}$. A minimum delay rate α, a minimum damping ratio $\boldsymbol{\xi = cos\theta}$, and a maximum undamped natural frequency $\boldsymbol{\omega = rsin\theta}$ is ensured when such a region is used. The value used for LMI region are as follow, the left haft-plane α = -10, the disk center at zero and radius *r=200*, and the conic sector origin at 0 and half inner angle $\theta=3\pi/2$, as shown in Figure 5.7.

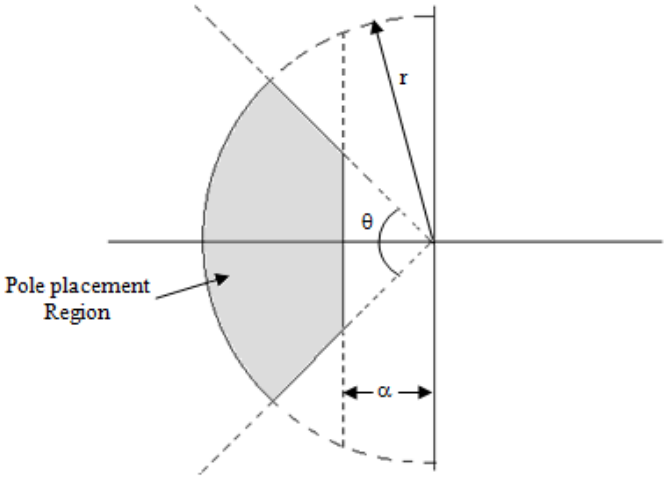

Figure 5.7: *The Pole Placement Region*

The poles are chosen such that the settling time is less than one sec. The rationale for this settling time specification comes from the observed quasi-frequency of ocean waves (taken as disturbance). A wide variation in this disturbance is expected with seasonal and geographic changes and also due to tracking orientation of asymmetric payload. A safety factor of ten is assumed for this purpose. For the mentioned rise time, the desired natural frequency comes out to be 2 rad/sec. If the lower limit of the desired Eigenvalue region is kept at -2 rad/sec then the closed loop dynamics at the rig are observed to be too slow, so this is set at -10 rad/sec. Similarly the angle theta for the chosen conic sector is kept at $3\pi/4$ which corresponds to damping ratio of 0.707 which is realistic for the mechanical structure being considered. The upper bound on the Eigenvalues comes from the need for keeping the actuators in linear region, away from saturation. Confining the closed-loop poles between these constraints ensures the desired performance. This pole-placement minimizes the overshoot and oscillation in the system response and also decreases its rise time and settling time.

5.7 Robustness and Performance Evaluations

This Section contains the details of experimentations furnished for the comparative studies. First a brief overview of experimental rig is given and in the next subsection control law and state-disturbance observer structure for the stabilized platform using robust feedback linearization technique is proposed. In the last subsection results are compared with previously designed robust H_∞ controller with LMI optimization.

5.7.1 Experimental Setup

For controller validation, a state of the art test platform is setup with a variety of actuators and sensors. Two ball-screw actuators (Duff-Norton Ball Skew) are deputed for roll and pitch movement of payload. These actuators used AC servo motors (Mitsubishi HC-SFS152B) driven by 50Hz PWM generator amplifier (Mitsubishi MR-J2S-200A). The optical and magnetic sensors (Motion Sensor OCTANS and AHRS 400CA respectively) utilized to sense the outputs of the system. The closed-loop control algorithm is implemented in DSP board (*Trio motion MC206x*). The actual routines have been written in Trio Basic language. The details of hardware configuration are outlined in Table 5.3. The stabilized platform of 550 Kilogram weight is used to stabilize 500 Kilogram payload in deep turbulent sea.

Actuator (Duff-Norton Ball Skew)	
Force	*4595 N*
Capacity	*5 Tons*
Max Speed	*27.2 inch/min*
Servo Motor (Mitsubishi HC-SFS152B)	
Max PRM	*3000 RPM*
Max Torque	*21.6 Nm*
Servo Amplifier (Mitsubishi MR-J2S-200A)	
Voltage	*3 Phase 200-230 V AC*
Frequency	*50/60 Hz*
Controller (Trio motion MC206x)	
Technology	*32-bit DSP*
Software Language	*Motion Perfect*
Sensor (AHRS400 CA)	
Range roll, pitch and heading	*± 180°, ± 90° and ± 180°*
Update Rate	*100 Hz*
Resolution	*< 0.05 degrees/sec*

***Table 5.3**: Hardware Configurations of Stabilized Platform*

5.7.2 Robust Feedback Linearization Design

From the previous system analyses, it is clear that three states dynamical model can represent the stabilized platform properly. In this scenario the robust smooth real twisting algorithm is not applicable, because it works only for relative degree two systems. The robust pole placement technique has been chosen for the comparison with LMI based polytopic controller. For this experiment, three poles are placed at -8, -10 and -12. The controller parameters to achieve this are $k_1 = 30$, $k_2 = 296$ and $k_3 = 960$. Thus the proposed controller is given as

$$u = \frac{1}{b_0}\left(-\hat{f}_1 - k_1\xi_1 - k_2\hat{\xi}_2 - k_3\hat{\xi}_3\right) \tag{5.7.1}$$

where $\hat{f}_1$ is the estimate of the drift term $f(.)$, $\hat{\xi}_2$ and $\hat{\xi}_3$ are the estimates of the states ξ_2 and ξ_3 respectively. The proposed state-disturbance observer structure for the system is as follows:

$$\dot{\hat{\xi}}_1 = v_1$$

$$v_1 = -\lambda_4 L^{1/4} \left|\hat{\xi}_1 - \xi_1\right|^{3/4} sign\left(\hat{\xi}_1 - \xi_1\right) + \hat{\xi}_2$$

$$\dot{\hat{\xi}}_2 = v_2$$

$$v_2 = -\lambda_3 L^{1/3} \left|\hat{\xi}_2 - v_1\right|^{2/3} sign\left(\hat{\xi}_2 - v_1\right) + \hat{\xi}_3$$

$$\dot{\hat{\xi}}_3 = \hat{f}_1 + b_0 u$$

$$\hat{f}_1 = -\lambda_2 L^{1/2} \left|\hat{\xi}_3 - v_2\right|^{1/2} sign\left(\hat{\xi}_3 - v_2\right) + \hat{\xi}_4$$

$$\dot{\hat{\xi}}_4 = -\lambda_1 L \, sign\left(\hat{\xi}_4 - \hat{f}_1\right) \qquad (5.7.2)$$

where $\lambda_1 = 10,\ \lambda_2 = 20, \lambda_3 = 40$ and $\lambda_4 = 10$.

The stabilized platform is placed on a moving surface (termed as Test Table) which simulates a ship deck in a turbulent sea. For testing the controllers the stabilized platform is mounted on the Test Table and the Test Table is given a pitching command which acts as an external disturbance to the stabilized platform. The experimental results of each controller are given in the next subsection.

5.7.3 Experimental Results

A step disturbance is applied in the first test. The rig test results of disturbance rejection of robust feedback linearization and LMI controller are shown in Figure 5.8. It can be observed that disturbance recovery time of LMI based controller is greater than other two controllers. Moreover error amplitude in LMI case is also large.

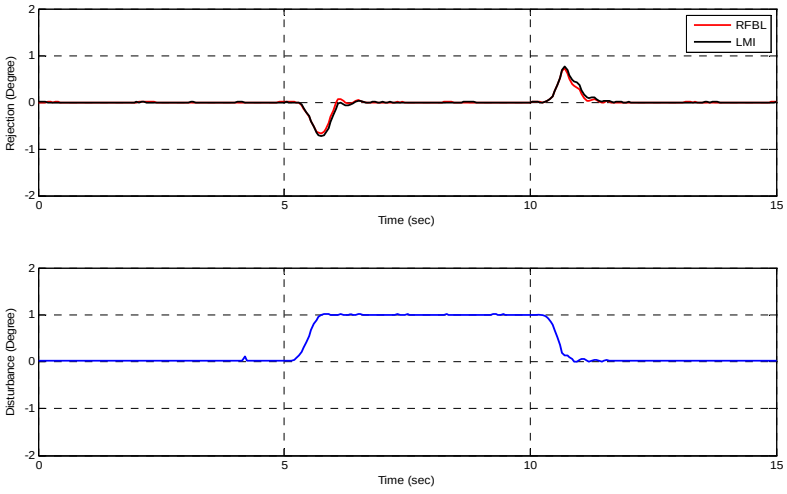

Figure 5.8: Disturbance Rejection with Stabilized Platform

Parameter	*LMI Controller*	*Robust Feedback Linearization Controller*
Disturbance Rejection Time	*1.0 sec*	*0.8 sec*
Percentage overshoot	*0%*	*0%*

***Table 5.4**: Summary of Controllers characteristics by Experiments*

In the next test, a sine signal with amplitude of 5 degree and frequency equal to 0.055 Hz is applied on the rig to predict continuous disturbance response. The results of sinusoidal disturbance with two controllers are shown in Figure 5.9 and summarized in Table 5.5. It is again observed that the proposed technique perform better performance as compare to LMI based controller.

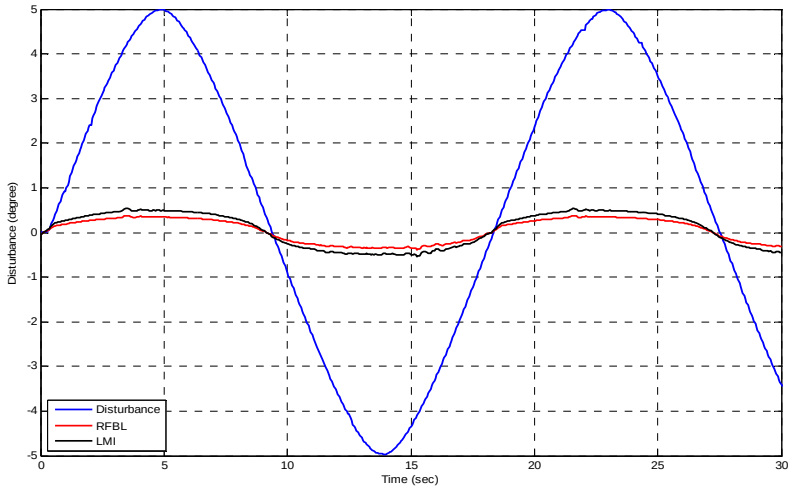

***Figure 5.9:** Sine Wave Disturbance Rejection with Stabilized Platform*

Parameter	*LMI Controller*	*Robust Feedback Linearization Controller*
Error Amplitude (in Degree)	0.5°	0.35°

***Table 5.5**: Summary of Controllers characteristics by Experiments*

5.8 Summary

In this chapter, previously proposed robust feedback linearization techniques are compared with polytopic based LMI controller. The experimentation shows that the

proposed robust control techniques perform well as compare to LMI based robust linear control technique.

Next chapter conclude the thesis along with suggestions for further work.

Chapter 6

CONCLUSIONS & FUTURE WORK

In this chapter a brief summary of the thesis is given. Moreover some future research proposals are suggested for researchers working in the area of higher order sliding mode control.

6.1 Thesis Summary

In this thesis, first a disturbance observer is proposed for single input single output (SISO) systems that estimate drift terms or internal and external disturbances for relative degree two systems. The work is an extended version of (Shtessel, Shkolnikov and Levant, 2007) in which they proposed a disturbance observer for relative degree one systems. Next the work is further extended to a state-disturbance observer for systems with relative degree less than or equal to the system order. The structure of the observer is independent from system model and based on robust exact differentiator proposed by (Levant, 1998; Levant, 2003). The state-disturbance observer can estimate states as well as the drift terms of the system. The drift term can be used to cancel out uncertainties and disturbances of the system online, in this way the system behaves like an nth order integrator. The states could be used to design any modern or state-space control. The finite time convergence analyses of both observers are given in noisy and noise free environment.

Further, two novel control techniques are proposed using the state-disturbance observer. Both techniques are robust and provide smooth control effort; moreover no particular model of the plant is required. Details of the proposed techniques are given within the following lines.

First proposed technique is robust smooth real twisting second order sliding mode for relative degree two systems using modified “twisting” algorithm. The robust disturbance observer is used to estimate the drift terms of the system. This information is used to compensate for the undesired dynamics in the closed-loop system. Finite time

stability of the overall system is proven using a homogeneity-based approach. The simulation and experimental results validate the theory.

Next, robust feedback linearization scheme is proposed in combination with robust state-disturbance observer in the closed loop system. The states and uncertainties are estimated with the help of state-disturbance observer. Finite time convergence of the overall closed-loop system is given using separation principle. The design is verified through simulations and experimentations on an academic benchmark example of DC motor.

Further, the techniques are implemented on industrial application to verify their usage for industry. The stabilized platform is a parallel robot manufactured for ocean-going crafts to reject torque disturbances caused by sea waves and kept top of the platform leveled with horizontal axis. A well established H_∞ robust control technique with LMI optimization is used as a benchmark to evaluate the performance of the proposed techniques. The system identification is used to extract models of the stabilized platform with different payload conditions. The models construct the vertices of a polytope system. This polytopic system is then used for the construction of the robust H_∞ control based on LMI optimization. Experimental results of LMI control are compared with the thesis contributions. It is concluded that the proposed techniques perform good as compare to robust LMI control design.

In the next Section some future work recommendations are given for researchers working in the same area.

6.2 Future Work

i. The proposed disturbance observer is for SISO systems, but mostly system in the industry are Multi Input Multi Output (MIMO) systems. In future, the work can be extended for MIMO systems. The MIMO disturbance observer can estimate drift terms for MIMO system.
ii. The proposed state-disturbance observer is again valid for SISO case. In future it can also be extended for MIMO systems so state and drift term of MIMO systems can be estimated.

iii. Robust feedback linearization technique and robust smooth real twisting second order sliding mode is also for SISO systems, it can also be extended to MIMO systems.

iv. The limitation of robust smooth real twisting algorithm is that it is valid only for second order sliding mode. In future the smoothness control can be extended for higher order sliding mode control.

REFERENCES

Ahmed, Q., A. I. Bhatti and M. Iqbal, (2011a), *Virtual Sensors for Automotive Engine Sensors Fault Diagnosis in Second Order Sliding Modes*, IEEE Sensors Journal, Vol. 11(9), pp. 1832 - 1840

Ahmed, Q., and A. I. Bhatti, (2011b), *Estimating SI Engine Efficiencies and Parameters in Second Order Sliding Modes*, IEEE Transactions on Industrial Electronics, Issue 99,

Bacciotti, A. and L. Rosier, (2001), *Liapunov Functions and Stability in Control Theory*, Lecture Notes in Control and Information Sciences, Springer, London.

Baev, S., Y. Shtessel and I. Shkolnikov, (2008), *Nonminimum-phase output tracking in causal systems using higher-order sliding modes*, Int. J. Robust Nonlinear Control, 18:454–467

Bartolini, G., A. Ferrara and E. Usai, (1998), *Chattering Avoidance by Second-Order Sliding Mode Control*, IEEE Transactions of Automatic Control, Vol. 43, pp.241-246.

Bartolini G., A. Ferrara, E. Punta, (2000), *Multi-Input Second-Order Sliding-Mode Hybrid Control of Constrained Manipulators*, Dynamics and Control, Vol. 10(3), pp. 277-296.

Bartolini, G., Levant, A., Pisano, A., and Usai, E., (2002), *Higher-order sliding modes for output-feedback control of nonlinear uncertain systems,* In X. Yu and J. X. Xu (Eds) Variable Structure Systems: Towards the 21st Century, Lecture Notes in Control and Information Sciences, Springer-Verlag, 274, pp. 83–108.

Bartolini G., A. Pisano, E. Punta, E. Usai,(2003), *A Survey of Applications of Second-Order Sliding Mode Control to Mechanical Systems,* International Journal of Control, Vol. 76(9/10), pp. 875-892.

Benallegue, A., A. Mokhtari and L. Fridman, (2008), *High-order Sliding-mode Observer for a Quadrotor UAV*, International Journal of Robust and Nonlinear Control, Vol. 18, pp. 427 – 440.

Besnard, L., Y. B. Shtessel, and B. Landrum, (2007), Control of a Quad rotor Vehicle Using Sliding Mode Disturbance Observer, Proceedings of the American Control Conference, NY, July 2007.

Bhatt, S. and D. Bernstein, (2000), *Finite Time Stability of Continuous Autonomous Systems,* SIAM Journal on Control and Optimization, Vol. 38(3), pp.751-766.

Butt, Q. R., A.I. Bhatti, (2008), *Estimation of Gasoline-Engine Parameters Using Higher Order Sliding Mode*, IEEE Transactions on Industrial Electronics, Volume: 55, Issue: 11, page 3891-3898

Boyd, S., L. El Ghaoui, E. Feron and V. Balakrishnan, (1993), *Linear Matrix Inequalities in System and Control Theory*, SIAM Press.

Burton, J. A. and A. S. I. Zinober, (1986), *Continuous Approximation of Variable Structure Control*, International Journal of Systems Science, Vol. 17, pp.875– 885.

Canudas deWit, C., H. Olsson, K. J. Astrom, and P. Lischinsky, (1995), *A new model for control of systems with friction*, IEEE Trans. on Automatic Control, Vol. 40, No 3, pp. 419-425.

Chilali, M., and P. Gahinet, (1996), H_∞ *Design with Pole placement Constraints: An LMI Approach*, IEEE Trans. on Automatic Control, 41 (3), pp. 358-367.

Davila, J., L. Fridman and A. Levant, (2005), *Second-Order Sliding-Mode Observer for Mechanical Systems*, IEEE Transactions of Automatic Control, Vol. 50 (11), pp. 1785-1789.

Edwards, C. and Sara K. Spurgeon, (1998), *Sliding Mode Control: Theory and Applications*, Taylor & Francis Ltd, London.

Edwards, C., Sara K. Spurgeon and R. Hebden, (2003), *On the Design of Sliding Mode Output Feedback Controllers*, invited paper prepared for a Special Issue of the International Journal of Control, Vol. 76(9/10), pp. 893-905.

Emel'yanov, S. V., Korovin, S. K., and Levantovsky, L. V., (1986), *Higher order sliding regimes in the binary control systems*, Soviet Physics, Doklady, 31, pp. 291-293.

Emel'yanov, S. V., Korovin, S. K., and Levantovsky, L. V., (1996), *High order sliding modes in control systems, Computational Mathematics and Modeling*, Vol. 7, No. 3, 294-318.

Emel'yanov, S. V., (2007), *Theory of Variable-Structure Systems: Inception and initial Development*, Computational Mathematics and Modeling, Vol. 18, No. 4, 321-331

Esfandiari, F., and H. K. Khalil, (1992), *Output feedback stabilization of fully linearizable systems*, International Journal of Control, Vol. 56(1), pp. 007-1037.

Ferrara, A.,and C. Lombardi, (2007), *Interaction control of robotic manipulators via second-order sliding modes*, International Journal of Adaptive Control and Signal Process. Vol. 21 pp. 708–730

Filippov, A. F., (1988), *Differential Equations with Discontinuous Right-Hand Side*, Kluwer Dordrecht, Nether-lands.

Franklin, G., J. D. Powell and A. Emami-Naeini, (2010), *Feedback Control of Dynamic Systems*, 6th Edition, Prentice Hall, London.

Fridman, L., and A. Levant, (1996), *Sliding Modes of Higher Order as a Natural Phenomenon in Control Theory*, Lecture Notes in Control and Information Science, Robust Control via Variable Structure and Lyapunov Techniques, Springer-Verlag London, pp.107–133

Freidovich, L. B., and H. K. Khalil, (2006), *Robust Feedback Linearization using Extended High-Gain Observer*, in proceeding of 45th IEEE Conference on Decision & Control, San Diego CA, USA.

Hall, C. and Y. B. Shtessel, (2006), *Sliding Mode Disturbance Observers-based Control for a Reusable Launch Vehicle*, AIAA Journal on Guidance, Control, and Dynamics, Vol. 29,No. 6, pp. 1315-1329.

Hunt, K. J., D. Sbarbaro, R. Zbikowski, P.J. Gawthrop (1992), *Neural Networks for Control Systems - A Survey*, Automatica, Vol. 28, No. 6, pp. 1083-1112.

Iqbal, S., M. Akhtar and N. Mehdi, (2005), *System Identification and H_∞ Loop-shaping Design for 3DOF Stabilized Platform,* in Proceeding of 4th International Bhurban Conference on Science and Technology, IBCAST Bhurban, Pakistan, July 2005, pp. 75 − 82.

Iqbal, S., A. I. Bhatti, M. Akhtar and S. Ullah, (2007), *Design and Robustness Evaluation of an H_∞ Loop Shaping Controller for a 2DOF Stabilized Platform*, in Proceeding of European Control Conference, ECC, Kos Greece, July 2007 pp. 2098 − 2104.

Iqbal, S., A. I. Bhatti and Q. Ahmed, (2008), *Dynamic Analysis and Robust Control Design for Stewart Platform with Moving Payloads*, in Proceeding of 17th IFAC World Congress, IFAC WC, Seoul, Korea, July 2008, pp. 5324 – 5329.

Iqbal, S., C. Edwards and A. I. Bhatti, (2010), *A Smooth Second-Order Sliding Mode Controller for Relative Degree Two Systems*, in proceeding of 36th Annual Conference of the IEEE Industrial Electronics Society, Glendale, AZ, USA, Nov 07-10, 2010.

Iqbal, S., C. Edwards and A. I. Bhatti, (2011), *Robust Output Feedback Linearization for Minimum Phase Systems*, Proc. of 18th IFAC World Congress, Milano, Italy, August 28 – September 2, 2011.

Iqbal, M., A. I. Bhatti, S. Iqbal, and Q. Khan, (2011), *Robust Parameter Estimation of Nonlinear Systems Using Sliding-Mode Differentiator Observer*, IEEE Transactions on Industrial Electronics, vol. 58(2), February 2011

Isidori, A., (1995), *Nonlinear Control Systems - An Introduction*, 3rd Edition, Springer-Verlag, New York.

Kalman, R. E., (1960), *A New Approach to Linear Filtering and Prediction Problems,* Transactions of the ASME--Journal of Basic Engineering, Vol. 82, pp.35-45.

Khalil, H., (1999), *High-Gain Observers in Nonlinear Feedback Control*, Lecture Notes in Control and Information Sciences, Volume 244, pp. 249-268.

Khalil, H., (2002), *Nonlinear Systems*, 3rd Edition, Prentice Hall, New York.

Khan, M. K., and Sara K. Spurgeon, P. F. Puleston, (2001), *Robust Speed Control of an Automotive Engine Using Second Order Sliding Modes*, Proceedings of European Control Conference, 974-978, Porto, Portugal.

Khan, M. K., Goh K. B., and Sara K. Spurgeon, (2003), *Second order sliding mode control of a diesel engine*, Asian Journal of Control, 5(4).

Khan, M. K., Sara K. Spurgeon, (2006), *Robust MIMO water level control in interconnected twin-tanks using second order sliding mode control*, Control Engineering Practice 14, 375–386.

Khan, Q., A.I. Bhatti, M. Iqbal and Q. Ahmed, (2011a), *Dynamic Integral Sliding Mode Control of Uncertain Nonlinear Systems*, Accepted for publication in International Journal of Innovative Computing Information and Control.

Khan, Q., A. I. Bhatti, S. Iqbal, M. Iqbal, (2011b), *Dynamic Integral Sliding Mode for MIMO Uncertain Nonlinear Systems*, International Journal of Control, Automation and Systems. Vol. 9(1), pp.151 – 160.

Khan, Q., A.I. Bhatti, and Q. Ahmed, (2011c), *Dynamic Integral Sliding Mode Control of Nonlinear SISO Systems with States Dependent Matched and Mismatched Uncertainties*, in proceeding of 18th IFAC World Congress, Milano, Italy, August 28 – September 2, 2011.

Khargonekar, P. P., and Mario A. Rotea, (1991), *Mixed H_2 / H_∞ Control: A Convex Optimization Approach*, IEEE Transaction on Automatic Control. 36 (7), pp. 824–837.

Landau, I. D., (1990), *System Identification and Control Design*, Prentice Hall.

Levant, A., (1993), *Sliding Order and Sliding Accuracy in Sliding Mode Control*, International Journal of Control, Vol. 58 (6), pp. 1247-1263.

Lee, C. C., (1990), *Fuzzy logic in control systems: fuzzy logic controller-parts 1 and 2*, IEEE Transactions on Systems, Man, and Cybernetics, Vol. 20, No. 2, pp 404-435.

Levant, A., (1998), *Robust Exact Differentiation via Sliding Mode Technique*, Automatica, Vol. 34(3), pp. 379 – 384.

Levant, A., A. Pridor, R. Gitizadeh, I. Yaesh, J. Z. Ben-Asher (2000), *Aircraft Pitch Control via Second Order Sliding Technique*, AIAA Journal of Guidance, Control and Dynamics, Vol. 23(4), pp. 586-594

Levant, A. (2002), *Universal SISO Output-Feedback controller*, in proceedings of 15th IFAC World Congress, Barcelona, Spain.

Levant, A. (2003), *Higher-Order Sliding Modes, Differentiation and Output-Feedback Control*, International Journal of Control, 76 (9/10), pp. 924–941.

Levant, A., (2005), *Homogeneity Approach to High-order Sliding Mode Design*, Automatica, Vol. 41(5), pp 823-830.

Levant, A., (2008), *Homogeneous High-Order Sliding Modes*, Proceedings of the 17th IFAC World Congress, Seoul, Korea, pp. 3799-3810.

Massey, T. and Y. Shtessel (2005). *Continuous traditional and high order sliding modes for satellite formation control*, AIAA J. Guidance, Control, and Dynamics, 28(4), 826-831.

Ljung, L., (1989), *System Identification: Theory for the User*, PTR Prentice Hall.

Ljung, L., and T. Glad, (1994), *Modeling of Dynamic Systems*, PTR Prentice Hall.

Lu, X. Y., and Sara K. Spurgeon, (1999), *Output Feedback Stabilization of MIMO Nonlinear Systems via Dynamic Sliding Mode*, International Journal of Robust and Non-linear Control, Vol. 9, pp. 275-306.

Luenberger, D. G., (1964), *Observing the state of a linear system,* IEEE Transaction on Military Electronics Vol. 8, pp. 290-293.

Man, Z., A. P. Paplinski and H. Wu, (1994), *A Robust MIMO Terminal Sliding Mode Control Scheme for Rigid Robotic Manipulators*. IEEE Transactions on Automatic Control, Vol. 39(12), pp. 2464–2469.

Ogata, K., (2009), *Modern Control Engineering*, 5th edition, Prentice Hall, London.

Orlov, Y., (2005), *Finite Time Stability and Robust Control synthesis of Uncertain Switched Systems*, SIAM Journal of Control and Optimization, Vol. 43(4), pp. 1253-1271.

Qaiser, S. H., A. I. Bhatti, M. Iqbal, R. Samar, J. Qadir (2009a), *Model validation and higher order sliding mode controller design for a research reactor*, Annals of Nuclear Energy, vol. 36, pp. 37-45.

Qaiser, S. H., A.I. Bhatti, M. Iqbal, and J. Qadir, (2009b), *Estimation of Precursor Concentration in a Research Reactor by using Second Order Sliding Mode Observer,* Nuclear Engineering and Design, Vol. 239(10), Pages 2134-2140.

Radke, A., and Z. Gao, (2006), *A Survey of State and Disturbance Observers for Practitioners*, Proceedings of the American Control Conference, Minneapolis, Minnesota, USA, June 14-16, 2006.

Sastry, S., (1999), *Nonlinear Systems: Analysis, Stability and Control*, Springer Verlag, New York.

Shtessel, Y. B., I. A. Shkolnikov, and M. D. J. Brown, (2003), *An Asymptotic Second-Order Smooth Sliding Mode Control*, Asian Journal of Control, Vol. 5(4), pp. 498-504.

Shtessel, Y. B., I. A. Shkolnikov, and A. Levant, (2007), *Smooth Second-Order Sliding Modes: Missile Guidance Application*, Automatica, Vol. 43, issue. 8, pp. 1470-1476.

Sira-Ramirez, H., (1993), *On the Dynamical Sliding Mode Control of Nonlinear Systems*, International Journal of Control, Vol. 57(7), pp. 1039-1061.

Slotine, J.-J. E., and Li, W., (1991), *Applied Nonlinear Control*, Prentice-Hall, London.

Soderstrom, T., and P. Stoica, (1989), *System Identification*, Prentice Hall, London.

Spurgeon, S., K. B. Goh and N. B. Jones (2002). *An application of higher order sliding modes to the control of a diesel generator set (genset)*, Advances in Variable Structure Systems, Proc. of the 7th VSS Workshop, July 2002, Sarajevo.

Utkin, V. I., (1977), *Sliding Variable Structure Systems with Sliding Modes*, IEEE Transactions on Automatic Control, Vol. 22 (2), pp 212-222.

Utkin, V. I., (1992), *Sliding Modes in Optimization and Control Problems*, Springer Verlag, New York.

Utkin, V. I., J. Guldner and J. Shi (1999), *Sliding Mode Control in Electromechanical Systems*, Taylor and Francis, London.

Yan, X. Y., Sara K. Spurgeon and C. Edwards, (2005), *Dynamic Output Feedback Sliding Mode Control for a Class of Nonlinear Systems with Mismatched Uncertainty*, European Journal of Control, Vol. 11(1), pp. 1-10.

Yu, X., and Z. Man, (2002), *Variable Structure Systems with Terminal Sliding Modes*, Lecture Notes in Control and Information Sciences, Variable Structure Systems: Towards the 21st Century, Springer Berlin / Heidelberg, Vol. 274, pp. 109-127.

APPENDICES

Appendix – A

Stability Analysis for Real Twisting Algorithm

In general, Lyapunov-based approach is used for the stability analysis of a dynamical system in control systems. However, the method is applicable only for relative degree one with respect to candidate Lyapunov function. For the relative degree two systems, Lyapunov method cannot be used directly. Some other techniques, e.g. geometric based methods are used in that case for stability proof.

For the stability analysis of higher order sliding mode (HOSM), the geometric approach is used and convergence of the trajectories has been presented in literature (Levant, 2002). Two most popular algorithms of HOSM are commonly used in this thesis. Here for completeness the stability analysis of the algorithms are given.

In this appendix, a detail analysis of real twisting algorithm using geometric approach is given.

A.1 Stability Analysis

Let an uncertain second order dynamical system can be represented as

$$\ddot{x} = a(t) + b(t)u \tag{A.1}$$

where $|a(t,x)| \leq C, \qquad 0 < K_m \leq b(t,x) \leq K_M,$ (A.2)

Let the control law be

$$u = -r_1 signx - r_2 sign\dot{x}, \qquad r_1 > r_2 > 0 \tag{A.3}$$

Lemma [Levant, 1993]

Let r_1 and r_2 satisfy the conditions

$$K_m(r_1 + r_2) - C > K_M(r_1 - r_2) + C, \qquad K_m(r_1 - r_2) > C \tag{A.4}$$

Then the controller (A.3) provides for the appearance of a 2-sliding mode $x = \dot{x} = 0$ attracting the trajectories in finite time.

Proof:

From equation (A.1) and (A.3) we have

$$\ddot{x} = a - b(r_1 signx + r_2 sign\dot{x}) \quad \text{(A.5)}$$

The equation (A.5) is replaced by an equivalent differential inclusion by using (A.2)

$$\ddot{x} \in [-C, C] - [K_m, K_M](r_1 signx + r_2 sign\dot{x}) \quad \text{(A.6)}$$

In 1st quadrant, upper bounds of inclusion can give trajectory $\dot{x}_0 x_M$ of Figure A.1.

$\ddot{x} \leq C - K_M(r_1 + r_2)$

by using constraints given in (A.4), we get

$\ddot{x} < 0$

In 3rd quadrant, taking lower bounds of inclusion can give outer trajectory, i.e.

$\ddot{x} \geq -C + K_m(r_1 + r_2)$

by employing constraints given in (A.4), we get

$\ddot{x} > 0$

This implies that by using control law (A.3), we get $sign(x)sign(\ddot{x}) < 0$ in first and third quadrants. It means that the system trajectories in first and third quadrants must across line $\dot{x} = 0$.

In 2nd quadrant, taking lower bounds we get

$\ddot{x} \geq -C + K_m(r_1 + r_2)$

by applying constraints given in (A.4), we get

$\ddot{x} > 0$

In 4th quadrant, taking upper bounds can give outer boundaries, i.e.

$\ddot{x} \leq C - K_M(r_1 - r_2)$

by introducing constraints given in (A.4), we get

$\ddot{x} < 0$

It means that by using control law (A.3) the system trajectories in second and fourth quadrant go away from the line $\dot{x} = 0$, but due to its parabolic nature and $sign(x)sign(\ddot{x}) < 0$ and $sign(x)sign(\dot{x}) < 0$, the system trajectories must converge to the origin and cross line $x = 0$.

The upper and lower bounds of trajectories in each quadrant can be found by taking (A.6) and multiplying both sides by $sign(x)$ function

$$\ddot{x}signx \in [-C, C] - [K_m, K_M](r_1 signx + r_2 sign\dot{x})signx$$

For $x > 0,\ \dot{x} > 0$ and $x < 0,\ \dot{x} < 0$, lower bounds of (A.2) in first and third quadrant is

$$\ddot{x}signx \geq -C - K_M(r_1 + r_2) < 0, \tag{A.7}$$

Upper bounds of (A.2) in first and third quadrant are

$$\ddot{x}signx \leq C - K_m(r_1 + r_2) < 0, \tag{A.8}$$

For $x < 0,\ \dot{x} > 0$ and $x > 0,\ \dot{x} < 0$, lower bounds of (A.2) in second and fourth quadrant is

$$\ddot{x}signx \geq -C - K_M(r_1 - r_2) < 0, \tag{A.9}$$

Upper bounds of (A.2) in second and fourth quadrants are

$$\ddot{x}signx \leq C - K_m(r_1 - r_2) < 0, \tag{A.10}$$

by (A.8) - (A.10) we can write

$$-[K_M(r_1 + r_2) + C] \leq \ddot{x}signx \leq -[K_m(r_1 + r_2) - C] < 0, \quad with\ x\dot{x} > 0,$$

$$-[K_M(r_1 - r_2) + C] \leq \ddot{x}signx \leq -[K_m(r_1 - r_2) - C] < 0, \quad with\ x\dot{x} < 0, \tag{A.11}$$

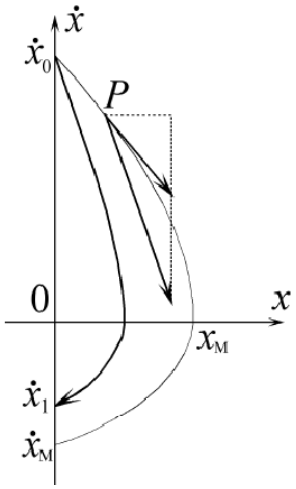

***Figure A.1**: The convergence of the twisting controller*

The graphical representation of the upper bounds of (A.11) i.e. $\dot{x}_0 x_M \dot{x}_M$ can be seen in Figure A.1. The equation of the trajectory can be simplify as

$$\ddot{x} = \begin{cases} -[K_m(r_1 + r_2) - C]signx, & \text{with } x\dot{x} > 0 \\ -[K_M(r_1 - r_2) + C]signx & \text{with } x\dot{x} < 0' \end{cases} \quad \text{(A.12)}$$

The solution of (A.11) with initial conditions $x = 0,\ \dot{x} = \dot{x}_M$ at *t=0*.

Let the solution of the differential equation for $\dot{x} > 0$,

$$\ddot{x} = -[K_m(r_1 + r_2) - C]$$

Integrate once with respect to time *t*, we get

$$\dot{x} = -[K_m(r_1 + r_2) - C]t + A \quad \text{(A.13)}$$

Let the solution holds in the small vicinity of the origin i.e. $A = 0$, we get

$$t = -\frac{\dot{x}}{K_m(r_1 + r_2) - C} \quad \text{(A.14)}$$

Again integrating (A.13) with respect to time *t*, we get

$$x = -\frac{1}{2}[K_m(r_1 + r_2) - C]t^2 + B$$

Putting value of *t* from (A.14), we get

$$x = -\frac{\dot{x}}{2[K_m(r_1 + r_2) - C]} + B$$

Apply boundary value conditions $\dot{x} = 0,\ x = x_M,$ we get $B = x_M$

$$x = x_M - \frac{\dot{x}^2}{2[K_m(r_1 + r_2) - C]}$$

Similarly the solution of the differential equation for $\dot{x} < 0$, is

$$x = x_M - \frac{\dot{x}^2}{2[K_M(r_1 - r_2) + C]}$$

We can write the both results as

$$x = \begin{cases} x_M - \frac{\dot{x}^2}{2[K_m(r_1 + r_2) - C]} & \text{with } \dot{x} > 0 \\ x_M - \frac{\dot{x}^2}{2[K_M(r_1 - r_2) + C]} & \text{with } \dot{x} < 0 \end{cases}, \quad \text{(A.15)}$$

Solve (A.15) for $\dot{x}_0$ by putting $x = 0$ we get

$\dot{x}_0^2 = 2[K_m(r_1 + r_2) - C]x_M$

Let the trajectories cut axis $\boldsymbol{x = 0}$ at $\boldsymbol{\dot{x}_1}$ and obviously $|\boldsymbol{\dot{x}_1}| < |\boldsymbol{\dot{x}_M}|$, and again we have

$$\left|\frac{\dot{\boldsymbol{x}}_1}{\dot{\boldsymbol{x}}_0}\right| = \sqrt{\frac{[\boldsymbol{K_m(r_1 - r_2) + C}]}{[\boldsymbol{K_m(r_1 + r_2) - C}]}}$$

By considering condition (A.4) we have

$$\left|\frac{\dot{\boldsymbol{x}}_1}{\dot{\boldsymbol{x}}_0}\right| = \boldsymbol{q} < 1$$

Through same procedure, the trajectories for $x < 0$ can also provide the same results, i.e.

$|\boldsymbol{\dot{x}_{i+1}}|/|\boldsymbol{\dot{x}_i}| \leq \boldsymbol{q} < 1$. Therefore the real twisting algorithm converges to origin in finite time.

A.2 Convergence Time

The trajectory $\boldsymbol{\dot{x}_0 x_1 \dot{x}_1}$ can be written as

$$[K_m(r_1 - r_2) - C] \leq |\ddot{x}| \leq [K_M(r_1 + r_2) + C] \tag{A.16}$$

This solution holds within small vicinity of origin, so we can write

$$|\ddot{\boldsymbol{x}}| \geq [\boldsymbol{K_m(r_1 - r_2) - C}]$$

Integrating both sides, we get

$$|\dot{\boldsymbol{x}}| \geq [\boldsymbol{K_m(r_1 - r_2) - C}]\boldsymbol{t}$$

Solution for all trajectories is therefore

$$|\boldsymbol{\dot{x}_i}| \geq [\boldsymbol{K_m(r_1 - r_2) - C}]\boldsymbol{t_i}$$

Where t_i is time for successive interval between crossing the line $\boldsymbol{x = 0}$. From above equation we can write

$$t_i = \frac{|\dot{x}_i|}{[K_m(r_1 - r_2) - C]} \tag{A.17}$$

Total time for convergence is the sum of all t_i,

$$T \leq \sum \frac{|\dot{x}_i|}{[K_m(r_1 - r_2) - C]} \tag{A.18}$$

$$\boldsymbol{Var}\big(\dot{\boldsymbol{x}}(.)\big) = \sum |\dot{\boldsymbol{x}}_{\boldsymbol{i}}| \leq |\dot{\boldsymbol{x}}_{\boldsymbol{0}}| + |\dot{\boldsymbol{x}}_{\boldsymbol{1}}| + |\dot{\boldsymbol{x}}_{\boldsymbol{2}}| + \cdots$$

$$\leq |\dot{\boldsymbol{x}}_{\boldsymbol{0}}| + \boldsymbol{q}|\dot{\boldsymbol{x}}_{\boldsymbol{0}}| + \boldsymbol{q}^{\boldsymbol{2}}|\dot{\boldsymbol{x}}_{\boldsymbol{0}}| + \cdots$$

$$\leq |\dot{\boldsymbol{x}}_{\boldsymbol{0}}|(\boldsymbol{1} + \boldsymbol{q} + \boldsymbol{q}^{\boldsymbol{2}} + \cdots)$$

$$\sum|\dot{\boldsymbol{x}}_{\boldsymbol{i}}| \leq \frac{|\dot{\boldsymbol{x}}_{\boldsymbol{0}}|}{(\boldsymbol{1}-\boldsymbol{q})} \tag{A.19}$$

Put value from (A.19) in (A.18) we get

$$\boldsymbol{T} \leq \frac{|\dot{\boldsymbol{x}}_{\boldsymbol{0}}|}{(\boldsymbol{1}-\boldsymbol{q})[\boldsymbol{K}_{\boldsymbol{m}}(\boldsymbol{r}_{\boldsymbol{1}} - \boldsymbol{r}_{\boldsymbol{2}}) - \boldsymbol{C}]}$$

Therefore the total convergence time for real twisting algorithm is calculated by above equation.

A.2 Analysis

By control law (A.3) and constraints (A.2) the trajectories of system (A.1) will spiral around the origin. To prove the convergence, one have to show that the magnitude of $\dot{\boldsymbol{x}}_{\boldsymbol{i}}$ remains always less than $\dot{\boldsymbol{x}}_{\boldsymbol{i+1}}$. For this purpose, the bounds of differential inclusion have been calculated. After that worst trajectory differential equation was solved to calculate $\dot{\boldsymbol{x}}_{\boldsymbol{i}}$. Therefore real twisting algorithm converges to the equilibrium point in finite time.

Appendix – B

Stability Analysis for Super Twisting Algorithm

Here we study in detail the stability analysis of most popular second order sliding mode algorithms e.g. super twisting algorithm.

B.1 Stability Analysis

Consider a dynamical system

$$\dot{\boldsymbol{x}} = \boldsymbol{a} + \boldsymbol{bu} \tag{B.1}$$

Let C, K_M, K_m, U_M, q are some positive constants.

$$|\dot{\boldsymbol{a}}| + \boldsymbol{U_M}|\dot{\boldsymbol{b}}| \leq \boldsymbol{C}, \qquad \boldsymbol{0} < K_{\boldsymbol{m}} \leq \boldsymbol{b}(\boldsymbol{t}, \boldsymbol{x}) \leq \boldsymbol{K_M}, \qquad |\boldsymbol{a}/\boldsymbol{b}| > q\boldsymbol{U_M}, \qquad \boldsymbol{0} < q < 1$$

(B.2)

and the control law

$$\boldsymbol{u} = -\boldsymbol{\lambda}|\boldsymbol{x}|^{\boldsymbol{1/2}}\boldsymbol{signx} + \boldsymbol{u_1} \quad \dot{\boldsymbol{u}}_{\boldsymbol{1}} = \begin{cases} -\boldsymbol{u}, & |\boldsymbol{u}| > \boldsymbol{U_M} \\ -\boldsymbol{\alpha signx}, & |\boldsymbol{u}| \leq \boldsymbol{U_M} \end{cases} \tag{B.3}$$

Lemma [Levant, 1993]

With K_m $\alpha > C$ and λ sufficiently large i.e.

$$\boldsymbol{\lambda} > \sqrt{\frac{\boldsymbol{2}}{(\boldsymbol{K_m\alpha - C})}}\frac{(\boldsymbol{K_m\alpha + C})\boldsymbol{K_M}(\boldsymbol{1+q})}{\boldsymbol{K_m^2}(\boldsymbol{1-q})} \tag{B.4}$$

then the controller provides for the appearance of a 2-sliding mode $\boldsymbol{x} = \dot{\boldsymbol{x}} = \boldsymbol{0}$ attracting the trajectories in finite time. The control u enters in finite time the segment $[-U_M, U_M]$ and stays there. It never leaves the segment if the initial value is inside at the beginning.

Proof:

First we calculate $\dot{\boldsymbol{u}}$ with $|\boldsymbol{u}| > \boldsymbol{U_M}$ and show that $\dot{\boldsymbol{u}}\boldsymbol{u} < 0$, it means that $|\boldsymbol{u}| \leq \boldsymbol{U_M}$will established in finite time, using (B.3) we have

$$\dot{\boldsymbol{u}} = \frac{\boldsymbol{d}}{\boldsymbol{dt}}(\boldsymbol{u}) = \frac{\boldsymbol{d}}{\boldsymbol{dt}}\left(-\boldsymbol{\lambda}|\boldsymbol{x}|^{\boldsymbol{1/2}}\boldsymbol{signx} + \boldsymbol{u_1}\right)$$

By using the property $\frac{\boldsymbol{d}}{\boldsymbol{dt}}|\boldsymbol{x}| = \dot{\boldsymbol{x}}\boldsymbol{signx}$

$$\dot{\boldsymbol{u}} = -\frac{\boldsymbol{1}}{\boldsymbol{2}}\boldsymbol{\lambda}|\boldsymbol{x}|^{-\boldsymbol{1/2}}(\dot{\boldsymbol{x}}\boldsymbol{signx})\boldsymbol{signx} - \boldsymbol{\lambda}|\boldsymbol{x}|^{\boldsymbol{1/2}}\frac{\boldsymbol{d}}{\boldsymbol{dt}}(\boldsymbol{signx}) + \dot{\boldsymbol{u}}_{\boldsymbol{1}}$$

The sign in quadrant I and IV is constant so $\frac{\boldsymbol{d}}{\boldsymbol{dx}}(\boldsymbol{signx}) = \boldsymbol{0}$ and using (B.3), we get

$$\dot{\boldsymbol{u}} = -\tfrac{\boldsymbol{1}}{\boldsymbol{2}}\boldsymbol{\lambda}|\boldsymbol{x}|^{-\boldsymbol{1/2}}\dot{\boldsymbol{x}} - \boldsymbol{u} \qquad \text{(B.5)}$$

Now we have to prove that $\dot{\boldsymbol{u}}\boldsymbol{u} < 0$

$$\dot{\boldsymbol{u}}\boldsymbol{u} = \left(-\frac{\boldsymbol{1}}{\boldsymbol{2}}\boldsymbol{\lambda}|\boldsymbol{x}|^{-\boldsymbol{1/2}}\dot{\boldsymbol{x}} - \boldsymbol{u}\right)\boldsymbol{u}$$

$$\dot{\boldsymbol{u}}\boldsymbol{u} = -\frac{\boldsymbol{1}}{\boldsymbol{2}}\boldsymbol{\lambda}|\boldsymbol{x}|^{-\boldsymbol{1/2}}\dot{\boldsymbol{x}}\boldsymbol{u} - \boldsymbol{u}^{\boldsymbol{2}}$$

In the above equation, if $\dot{\boldsymbol{x}}\boldsymbol{u} > 0$, then $\dot{\boldsymbol{u}}\boldsymbol{u} < 0$. Using (B.1) $\dot{\boldsymbol{x}}\boldsymbol{u}$ will be equal to

$$\dot{\boldsymbol{x}}\boldsymbol{u} = (\boldsymbol{a} + \boldsymbol{bu})\boldsymbol{u}$$

$$\dot{\boldsymbol{x}}\boldsymbol{u} = \boldsymbol{b}(\boldsymbol{a}/\boldsymbol{b} + \boldsymbol{u})\boldsymbol{u}$$

Form (B.2) and (B.3), we have $-\boldsymbol{a}/\boldsymbol{b} < q\boldsymbol{U_M} < \boldsymbol{a}/\boldsymbol{b}$, $\boldsymbol{u} > \boldsymbol{U_M}$ and $\boldsymbol{0} < q < 1$, by taking lower bounds we have

$$\dot{\boldsymbol{x}}\boldsymbol{u} \geq \boldsymbol{K_m}(\boldsymbol{qU_M} + \boldsymbol{U_M})\boldsymbol{U_M}$$

$$\dot{\boldsymbol{x}}\boldsymbol{u} \geq \boldsymbol{K_m}(\boldsymbol{1} + \boldsymbol{q})\boldsymbol{U_M^2} > 0$$

Hence prove that $\dot{\boldsymbol{u}}\boldsymbol{u} < 0$. This guarantees that $|\boldsymbol{u}| \leq \boldsymbol{U_M}$ can be established in finite time. For analysis of $|\boldsymbol{u}| \leq \boldsymbol{U_M}$ differentiate (B.1) with respect to time, we get

$$\ddot{\boldsymbol{x}} = \dot{\boldsymbol{a}} + \dot{\boldsymbol{b}}\boldsymbol{u} + \boldsymbol{b}\dot{\boldsymbol{u}}$$

(B.6)

From (B.3) we get

$$\ddot{\boldsymbol{x}} = \dot{\boldsymbol{a}} + \dot{\boldsymbol{b}}\boldsymbol{u} + \boldsymbol{b}\frac{\boldsymbol{d}}{\boldsymbol{dt}}\left(-\boldsymbol{\lambda}|\boldsymbol{x}|^{\boldsymbol{1/2}}\boldsymbol{signx} - \boldsymbol{u}_{\boldsymbol{1}}\right)$$

In I and IV quadrants we have

$$\ddot{\boldsymbol{x}} = \dot{\boldsymbol{a}} + \dot{\boldsymbol{b}}\boldsymbol{u} - \boldsymbol{b}\frac{\boldsymbol{1}}{\boldsymbol{2}}\boldsymbol{\lambda}\frac{\dot{\boldsymbol{x}}}{|\boldsymbol{x}|^{\boldsymbol{1/2}}} - \boldsymbol{b}\dot{\boldsymbol{u}}_{\boldsymbol{1}}$$

For $|\boldsymbol{u}| \leq \boldsymbol{U_M}$

$$\ddot{\boldsymbol{x}} = \dot{\boldsymbol{a}} + \dot{\boldsymbol{b}}\boldsymbol{u} - \boldsymbol{b}\tfrac{\boldsymbol{1}}{\boldsymbol{2}}\boldsymbol{\lambda}\frac{\dot{\boldsymbol{x}}}{|\boldsymbol{x}|^{\boldsymbol{1/2}}} - \boldsymbol{b}\boldsymbol{\alpha}\boldsymbol{sign}(\boldsymbol{x}) \qquad \forall\, \boldsymbol{x} \neq \boldsymbol{0}$$

From (B.2) we get an equivalent differential inclusion of the above equation as

$$\ddot{x} \epsilon [-C, C] - [K_m, K_M] \left(\frac{1}{2} \lambda \frac{\dot{x}}{|x|^{1/2}} + \alpha sign x \right)$$

(B.7)

For first quadrant, i.e. $x > 0$ **and** $\dot{x} > 0$, (B.7) becomes

$$\ddot{x} \leq C - K_m \left(\frac{1}{2} \lambda \frac{\dot{x}}{|x|^{1/2}} + \alpha \right) < 0 \quad \text{(B.8)}$$

Now we can find the condition $K_m \alpha > C$ for convergence which makes $\ddot{x}$ negative definite. Hence trajectories in first quadrant will always approach to the axis $\dot{x} = 0$. Convergence of the algorithm in different quadrant can be seen in Figure B.1.

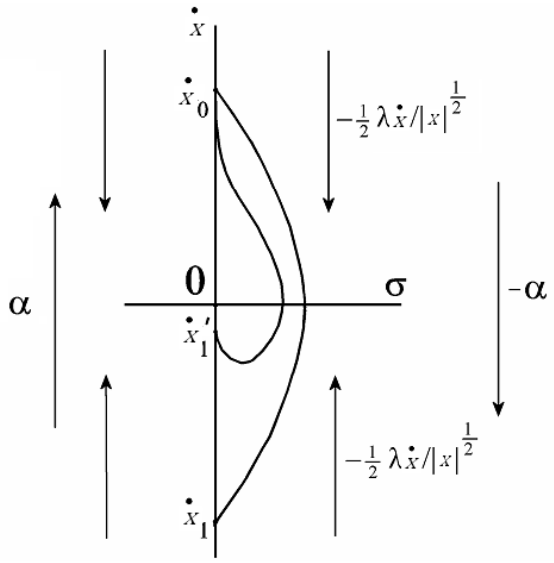

Figure B.1*: Convergence of Super Twisting in Different Quadrant*

Second term in (B.7) has sign negative, in first quadrant addition of any positive term will decrease its quantity. Hence the upper bounds of trajectories in first quadrant are

$$\ddot{x} = [-C, C] - \alpha [K_m, K_M] sign x \quad \text{(B.9)}$$

Multiplying both sides of (B.9) with $sign(x)$ function, we get

$$\ddot{x} sign x = ([-C, C] - \alpha [K_m, K_M] sign x) sign x$$

By using upper bounds, we have

$$\ddot{x} sign x \leq C - K_m \alpha < 0$$

$$-[K_M \alpha + C] \leq \ddot{x} sign x \leq -[K_m \alpha - C] < 0$$

(B.10)

The trajectories of $\dot{x}_0 x_M$ (line a in Figure B.2)

$$\ddot{\boldsymbol{x}} = -[\boldsymbol{K_m\alpha - C}] \qquad \textbf{with } \dot{\boldsymbol{x}} > 0, \tag{B.11}$$

For solution of (B.11) with initial conditions $\boldsymbol{x = 0},\ \dot{\boldsymbol{x}} = \dot{\boldsymbol{x}}_{\boldsymbol{M}}$ at $\boldsymbol{t = 0}$ integrate with respect to time *t*, we get

$$\dot{\boldsymbol{x}} = -[\boldsymbol{K_m\alpha - C}]\boldsymbol{t} + \boldsymbol{A} \tag{B.12}$$

Let the solution holds in the small vicinity of the origin i.e. $\boldsymbol{A = 0}$, we get

$$\boldsymbol{t} = -\frac{\dot{\boldsymbol{x}}}{\boldsymbol{K_m\alpha - C}} \tag{B.13}$$

Again integrating (B.12) with respect to time, we get

$$\boldsymbol{x} = -\frac{\mathbf{1}}{\mathbf{2}}[\boldsymbol{K_m\alpha - C}]\boldsymbol{t}^{\mathbf{2}} + \boldsymbol{B}$$

Putting value of *t* from (B.13), we get

$$\boldsymbol{x} = -\frac{\dot{\boldsymbol{x}}}{\mathbf{2}[\boldsymbol{K_m\alpha - C}]} + \boldsymbol{B}$$

Apply boundary value conditions $\dot{\boldsymbol{x}} = \boldsymbol{0},\ \boldsymbol{x = x_M},$ we get $\boldsymbol{B = x_M}$

$$\boldsymbol{x} = \boldsymbol{x_M} - \frac{\dot{\boldsymbol{x}}^{\mathbf{2}}}{\mathbf{2}[\boldsymbol{K_m\alpha - C}]} \tag{B.14}$$

In (B.14), putting $\boldsymbol{x = 0}$, we can find the values of $\dot{\boldsymbol{x}}_{\boldsymbol{0}}$

$$\dot{\boldsymbol{x}}_{\boldsymbol{0}}^{\mathbf{2}} = \mathbf{2}[\boldsymbol{K_m\alpha - C}]\boldsymbol{x_M} \tag{B.15}$$

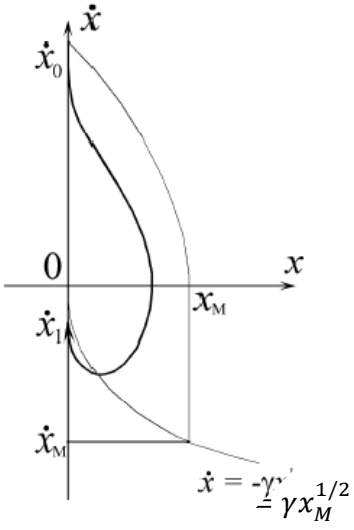

Figure B.2*: The Super Twisting Controller convergence*

Again from (B.14), we can write

$$\dot{x}^2 = -2[K_m\alpha - C](x - x_M)$$

(B.16)

This is equation of parabola with vertex at x_M. Hence trajectories in 4th quadrant will cut line $x = 0$ in finite time. The trajectories in fourth quadrant can be bounded in region called majorant (Levant, 1993). The region majorant is bounded by $x = 0$ and the curve b and c (in Figure B.2).

For fourth quadrant we have $x > 0$ **and** $\dot{x} < 0$, so

$$\ddot{x} \geq -C - K_m\left(\alpha - \frac{1}{2}\lambda\frac{|\dot{x}|}{|x|^{1/2}}\right)$$

In fourth quadrant $\ddot{x} > 0$ if

$$\frac{1}{2}\lambda\frac{|\dot{x}|}{|x|^{1/2}} > \frac{C}{K_m} + \alpha \qquad \text{(B.17)}$$

From (B.17) we have

$$\dot{x} \geq -\frac{2}{\lambda}\left(\frac{C}{K_m} + \alpha\right)x^{1/2}$$

The curve b is start from $(x_M, 0)$ to $\left(x_M, -\frac{2}{\lambda}\left(\frac{C}{K_m} + \alpha\right)x_M^{1/2}\right)$, and the curve c is from $\left(x_M, -\frac{2}{\lambda}\left(\frac{C}{K_m} + \alpha\right)x_M^{1/2}\right)$ to $(0, \dot{x}_M)$.

For $|u| < U_M$, condition $|\dot{x}_M/\dot{x}_0| < 1$ is sufficient for convergence, so we have

$$\frac{2(K_m\alpha+C)^2}{\lambda^2 K_m^2(K_m\alpha-C)} < 1 \qquad \text{(B.18)}$$

This equality is not valid for $x > 0$ **and** $\dot{x} > 0$, in this case $\dot{u}$ stay negative and does change sign. Again taking (B.1) and (B.2) for $|u| \leq U_M$

$$|\dot{x}| = b|(a/b + u)|$$

$$|\dot{x}| \leq b(|a/b| + |u|)$$

$$|\dot{x}| \leq K_M|qU_M + U_M|$$

$$|\dot{x}| \leq K_M(1 + q)U_M$$

Similarly we have

$$|\dot{x}| = b|(a/b + u)|$$

$$|\dot{x}| \geq K_m|-qU_M + U_M|$$

It always remains positive, so that we can write

$$|\dot{x}| \geq K_m(1-q)U_M$$

$$\dot{x}_0 \leq K_M(q+1)U_M$$

$$\left|\frac{\dot{x}_M}{\dot{x}_0}\right| = \frac{K_m(1-q)U_M}{K_M(1+q)U_M} = \frac{K_m(1-q)}{K_M(1+q)} < 1 \quad \text{(B.19)}$$

Comparing (B.18) and (B.19) we have

$$\frac{K_m^2(1-q)^2}{K_M^2(1+q)^2} < \frac{2(K_m\alpha + C)^2}{\lambda^2 K_m^2(K_m\alpha - C)}$$

From the above equation, we can find the bounds for λ i.e.,

$$\lambda > \sqrt{\frac{2}{(K_m\alpha - C)}} \frac{(K_m\alpha + C)K_M(1+q)}{K_m^2(1-q)} < 1$$

B.2 Convergence Time

The trajectory $\dot{x}_0 x_1 \dot{x}_1$ can be written as

$$[K_m\alpha - C] \leq |\ddot{x}| \leq [K_M\alpha + C]$$

This solution holds within small vicinity of origin, so that we can write

$$|\ddot{x}| \geq [K_m\alpha - C]$$

Integrating both sides, we have

$$|\dot{x}_i| \geq [K_m\alpha - C]t_i$$

Where t_i is time for successive interval between crossing the line $x=0$. From the above equation we can write,

$$t_i = \frac{|\dot{x}_i|}{[K_m\alpha - C]}$$

And total time for convergence is the sum of all t_i

$$T \leq \sum \frac{|\dot{x}_i|}{[K_m\alpha - C]} \quad \text{(B.20)}$$

$$Var(\dot{x}(.)) = \sum |\dot{x}_i| \leq |\dot{x}_0| + |\dot{x}_1| + |\dot{x}_2| + \cdots$$

$$\leq |\dot{x}_0| + q|\dot{x}_0| + q^2|\dot{x}_0| + \cdots$$

$$\leq |\dot{x}_0|(1 + q + q^2 + \cdots)$$

$$\sum|\dot{x}_i| \leq \frac{|\dot{x}_0|}{(1-q)} \tag{B.21}$$

Put value from (B.21) in (B.20), we get

$$T \leq \frac{|\dot{x}_0|}{(1-q)[K_m\alpha - C]}$$

Therefore the total convergence time for super twisting algorithm is calculated by above equation.

B.3 Analysis

First of all, it has been proved that the control law (B.3) using by system (B.1) converges to bounds $[-U_M, U_M]$ within finite time. Trajectories of the system (B.1) using super twisting algorithm (B.3) are parabola type. Hence again to prove convergence, one have to show that the magnitude of $\dot{x}_i$ is always less than $\dot{x}_{i+1}$. The differential equation is solved for worst trajectory in 1st quadrant to calculate $\dot{x}_0$. After that magnitude of $\dot{x}_M$ is calculated by the help of majorant. Therefore super twisting algorithm converges to equilibrium point within finite time.

Appendix – C

System Identification of Stabilized Platform

All engineering system need dynamical model for the analysis, design and implementation of a high-performance control for the system. System identification is the tool for constructing the model of the system by simply input/output measurements. It doesn't require any apriori knowledge of system dynamics.

A linear system can be described by a transfer function $G(s)$. If the system has finite input energy, the following Fourier Transform of input/output relationship will hold (Ljung and Glad, 1994):

$$Y(\omega) = G(\omega)U(\omega) \tag{C.1}$$

If input and output are known and output of system is invertible, the frequency function $G(\omega)$ could be constructed by the following relation.

$$G(\omega) = Y(\omega)U(\omega)^{-1} \tag{C.2}$$

In other words, system identification is an experimental approach for determining the dynamical model of the system, it includes following steps: (Landau, 1990)

- Input/output data acquisition under an experimental protocol.
- Choice of model structure like Auto Regressive with eXternal inputs (ARX), Auto Regressive with Moving Average (ARMAX), etc.
- Estimation of model parameters and coefficients.
- Validation of the identified model (structure and values of the parameters).

The first step in system identification is data acquisition. The input signal $u(t)$ should contain enough frequencies, so it can cover the whole bandwidth of interest and excite the complete dynamics of the system. Common choices for input signal for the identification are Gaussian white noise signal, Chirp signal or Pseudo Random Binary Signal (PRBS) (Ljung, 1989; Ljung and Glad, 1994).

The selected input is given to the system and input/output data is recorded. The recorded data is used for model estimation.

Next step in the identification process is choice of model structure. Different methods like ARX, ARMAX etc. are common choices for model structure in identification process. The suitable choice of the model structure is perhaps the most difficult decision the user has to make (Ljung, 1989; Ljung and Glad, 1994). This choice is based on insight knowledge of the system and complete understanding of the identification procedure.

Further a decision about the order of the model should be taken by the user. It is also a difficult task in model identification. An over parameterized model structure can lead to unnecessary computations and an under parameterized model may be very inaccurate (Stoica, 1989).

Last step in identification process is model validation. For this purposes, a dataset different than the data used in the identification process is recommended (Ljung, 1989). The validation signal frequency should be according to worst scenarios so the model will remain valid for other frequencies.

C.1 Model Identification of the Stabilized Platform

The stabilized platform has two inputs and two outputs axes i.e. roll and pitch. Both axes are orthogonal and have no coupling effect on each other. The Single Input Single Output (SISO) case of system identification can be applicable on both axes separately. Only pitch axis system identification process is explained here in detail.

As stated above, first step in the system identification is data collection and common choices of input signal are White Noise, PRBS or Chirp signals. Due to discontinuous in nature, it is not recommended to apply white noise or PRBS on stabilized platform because of its sensitive and sluggish mechanical structure. Chirp signal is therefore selected as an input; it is a sinusoid with continuously varying frequency over a definite band Ω: $\omega_1 \leq \omega \leq \omega_2$ for certain time period $0 \leq t \leq M$ (Ljung 1989) i.e.

$$u(t) = A\cos(\omega_1 t + (\omega_2 - \omega_1)t^2/2M) \tag{C.3}$$

The Chirp signal should contain enough frequencies, so it covers the whole system's bandwidth to exalt all the dynamics of the stabilized platform. As mentioned earlier that the voltages through DAC are inputs to the stabilized platform and top plate angular positions, measured in degrees are the desired outputs. Input limit is ± 10V and output becomes saturate beyond $\pm 10^{\circ}$ both in roll and pitch axes. The frequency range

for Chirp signal is swept between 0.04 Hz to 2 Hz. This range is selected after studying the response of the system experimentally and the rough cut-off frequency range is founded. Therefore, the optimum value of input voltage for identification is set as ± 3 Volts to keep the system in operating range. If these limits are crossed then the actuators of the system becomes saturated and it may lead to lose important dynamics of the plant. The selected input signal is given to the platform and corresponding output data is measured. Figure C.1 shows the input/output signals graph.

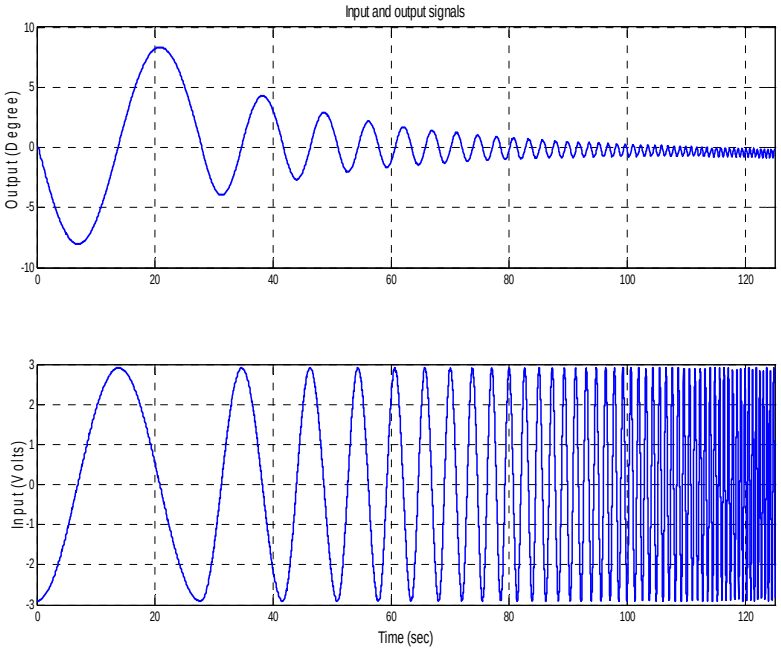

***Figure C.1**: Input Output Signal of Stabilized Platform*

The data collected from this experiment is used for model estimation. Before model estimation, it is also necessary to treat the raw data so it becomes appropriate for identification process. In the first step, a treatment is done to remove mean and trends from the raw data. In the next step the processed data is fitted into ARX model. The ARX model relates the current output to finite number of past inputs and outputs for model estimation. The estimated models have three poles and two zeros. The delay observed is too small and neglected to avoid complication. This model structure is chosen on the basis of best fits between model's and actual system's outputs. If order of the system is increased then poles are canceled by zeros and system can lose con-

trollability and observability properties. The resultant identified model has three states but these states don't have any physical meaning.

The equation of identified model can be represent as follow,

$$y(k) = -a_1 y(k-1) - a_2 y(k-2) - a_3 y(k-3) + b_1 u(k) + b_2 u(k-1) \qquad \text{(C.2)}$$

The identified parameters of three different load conditions for the above equation are given in following Table C.1.

Model	a_1	a_2	a_3	b_1	b_2
Without Payload	*-1.6432*	*0.7629*	*-0.1197*	*-0.0152*	*0*
Symmetric Payload	*-1.4203*	*0.6370*	*-0.2166*	*-0.0246*	*0*
Asymmetric Payload	*-1.6364*	*1.5107*	*-0.8741*	*0*	*-0.0176*

***Table C.1**: Parameters of the three identified models*

A cosine signal with 0.04Hz frequency is chosen for validation process. The validation frequency is set to be worst case scenario of sea dynamics, as the observed sea wave's frequency was found to be less then specified frequency during experimentation. The responses of the cosine signal were obtained from actual platform as well as from identified model. Figure C.2 shows the comparison results and Figure C.3 shows prediction errors. The errors are almost negligible and the identified model output signal is almost overlapped with the actual output of the system.

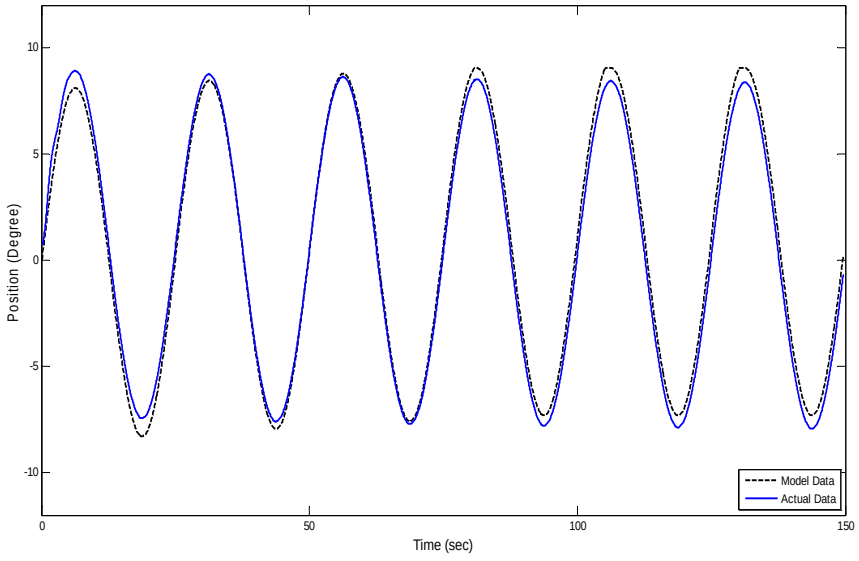

***Figure C.2**: Model Validation on Test Data*

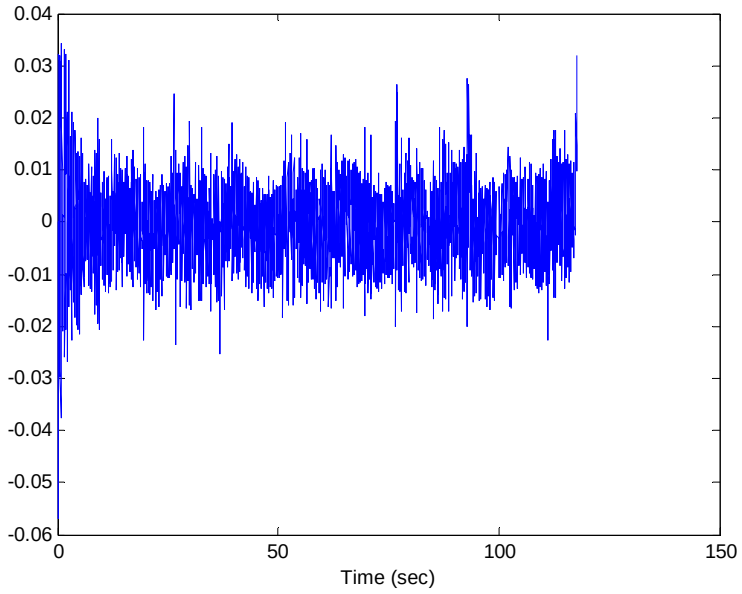

***Figure C.3**: Prediction Error over Test Data*

The state space models' $\boldsymbol{A^i, B^i, C^i, D^i} \quad \forall \boldsymbol{i = 1, 2, 3}$ of identified systems are given as:

$$\boldsymbol{A^1} = \begin{bmatrix} \mathbf{17.3100} & \mathbf{22.6900} & \mathbf{-22.6900} \\ \mathbf{-20.0261} & \mathbf{-19.9739} & \mathbf{59.9739} \\ \mathbf{2.7156} & \mathbf{-2.7156} & \mathbf{-37.2844} \end{bmatrix}$$

$$\boldsymbol{A^2} = \begin{bmatrix} \mathbf{15.5646} & \mathbf{24.4354} & \mathbf{-24.4354} \\ \mathbf{-20.8593} & \mathbf{-19.1407} & \mathbf{59.1407} \\ \mathbf{5.2933} & \mathbf{-5.2933} & \mathbf{-34.7067} \end{bmatrix}$$

$$\boldsymbol{A^3} = \begin{bmatrix} \mathbf{24.0672} & \mathbf{15.9328} & \mathbf{-15.9328} \\ \mathbf{-37.9951} & \mathbf{-2.0049} & \mathbf{42.0049} \\ \mathbf{13.9261} & \mathbf{-13.9261} & \mathbf{-26.0739} \end{bmatrix}$$

$$B^1 = \begin{bmatrix} -0.0086 \\ -0.0076 \\ 0.0010 \end{bmatrix} \qquad B^2 = \begin{bmatrix} 0.0151 \\ -0.0129 \\ -0.0033 \end{bmatrix} \qquad B^3 = \begin{bmatrix} -0.0070 \\ 0.0184 \\ -0.0290 \end{bmatrix}$$

$$C^1 = [11.3450 \quad -11.3450 \quad 11.3450]$$

$$C^2 = [12.2177 \quad -12.2177 \quad 12.2177]$$

$$C^3 = [7.9664 \quad -7.9664 \quad 7.9664]$$

$$D^1 = [0.0043] \qquad D^2 = [-0.0075] \qquad D^3 = [0.0035]$$

Appendix – D

LMI Control Design for the Stabilized Platform

Many engineering optimization problems can easily be approximated with Linear Matrix Inequalities (LMIs). The beauty in LMI is that it can accommodate a variety of design specification and constraints. Once a problem is formulated in terms of LMIs, it can be solved by efficient convex optimization methods. Moreover multiple LMIs can be expressed as a single LMI.

LMI is an expression of the form:

$$F(x) = F_0 + x_1F_1 + \cdots + x_nF_m \prec 0 \tag{D.1}$$

where $x = [x_1 \quad \cdots \quad x_m]$ is the vector of m decision variables, $F_i \in \mathcal{R}^{n\times n}\ \forall i = 0, \ldots, m$ are real symmetric matrices. The special inequality symbol $\prec$ in (D.1) means the matrix $F(x)$ is negative definite, i.e. all its eigenvalues $\lambda\big(F(x)\big)$ are negative. The main property of an LMI is that the inequality $F(x) \prec 0$ defines a convex set C on x, i.e. $\mathsf{C} = \{x|F(x) \prec 0\}$ is convex. Let $x_1, x_2 \in \mathsf{C}$ and $\alpha \in [0 \quad 1]$, we can define a convex set with:

$$F(\alpha x_1 + (1-\alpha)x_2) = \alpha F(x_1) + (1-\alpha)F(x_2) \prec 0 \tag{D.2}$$

The closed loop Root Means Square (RMS) gain from ω to z_∞ cannot exceed γ if and only if there exists a symmetric matrix $\boldsymbol{X} := \boldsymbol{X}_\infty$ and $\boldsymbol{Y} := \boldsymbol{KX}$ such that,

$$\begin{bmatrix} \boldsymbol{AX + XA^T + B_2Y + Y^TB_2^T} & \boldsymbol{B_1} & \boldsymbol{XC_1^T + Y^TD_{12}^T} \\ \boldsymbol{B_1^T} & \boldsymbol{-I} & \boldsymbol{D_{11}^T} \\ \boldsymbol{C_1X + D_{12}Y} & \boldsymbol{D_{11}} & \boldsymbol{-\gamma I} \end{bmatrix} < 0 \tag{D.3}$$

Moreover the closed loop H_2 norm of $\boldsymbol{T_{wz_2}}$ cannot exceed ν if there exists two symmetric matrices X and Q such that,

$$\begin{bmatrix} \boldsymbol{Q} & \boldsymbol{C_2X + D_{22}Y} \\ \boldsymbol{XC_2^T + Y^TD_{22}^T} & \boldsymbol{X} \end{bmatrix} > 0\,, \tag{D.4}$$

$$\boldsymbol{Trace}\,(\boldsymbol{Q}) < \boldsymbol{v_0^2}\,, \tag{D.5}$$

where

$$\boldsymbol{\gamma^2 < \gamma_0^2}. \tag{D.6}$$

The closed-loop poles lie in the LMI region

$$\boldsymbol{D = \{z \in C: L + Mz + M^T\bar{z} < 0\}} \tag{D.7}$$

where $\boldsymbol{L = L^T = \{\lambda_{ij}\}_{1\le i,j\le m}}$, $\boldsymbol{M = M^T = \{\mu_{ij}\}_{1\le i,j\le m}}$ and '*M* ' and '*L*' are fixed real matrices. These closed-loop poles lie in the region if and only if there exists a symmetric matrix X_{pol} and satisfying the following conditions:

$$\boldsymbol{\left[\lambda_{ij} + \mu_{ij}(AX + B_2Y)X_{pol} + \mu_{ji}\left(XA^T + Y^TB_2^T\right)\right]_{1\le i,j\le m} < 0} \tag{D.8}$$